Dissertation

submitted to the

Combined Faculties of the Natural Sciences and Mathematics
of the Ruperto-Carola University of Heidelberg, Germany

for the degree of

Doctor of Natural Sciences

Put forward by

Coralie Sophie Schneider

born in: Oberndorf am Neckar, Germany
Oral examination: December 15th, 2021

Towards Infrared QCD Correlation Functions With Functional Methods

Referees: Prof. Dr. Jan M. Pawlowski
Prof. Dr. Jörg Jäckel

Towards Infrared QCD Correlation Functions With Functional Methods

In this thesis, we study the infrared regime of QCD with functional methods. To this end, we present the *Mathematica* package *QMeS-Derivation*. It allows for the derivation of symbolic functional equations from a given master equation. We apply this tool to Landau gauge Yang-Mills theory, where gauge invariance is implemented via BRST symmetry. We solve a self-consistent set of momentum-dependent functional equations within a vertex expansion and compare the correlation functions obtained from different functional approaches. We find good agreement of the results, hinting at gauge consistency of our setup. We proceed by using the obtained Euclidean results to compute four-gluon correlation functions, from which we extract the scalar and pseudo-scalar glueball mass by finding spectral representations of the dressings. The obtained results agree well with the masses computed from other methods. Next, we consider QCD at finite temperature and finite chemical potential and provide a setup for thermal correlation functions, where we introduce a thermal split in the quark-gluon vertex. This setup allows for a study of the phase diagram of QCD, where special emphasis is put on the investigation of the chiral phase transition.

Fortschritte Zur Berechnung Niedrigenergetischer QCD Korrelationsfunktionen Mit Funktionalen Methoden

In dieser Arbeit untersuchen wir den QCD Niedrigenergie-Sektor mit Hilfe funktionaler Methoden. Dazu stellen wir das *Mathematica* Paket *QMeS-Derivation* vor. Es ermöglicht die Herleitung von symbolischen funktionalen Gleichungen aus einer gegebenen Mastergleichung. Wir wenden dieses Tool auf Yang-Mills Theorie in Landau Eichung an, bei der Eichinvarianz über BRST-Symmetrie implementiert wird. Wir lösen einen in sich konsistenten Satz impulsabhängiger funktionaler Gleichungen in einer Vertex-Entwicklung und vergleichen die Korrelationsfunktionen, die wir aus verschiedenen funktionalen Methoden erhalten. Wir finden eine gute Übereinstimmung der Ergebnisse, die auf Eichkonsistenz unseres Systems hindeutet. Wir fahren fort, indem wir die erhaltenen euklidischen Ergebnisse verwenden, um Vier-Gluon-Korrelationsfunktionen zu berechnen, aus denen wir die skalare und pseudoskalare Glueball-Masse extrahieren, indem wir spektrale Darstellungen der Dressings finden. Die erhaltenen Ergebnisse stimmen gut mit den Massen überein, die aus anderen Methoden berechnet wurden. Als Nächstes betrachten wir QCD bei endlicher Temperatur und endlichem chemischen Potential und stellen einen Ansatz für thermische Korrelationsfunktionen bereit, bei dem eine thermische Aufspaltung im Quark-Gluon-Vertex eingeführt wurde. Dieser Ansatz ermöglicht die Untersuchung des Phasendiagramms der QCD, wobei besonders Wert auf die Untersuchung des chiralen Phasenübergangs gelegt wird.

Contents

1. Introduction

1.1. Motivation

Our modern understanding of fundamental physics is captured in the Standard Model (SM) of elementary particle physics. It describes the three fundamental interactions, the electromagnetic, the weak, and the strong force, as well as the fundamental fermions that constitute matter. With the discovery of the Higgs boson [6, 7], the key ingredient for the mechanism [8–10] that gives rise to particle masses, the SM has become widely accepted and is today one of the most well-tested models in physics.

The theory of Quantum Chromodynamics (QCD) captures the strongly interacting sector of the Standard Model i.e. the interaction between colored particles such as quarks and gluons where the corresponding gauge theory is a non-Abelian $SU(3)$ Yang-Mills theory (YM) [11]. The interaction manifests in a plethora of different phenomena that are dependent on the energy scale. In the large momentum regime of QCD, the coupling becomes asymptotically small rendering the theory asymptotically free [12, 13]. This sector has been extensively studied with perturbative approaches and techniques. For low momenta, the strong coupling becomes large and the theory becomes strongly correlated. This particular infrared behavior is subject to many theoretical QCD studies, see e.g. [14] and experiments, such as heavy-ion collisions at RHIC [15], LHC [16], CBM [17] and NICA [18], as this sector exhibits two interesting features.

The emergence of hadrons in the strongly coupled regime is linked to (color-)confinement that describes the absence of colored particles from the physical spectrum and manifests itself in a linear potential between a pair of quarks. Thus, although the existence of quarks which are the constituents of hadrons is experimentally well established [19], a single quark cannot be detected or measured. The self-interacting or non-Abelian nature of QCD also allows for the formation of glueballs, bound states of gluons only.

The second characteristic effect in the non-perturbative sector of QCD is dynamical chiral symmetry breaking. Implications thereof can be seen when comparing the observed hadron mass to those of the constituent quark masses in the SM, that were acquired by the Higgs mechanism, making up only a fraction of the total hadron mass while the remaining observed mass difference is accounted for by QCD binding energy.

While the properties of most hadrons are experimentally well-known [20], a quantitative understanding of infrared QCD is necessary to provide theoretical insights and predictions. This goes hand in hand with the development of non-perturbative *ab initio* approaches, where during the last years mainly two methods have prevailed, lattice computations and functional methods.

The first has proven itself by yielding precise predictions of the hadronic bound state spectrum, see e.g. [21], and various studies on the QCD phase diagram at small chemical potential, see e.g. [22–25]. However, a major conceptual obstacle connected with lattice simulations is the sign problem preventing the efficient inclusion of fermionic matter as well as large chemical potentials in the computation, see e.g. [26, 27]. Furthermore, the

convergence in the continuum limit has to be established.

Functional methods yield a continuum description of the theory in terms of an infinite number of coupled equations for correlation functions, where the propagators play a central rôle. However, the exact equations can only be solved within truncations.

In this conceptual framework, two aspects have to be taken into consideration. Firstly, the convergence of results for increasing truncations has to be established. This goes hand in hand with the technical development of computer-algebraic tools for the self-consistent numerical computation and solution of the coupled equations within functional methods. And Secondly, the propagators of gauge theories are only well-defined if the redundant degrees of freedom are removed via a gauge-fixed formulation of the theory. This procedure breaks gauge invariance of the action, rendering the correlation functions to be only indirectly related to physical observables and where only combinations thereof are gauge-invariant. Thus, a study of the conservation of gauge symmetry or residuals thereof encoded in other emerging symmetries of the action within functional approaches, where cut-offs and regulators are required, is necessary. The smallness of violation of the underlying gauge symmetry within truncations is essential to guarantee the limit of physical gauge invariance of the full theory. This gauge consistency of the correlation functions is relevant to the understanding and manifestation of confinement in gauge-fixed settings.

Equipped with these insights into the technical numerical treatment of functional computations of gauge theories, one can start to study confinement and infrared gluon dynamics in the pure gauge sector of QCD. This is already sufficient since confinement can be directly related to a mass gap in the gluon propagator in Yang-Mills theory [28–30]. Proving the existence of this mass gap in quantum Yang-Mills theory is even one of the Millennium Prize Problems [31] and requires proving the existence of the underlying quantum field theory. First computations of signatures of the mass gap in Yang-Mills theory have already been performed with functional methods, see e.g. [32–40].

Methods for the computation of QCD bound states with functional equations, e.g. via dynamical hadronization [41–44] and via Bethe-Salpeter equations [45, 46], are still in development. Their predictive power and the obtained results are on a par with lattice computations.

Building on the gained insights in Yang-Mills theory, the inclusion of quarks is a feasible improvement of the truncation, leading to insights into the full theory of QCD. Additionally, including a finite chemical potential and finite temperature allows for a study of the phase diagram of Quantum Chromodynamics. Here the advantages of functional methods stand out as they do not face any technical difficulties with the inclusion of fermions and large chemical potentials.

Understanding the phase structure is closely linked to the two major non-perturbative effects of QCD, confinement and chiral symmetry breaking. Keeping the temperature low and going to very high chemical potential, quark-matter is in a color-flavor-locked phase [47], a chiral symmetry broken phase where color-superconduction occurs.

At vanishing temperature and chemical potential, matter is in the hadronic confined phase, meaning there are no free quarks and gluons but only bound states thereof. Increasing the temperature leads to a crossover at $T_c \approx 155\,\mathrm{MeV}$ [22, 23] into the deconfined quark-gluon plasma where (approximate) chiral symmetry is restored, this stage is comparable to the situation in the early universe. The chiral and the confinement-deconfinement phase transition are closely related [48], however, the true nature of this relation is not

yet fully understood. The chiral crossover turns into a phase transition of first order for higher chemical potential, potentially yielding a critical endpoint in the phase diagram.

The existence of a chiral critical endpoint for finite temperature and chemical potential is highly conjectured and subject of many theoretical and experimental studies, see e.g. [49–67]. Thus, from a theoretical point of view, the full understanding of the non-perturbative sector of QCD is a requirement for explorations of the QCD phase diagram.

In conclusion, this work contributes to the theoretical insights into infrared QCD dynamics by introducing a numerical tool for the systematic and theory-independent derivation of symbolic functional equations. Using this tool, we present a study of gauge consistency in truncated $SU(3)$ Yang-Mills theory with different functional methods, where we compare various solutions related to the mass gap. We provide an ansatz and first results for the extraction of glueball masses obtained within this framework. Finally, we present the setup for a study of QCD at finite temperature and finite chemical potential, where we are aiming at extracting the chiral order parameter and the critical temperature T_c. The individual projects presented in this thesis are motivated separately at the beginning of each chapter.

1.2. Publications

While the thesis was written by the author only, most of the results that are presented were obtained in collaborations. The respective content, as well as text and figures, were taken from the publications and not marked individually but rather cited at the beginning of the respective chapters.

The author was however main author of the following publication,

[1, 2] **QMeS-Derivation: Mathematica package for the symbolic derivation of functional equations**
Jan M. Pawlowski, Coralie S. Schneider, Nicolas Wink
E-Print: arXiv:2102.01410
Github: QMeS-Derivation

Furthermore the thesis includes so far unpublished works, listed here:

[3] **On Gauge Invariance in Gauge-Fixed Yang-Mills Theory**
Jan M. Pawlowski, Coralie S. Schneider, Nicolas Wink
Comment: We investigate gauge invariance in Landau gauge Yang-Mills theory with functional methods by solving a self-consistent set of transverse and longitudinal momentum-dependent correlation functions.

[4] **Glueball Masses from the fRG**
Jan M. Pawlowski, Coralie S. Schneider, Jonas Turnwald, Julian M. Urban
Comment: The scalar and pseudo-scalar glueball masses are extracted from the spectral function of the full fRG four-gluon vertex dressing via Padé approximants and Gaussian Process Regression.

[5] **Phase Structure of QCD**
Fei Gao, Jan M. Pawlowski, Coralie S. Schneider
Comment: A study of the phase structure of $2+1$-flavor QCD with thermal correlation functions at finite chemical potential.

1.3. Outline

We start by introducing the basics of non-Abelian gauge theories and Quantum Chromodynamics (QCD) in Chapter 2. Functional methods and different quantum master equations within our notation, as well as the vertex expansion of the effective action, a short discussion of truncations and different infrared cutoffs, are presented in Chapter 3. The full derivation of the equations can be found in Section A.1.

Chapter 4 presents *QMeS-Derivation*, a *Mathematica* package for the symbolic derivation of functional equations starting from a quantum master equation. The corresponding equations, as well as the general conventions and notations, were introduced in the previous chapter and the functional derivative rules used by the package can be found in Section A.2. After introducing the workflow and defining the main objects within *QMeS-Derivation*, we give examples in Yang-Mills theory, and $N_f = 1$ and $N_f = 2$ Yukawa theory, where the corresponding *QMeS* outputs can be found in Section A.3.

In Chapter 5, the previously introduced package is applied to Euclidean $SU(3)$ Yang-Mills theory in Landau gauge where gauge invariance is implemented via BRST symmetry. Results obtained self-consistently from different functional methods are compared for several (non-)confining solutions. We compare the longitudinal correlation functions obtained from different functional methods and find good agreement hinting at gauge consistency of our setup. In-depth information about the respective computations can be found in Chapter B.

The obtained results are then used to extract masses for the scalar and pseudo-scalar glueball by finding a spectral representation of the appropriately projected four-gluon vertex dressings with Padé approximants and Gaussian Process Regression. After introducing both methods, as well as the relation between Euclidean correlation functions and spectral representations thereof in Minkowski space, the results are presented in Chapter 6. Chapter C contains additional information on the numerical details of this topic.

Chapter 7 contains the motivation and a setup for the derivation of functional equations at finite temperature and chemical potential in $2+1$-flavour QCD, where we have introduced a thermal split in the quark-gluon vertex. The chapter contains preliminary results at vanishing chemical potential that are compared within different truncations. Further technical information is given in Chapter D.

Finally, we give a summary of the results obtained in this work and an overall conclusion containing an outlook and future projects in Chapter 8.

2. Quantum Chromodynamics

The study of Quantum Chromodynamics (QCD) entails strongly interacting quarks and gluons exhibiting interesting features. The non-Abelian nature of the theory allows for gluonic self-interactions and the theory exhibits a phenomenon called asymptotic freedom: At high energies, i.e. at a small coupling constant, the theory becomes asymptotically free, meaning that the coupling approaches the Gaussian fixed point [12, 13]. The self-interaction of gluons also allows for the formation of glueballs, i.e. bound states consisting solely of gluons. These theoretically predicted states have not yet been detected conclusively in experiments. For a general overview, see [68]. This topic will be discussed in more detail in Chapter 6.

Furthermore, all observed states are color-neutral, one cannot detect a single quark or gluon. In fact, a quark-anti-quark pair experiences a linearly rising potential when pulled apart. This (color-)confinement can be linked to the existence of a mass gap in the gauge sector of QCD, called Yang-Mills theory [28–30]. For studies of the gapped gluon in Landau gauge Yang-Mills theory and QCD with functional methods, see e.g. [32–40, 69].

Signatures thereof and a study of gauge invariance within different functional methods, is presented in Chapter 5. For an introduction to different confinement scenarios that are relevant in the context of functional methods, see e.g. [14, 70–73]. For topological and other approaches to confinement, see e.g. [74–77].

When comparing the quark masses with the masses of mesons and hadrons, one discovers that the former are significantly lighter than the latter. In fact, the mass of a proton is around 938 MeV, whereas the sum of the (current) masses of the constituent quarks, makes up only about 1 % of the proton mass [20, 78]. This phenomenon can be explained by dynamical chiral symmetry breaking. We will go into more details on this in Section 2.3 and in Chapter 7 which contains a setup for a study of QCD at finite temperature and chemical potential, delving deeper into the relation between chiral symmetry breaking and confinement while exploring the phase structure of QCD. For literature on chiral symmetry breaking within functional methods, see [44, 60, 69, 79–91].

In the following, we give a brief overview of QCD in Euclidean space-time. The discussion closely follows [92, 93]. For further details, see e.g. [14, 94, 95].

2.1. Non-Abelian Gauge Theories

We start by investigating the gauge invariant QCD action. For this, we consider a Dirac fermion q in a fundamental representation of the gauge group together with the $SU(3)$ Yang-Mills action. Implementing gauge invariance of the Euclidean action under a local transformation $U \in SU(3)$ one arrives at,

$$\begin{aligned} S[q,\bar{q},A] &= S_D[q,\bar{q}] + S_{YM}[A] \\ &= \int_x \bar{q}(\not{D} + m_q)q + \frac{1}{2}\int_x \operatorname{Tr} F_{\mu\nu}F_{\mu\nu}\,, \end{aligned} \tag{2.1}$$

where the Gamma matrices obey $\{\gamma_\mu, \gamma_\nu\} = 2\delta_{\mu\nu}$ and the covariant derivative that depends on the gauge field A_μ is given as,

$$D_\mu = \partial_\mu - igA_\mu \,. \tag{2.2}$$

One proceeds by constructing a kinetic term for the gauge field from the commutator of the covariant derivative,

$$\begin{aligned} F_{\mu\nu} &= \frac{i}{g}\left[D_\mu, D_\nu\right] \\ &= \partial_\mu A_\nu - \partial_\nu A_\mu - ig\left[A_\mu, A_\nu\right] \,. \end{aligned} \tag{2.3}$$

Since the gauge fields live in the Lie algebra of $SU(3)$, they are matrix-valued and therefore non-commuting, hence the non-Abelian nature of the theory. One can therefore write,

$$\begin{aligned} A_\mu &= A_\mu^a T^a \\ F_{\mu\nu}^a &= \partial_\mu A_\nu^a - \partial_\nu A_\mu^a + g f^{abc} A_\mu^b A_\nu^c \,, \end{aligned} \tag{2.4}$$

with the generators T^a of the Lie algebra,

$$\left[T^a, T^b\right] = i f^{abc} T^c \,, \tag{2.5}$$

and $\mathrm{Tr}(T^a T^b) = \frac{1}{2}\delta^{ab}$ and where f^{abc} are the structure constants of the Lie algebra. The non-Abelian nature of the gauge fields lead to self-interaction terms of the form,

$$A_\mu^a A_\nu^b \partial_\mu A_\nu^c \quad \text{and} \quad A_\mu^a A_\nu^b A_\rho^c A_\sigma^d \,. \tag{2.6}$$

The gauge transformation of the fields and the field strength tensor are then given as,

$$\begin{aligned} &q \to q^U = Uq \,, \quad \bar{q} \to \bar{q}^U = \bar{q}U^\dagger \,, \quad A_\mu \to A^U = UA_\mu U^\dagger - \frac{i}{g}(\partial_\mu U)U^\dagger \,, \\ &F_{\mu\nu} \to F_{\mu\nu}^U = UF_{\mu\nu}U^\dagger \,, \end{aligned} \tag{2.7}$$

with the gauge transformation,

$$U = e^{iT^a \Theta^a(x)} \,. \tag{2.8}$$

It is worth mentioning that in contrast to QED the field strength tensor itself, i.e. the color-electric and color-magnetic fields,

$$\begin{aligned} E_i^a &= F_{0i}^a \,, \\ B_i^a &= \frac{1}{2}\epsilon_{ijk} F_{jk}^a \,, \end{aligned} \tag{2.9}$$

with the totally anti-symmetric tensor ϵ_{ijk}, are no observables as they are not gauge invariant.

2.2. Quantization of Non-Abelian Gauge Theories

The gauge transformation (2.8) yields an infinite number of equivalent gauge configurations. This means we cannot simply derive Feynman Rules from the generating functional of Yang-Mills theory,

$$Z[J] = \int DA \exp\left(S_{YM}[A] + \int_x J^a_\mu A^a_\mu\right) . \tag{2.10}$$

The necessity to remove this ambiguity by fixing the gauge via the condition $\mathcal{F}[A_{gf}] = 0$, arises. This does however not account for Gribov copies, as it is only a locally unique condition, [96, 97]. We proceed by considering general covariant gauges, $\partial_\mu A_\mu = 0$.

Generally the gauge-fixing condition allows for a split of the path integral measure,

$$DA = \mathcal{J} DA_{gf} DU \,, \tag{2.11}$$

with the Jacobi determinant $\mathcal{J}$ of the transformation U. Following the Faddeev-Popov method [98], one can insert the following identity into the path integral,

$$1 = \Delta_\mathcal{F}[A] \int DU \delta\left(\mathcal{F}[A^U]\right) , \tag{2.12}$$

where $\Delta_\mathcal{F}[A]$ is gauge invariant.

This can be illustrated by considering a general observable O, which is by definition gauge invariant,

$$\begin{aligned}\langle O\rangle = \frac{\int DAO[A]e^{S_{YM}[A]}}{\int dAe^{-S_{YM}[A]}} &= \frac{\int DADU\delta\left(\mathcal{F}[A^U]\right)\Delta_\mathcal{F}[A]O[A]e^{-S_{YM}[A]}}{\int DADU\delta\left(\mathcal{F}[A^U]\right)\Delta_\mathcal{F}[A]e^{-S_{YM}[A]}} \\ &= \frac{\int D\bar{A}\delta\left(\mathcal{F}[\bar{A}]\right)\Delta_\mathcal{F}[\bar{A}]O[\bar{A}]e^{-S_{YM}[\bar{A}]}}{\int D\bar{A}\delta\left(\mathcal{F}[\bar{A}]\right)\Delta_\mathcal{F}[\bar{A}]e^{-S_{YM}[\bar{A}]}} ,\end{aligned} \tag{2.13}$$

with $A = \bar{A}^{U^\dagger}$, $D\bar{A}^{U^\dagger} = D\bar{A}$ and $\Delta_\mathcal{F}[\bar{A}^{U^\dagger}] = \Delta_\mathcal{F}[A]$. We can then compute the Jacobian determinant via,

$$\delta\left(\mathcal{F}[A^U]\right) = \frac{\delta(\Theta - \Theta_0)}{\left|\det\frac{\delta\mathcal{F}}{\delta\Theta}\right|} , \tag{2.14}$$

and the transformation $U = e^{i\Theta}$ and the gauge fixing,

$$\mathcal{F}[A_{gf} = A^{U(\Theta_0)}] = 0 . \tag{2.15}$$

The Faddeev-Popov determinant is then,

$$\Delta_\mathcal{F}[A] = \left|\det \mathcal{M}_\mathcal{F}[A_{gf}]\right| \quad \text{with} \quad \mathcal{M}_\mathcal{F}[A] = \left.\frac{\delta\mathcal{F}}{\delta\Theta}\right|_{\Theta=0} = \left.\frac{\delta\mathcal{F}}{\delta A}\frac{\delta A}{\delta\Theta}\right|_{\Theta=0} , \tag{2.16}$$

with indices dropped for simplicity. In a general covariant gauge, $\mathcal{F}[A] = \partial_\mu A_\mu$, this determinant can be represented by a Gaussian integral containing the anti-commuting Grassmann-valued fields c and $\bar{c}$,

$$\det \mathcal{M}_\mathcal{F}[A_{gf}] = \int Dc D\bar{c} \exp\left(\int_{x,y} d^4x \bar{c}(x)^a \left(-\partial_\mu D_\mu\right)^{ab}(x,y) c^b(y)\right) , \tag{2.17}$$

with $D_\mu^{ab} = \partial_\mu \delta^{ab} - g f^{abc} A_\mu^c$.

By using an average of gauges, one modifies (2.13) by,

$$\delta\left(\mathcal{F}[A^U]\right) \to \int DC\delta\left(\mathcal{F}[A^U - C]\right) \exp\left(\frac{1}{2\xi}\int_x C^a C^a\right), \tag{2.18}$$

with the gauge fixing parameter ξ. In summary, the gauge fixed Yang-Mills action is given as,

$$S_A[A,c,\bar{c}] = \frac{1}{4}\int_x F^a_{\mu\nu}F^a_{\mu\nu} + \frac{1}{2\xi}\int_x \left(\partial_\mu A^a_\mu\right)^2 - \int_x \bar{c}^a(\partial_\mu D_\mu)^{ab}c^b\,. \tag{2.19}$$

The final form of the generating functional then is,

$$Z[J_A, J_c, J_{\bar{c}}] = \int DADcD\bar{c}e^{-S_A[A,c,\bar{c}]+\int_x (J_A\cdot A + J_{\bar{c}}\cdot c - \bar{c}\cdot J_c)}\,. \tag{2.20}$$

A derivation of the effective action from the generating functional used in functional methods can be found in Chapter 3.

This gauge fixing procedure renders an action that is not gauge invariant anymore. The underlying gauge symmetry however manifests itself in a new symmetry of S_A, the BRST symmetry. Further details can be found in Section 2.3, 3.1.3 and A.1.3.

In the present work we only work in Landau gauge, meaning $\xi = 0$ and,

$$\partial_\mu A_\mu = 0\,. \tag{2.21}$$

For advantages of this gauge and its implications in this work, see Section 5.1.4.

2.3. QCD

The fully quantized and gauge-fixed QCD action is given as,

$$S_{QCD}[q,\bar{q},A,c,\bar{c}] = \frac{1}{4}\int_x F^a_{\mu\nu}F^a_{\mu\nu} + \frac{1}{2\xi}\int_x \left(\partial_\mu A^a_\mu\right)^2 - \int_x \bar{c}^a(\partial_\mu D_\mu)^{ab}c^b + \int_x \bar{q}(\not{D} + m_q)q\,. \tag{2.22}$$

For massless quarks $m_q = 0$ the action (2.22) exhibits an $U(N_f)_L \times U(N_f)_R$ flavor symmetry, where N_f is the number of quarks and the indices R/L indicate a projection with the right-/left-handed chiral projection operator $P_{R/L} = \frac{1\pm\gamma_5}{2}$, and $\gamma_5 = \gamma_1\gamma_2\gamma_3\gamma_4$.

Generally, there are six flavors of quarks, divided into three generations containing two quarks each. The up and the down quark from the first generation have a mass considerably smaller than the scale of the theory, Λ_{QCD}, whereas all other quark masses are significantly larger. Therefore only taking into account the first two quarks and considering them approximately massless, i.e. a 2-flavor approximation still captures the relevant features of the theory and exhibits an approximate flavor symmetry, $SU(2)$. This generalizes to $SU(N_f)$ with $N_f = 3$, if we also consider the strange quark as light.

For further discussions, it is useful to rewrite the chiral symmetry of the action (with massless quarks) as,

$$U(N_f)_L \times U(N_f)_R \to U(1)_V \times SU(N_f)_V \times U(1)_A \times SU(N_f)_A\,, \tag{2.23}$$

with the vector $V = L + R$ and axial vector $A = L - R$ transformations. Additionally the action is symmetric under $SU(N_c)$ gauge transformations.

While the $U(1)_V$ is a symmetry of the full action and implies baryon number conservation, the $SU(N_f)_V$ symmetry is broken by the quark mass terms. The axial symmetries $U(1)_A$ and $SU(N_f)_A$ are also broken, the first one is broken explicitly by the axial anomaly, [99–102], which manifests itself as the observed large mass difference in the η and η' meson [103]. The $SU(N_f)_A$ symmetry is spontaneously broken [104]. For a more detailed discussion of the symmetries, see e.g. [95].

The quark pair condensate serves as an order parameter for this spontaneous symmetry breaking,

$$\langle\bar{q}q\rangle = \langle\bar{q}_L q_R + \bar{q}_R q_L\rangle \neq 0\,, \tag{2.24}$$

with group indices dropped for simplicity and $q_{R/L} = P_{R/L}q$. The expectation value indicates a mixing of left- and right-handed quarks in the vacuum, allowing them to acquire an effective mass [92]. A study thereof at finite temperature and finite chemical potential is presented in Chapter 7.

Furthermore, the spontaneous breaking of the symmetry with massless quarks gives rise to three massless Goldstone bosons [105–107]. Due to the non-vanishing quark masses in QCD, the symmetry is also explicitly broken and thus all pseudo-Goldstone bosons are massive and are identified with three relatively light pseudo-scalar pions in QCD, [104, 108].

Interestingly, there is an intricate interplay of chiral symmetry breaking and confinement in the low energy region of QCD (for $N_f \geq 3$): on one hand, chiral symmetry breaking being fueled by a growing coupling and confinement being characterized by an emergent

mass gap in the gluon, hindering and finally stopping this growth of the coupling and on the other hand, massless quarks leading to a massless gluon dispersion and thus no confinement [109].

We will now proceed and introduce another symmetry of the QCD action (2.22): BRST symmetry [110, 111] which encodes the underlying gauge-invariance of the gauge-fixed theory. To this end, we rewrite the gauge-fixing term in the action,

$$S_{gf}[A] = \frac{1}{2\xi}\int_x \left(\partial_\mu A^a_\mu\right)^2 \to S_{gf}[A,B] = \int_x \left(B^a\partial_\mu A^a_\mu - \frac{\xi}{2}B^aB^a\right) . \tag{2.25}$$

The infinitesimal BRST transformations of the fields in QCD are given as,

$$\begin{aligned}
\mathfrak{s}q &= igc^aT^aq \\
\mathfrak{s}\bar{q} &= -ig\bar{q}c^aT^a \\
\mathfrak{s}A^a_\mu &= D^{ab}_\mu c^b \\
\mathfrak{s}c^a &= \frac{1}{2}gf^{abc}c^bc^c \\
\mathfrak{s}\bar{c}^a &= B^a \\
\mathfrak{s}B^a &= 0\,.
\end{aligned} \tag{2.26}$$

with the BRST transformation of a general field $\phi_i = \left(q,\, \bar{q},\, A^a_\mu,\, \bar{c}^a,\, c^a,\, B^a\right)$,

$$\delta_{\mathrm{BRST}}\phi_i = \mathfrak{s}\Phi_i\delta\lambda\,, \tag{2.27}$$

and the Grassmann valued transformation parameter $\delta\lambda$ and where we have introduced the auxiliary Nakanishi-Lautrup field B^a. We then have $\mathfrak{s}^2\phi_i = 0$ and we can integrate out the auxiliary field. These transformations are coupled to the respective BRST sources $Q_i = \left(Q_q,\, Q_{\bar{q}},\, Q^a_{A,\mu},\, Q^a_c,\, Q^a_{\bar{c}}\right)$. This yields additional terms in the action (2.22),

$$\begin{aligned}
S_{BRST}[q,\bar{q},A,c,\bar{c}] = &-\int_x igQ_qc^aT^aq + \int_x igQ_{\bar{q}}\bar{q}c^aT^a \\
&-\int_x Q^a_{A,\mu}\left(\partial_\mu c^a + gf^{abc}A^b_\mu c^c\right) \\
&-\frac{1}{2}\int_x gf^{abc}Q^a_cc^bc^c + \frac{1}{\xi}\int_x Q^a_{\bar{c}}\partial_\mu A^a_\mu\,.
\end{aligned} \tag{2.28}$$

Using the STI (3.17), one can derive equations that relate longitudinal to transverse correlation functions in the theory. Assuming regularity of longitudinal and transverse couplings for perturbative momenta the STI constrains the transverse couplings and demands equality of coupling constants in this regime,

$$\alpha_i(p) = \alpha_s(p) = \frac{g^2}{4\pi Z_A(p)Z^2_c(p)} \quad \text{with} \quad i = \{A\bar{q}q,\, A\bar{c}c,\, A^3,\, A^4\}\,, \tag{2.29}$$

where $Z_A(p)$ and $Z_c(p)$ are the non-trivial momentum dependent gluon and ghost propagator dressings.

We can compute the beta function of the strong running coupling as a series of perturbative coefficients. One then obtains at one-loop order[12],

$$\beta(\alpha_s) = \frac{p^2}{4\pi}\frac{d\alpha_s}{dp^2} = \frac{\alpha_s^2}{16\pi^2}\underbrace{\left(-\frac{11}{3}N_c + \frac{2}{3}N_f\right)}_{\beta_1} + \mathcal{O}(\alpha_s^3)\,, \tag{2.30}$$

where $\alpha_s = \alpha_s(\bar{p})$ is the coupling constant at the renormalisation scale $\bar{p}$, N is the number of colors in the $SU(N)$ gauge theory and N_f is the fermion number.

From the integration of the first order in (2.30) one obtains the one-loop running coupling,

$$\alpha_s(p) = \frac{\alpha_s(\bar{p})}{1 - \frac{\beta_1}{4\pi}\alpha_s(\bar{p})\ln\frac{p^2}{\bar{p}^2}}\,. \tag{2.31}$$

For $p \to \infty$ the strong coupling approaches the Gaussian fixed point, $\alpha_s(p) \to 0$. The theory becomes asymptotically free and one can investigate QCD within a perturbative expansion.

For low energies however, the coupling grows and perturbation theory is not applicable anymore. This renders the necessity for non-perturbative methods such as functional methods that are presented in Chapter 3 to investigate the infrared regime of QCD.

3. Functional Methods

This chapter is in parts based on [1].
Functional approaches are a well-established tool to study non-perturbative aspects of quantum field theories. They have been successfully used for a wide class of non-perturbative physics problems, ranging from strongly correlated condensed matter and statistical physics systems over nuclear physics, QCD, and high energy physics to beyond the Standard Model physics, cosmology, and quantum gravity. Applications also include real-time aspects in and out of equilibrium. For reviews on various physics applications of functional methods see e.g. [14, 59, 64, 71, 72, 112–136].

In these approaches, one solves a set of functional integro-differential loop relations between correlation functions of the theory at hand. These relations are typically closed at one or two-loop order in full correlation functions. If aiming for quantitative precision this requires setting up and solving a large set of loop equations involving the full tensor structure and momentum dependencies of the correlation function involved. This requires the use of elaborate computer-algebraic tools as well as well-structured numerics.

In this chapter, we introduce the master equation for fRG, DSE, and mSTI as well as our condensed notation. We give an example of an expansion scheme for the effective action and discuss the infrared cutoff and its properties.

3.1. Quantum Master Equations

In this section, we discuss the quantum master equation for the fRG, mSTI, and DSE. Full derivations can be found in Section A.1. We use a superfield notation throughout the paper, introduced below.

For a general quantum field theory, the Euclidean action $S[\phi]$ reads

$$S[\phi] = \sum_{n=2} S^{a_1 \dots a_n} \phi_{a_1} \dots \phi_{a_n} \,. \tag{3.1}$$

In (3.1) we have introduced deWitt's condensed notation, for the form used here see [115]. The a_i comprise internal and Lorentz indices, as well as species of fields and a sum/integration over space-time or momenta. Lowering and rising indices is done with the metric γ^{ab}, which is diagonal in bosonic subspaces and symplectic in fermionic ones. For a single fermion anti-fermion pair $(f, \bar{f})$ the metric is given by,

$$(\gamma^{ab}) = \begin{pmatrix} 0 & -1 \\ 1 & 0 \end{pmatrix} . \tag{3.2}$$

For the complete metric, we have the normalisation

$$\begin{aligned} \gamma_b{}^a &= \gamma^{ac}\gamma_{bc} = \delta_b^a \,, \\ \gamma^a{}_b &= \gamma^{ac}\gamma_{cb} = (-1)^{ab}\delta_b^a \,, \end{aligned} \tag{3.3}$$

with

$$(-1)^{ab} = \begin{cases} -1 & a \text{ and } b \text{ fermionic}, \\ 1 & \text{otherwise}. \end{cases} \tag{3.4}$$

Then, lowering and rising indices follows as,

$$\begin{aligned} \phi_a &= \phi^b \gamma_{ba} \,, \\ \phi^a &= \gamma^{ab} \phi_b \,. \end{aligned} \tag{3.5}$$

The condensed notation introduced above allows us to write the Master equations in a concise form. Moreover, the metric introduced here is also used in the program.

The Schwinger functional $W[J]$, the generating functional of connected correlation functions with the classical action (3.1), follows as,

$$e^{W[J]} = \int D\phi \exp\left(-S[\phi] + J^a \phi_a\right) = Z[J] \,. \tag{3.6}$$

In order to make the condensed notation more explicit, we write the source term as a sum over internal and Lorentz indices, and species of fields, α, and a space-time integral,

$$J^a \phi_a = \sum_\alpha \int d^d x \, J^\alpha(x) \phi_\alpha(x) \,. \tag{3.7}$$

While the derivation of master equations is best done with the Schwinger functional and they also take the simplest form if formulated in $W[J]$, for a discussion see e.g. [115], most applications are done for the effective action $\Gamma[\Phi]$, the generating functional of one-particle irreducible (1PI) correlation functions. The argument of Γ is the expectation value Φ of the field ϕ,

$$\frac{\delta W[J]}{\delta J^a} = W_a = \langle \phi_a \rangle_J = \Phi_a \,. \tag{3.8}$$

Then, the effective action $\Gamma[\Phi]$ is obtained as the Legendre transform of the Schwinger functional with respect to the source J,

$$\Gamma[\Phi] = \sup_J \Big(J^a \Phi_a - W[J] \Big) \,. \tag{3.9}$$

Equation (3.9) entails that the sources are related to the derivatives of $\Gamma[\Phi]$ w.r.t. the fields,

$$\frac{\delta \Gamma[\Phi]}{\delta \Phi_a} = \Gamma^a = \gamma^a{}_b J^b \,, \tag{3.10}$$

where we have used

$$J^a \Phi_a = \Phi^a J_a = J_a \Phi^b \gamma^a{}_b = \Phi_b J^a \gamma^a{}_b \,. \tag{3.11}$$

Finally, we are interested in master equations for correlation functions, provided by source- and field-derivatives of the Schwinger functional and the effective action respectively. We will use the notation,

$$\begin{aligned}\frac{\delta}{\delta\Phi_{a_1}}\dots\frac{\delta}{\delta\Phi_{a_n}}\Gamma[\Phi] &= \Gamma^{a_1\dots a_n}\,,\\ \frac{\delta}{\delta J^{a_1}}\dots\frac{\delta}{\delta J^{a_n}}W[J] &= W_{a_1\dots a_n}\,.\end{aligned} \tag{3.12}$$

The definition of the effective action entails, that the two-point function Γ^{ab} is the inverse of the propagator $G_{ab} = W_{ab}$,

$$G_{ab} = \langle\phi_a\phi_b\rangle - \langle\phi_a\rangle\langle\phi_b\rangle\,. \tag{3.13}$$

In our condensed notation this reads,

$$G_{ac}\Gamma^{cb} = \gamma^b{}_a\,. \tag{3.14}$$

With this setup, we now derive quantum master equations in terms of the effective action, the flow equation for the effective action in the functional renormalisation group, the quantum equation of motion (Dyson-Schwinger equations), as well as the modified Slavnov-Taylor identities.

3.1.1. Quantum Equations of Motion (DSE)

Dyson-Schwinger equations (DSEs) [137, 138] are the quantum equations of motion. They yield a complete description of the theory via 1PI correlation functions. In terms of the effective action they are given by,

$$\frac{\delta\Gamma[\Phi]}{\delta\Phi_a} = \frac{\delta S[\phi]}{\delta\phi_a}\bigg|_{\phi_b=\Phi_b+G_{bc}\frac{\delta}{\delta\Phi_c}}\,. \tag{3.15}$$

The full derivation of the DSE from the generating functional (3.6) can be found in Section A.1.1. The r.h.s. of (3.15) comprises a classical part as well as loops. It is evident from a theory with an nth-order interaction of the fields leads to up to $n-2$-loops in full propagators, full vertices as well as one classical vertex. This entails, that the DSE is a closed (exact) $n-2$-loop functional master equation. As such it allows for perturbative as well as non-perturbative approximations. For reviews see e.g. [14, 59, 71, 72, 130–136].

3.1.2. Flow Equation for the Effective Action (fRG)

The flow equation for the effective action within the *Functional Renormalisation Group* approach [41, 139–142] can be viewed as a differential DSE. Typically, one introduces an (infrared) momentum regularisation, that suppresses quantum fluctuations below the infrared cutoff scale k. This is done by changing the classical dispersion by $1/2\phi_a R^{ab}\phi_b$, where R^{ab} is a momentum-dependent cutoff functions, that acts as a mass for low momenta and decays sufficiently fast for large momenta. More details and the derivation of the fRG equation, see Section A.1.2. This approach allows us to integrate-out quantum fluctuations

successively within momentum shells, finally arriving at the full effective action at $k = 0$. With $\partial_t = k\partial_k$, the fRG flow equation is concisely given by,

$$\partial_t \Gamma = \frac{1}{2} \dot{R}^{ab} G_{ab} \,. \tag{3.16}$$

Equation (3.16) is a one-loop exact master equation. The propagator G_{ab} is infrared regularised via the cutoff mass. In turn, the equation is ultraviolet finite as $\dot{R}^{ab}$ decays for large momenta. In contradistinction to the DSE in (3.15), that is $n-2$-loop exact for an nth order interaction, the fRG-master equation is a closed (exact) one-loop equation for general theories. As for the DSEs, a complete set of fRG-equations solves the theory exactly. For reviews see e.g. [64, 112–129].

3.1.3. STI & mSTI

Within a gauge-fixed formulation of gauge theories the underlying gauge-invariance is carried by the BRST-symmetry (Becchi, Rouet, Stora, Tyutin). In their infinitesimal form, this symmetry is described by the *Slavnov-Taylor identities* (STI) [110, 111]. They ensure the gauge invariance of observables, and can be formulated in terms of a master equation for the effective action including BRST-sources, [143, 144],

$$\frac{\delta \Gamma}{\delta Q^a} \frac{\delta \Gamma}{\delta \Phi_a} = 0 \,. \tag{3.17}$$

For deriving (3.17) one adds source terms $Q^a \mathfrak{s}\phi_a$ for BRST transformations to the path integral, for more details see Section A.1.3. The BRST transformation in Yang-Mills theory transforms a gauge boson into a ghost. The explicit transformation can be found in (4.8). Q^a is a source term for the BRST transformation of the fields $\mathfrak{s}\phi_a$, see (A.25). For reviews see e.g. [14, 71, 72, 115, 130–133, 135, 136].

However, the introduction of a cutoff term in the effective action breaks BRST symmetry for non-vanishing k. This leads to a modification of the symmetry identities (mSTI) that appears as a 1-loop correction,

$$\frac{\delta \Gamma}{\delta Q^a} \frac{\delta \Gamma}{\delta \Phi_a} = R^{ab} G_{bc} \Gamma^c{}_{Q^a} \,. \tag{3.18}$$

for more details see Section A.1.4. In the above equation one can already see that for $k \to 0$ the mSTI reduces to the STI. Thus, satisfying the mSTI at all scales k, guarantees gauge invariance of observables at $k = 0$. For details beyond that provided in Section A.1.3 we refer to the reviews [64, 115, 117, 119, 120, 127–129] and references therein.

3.2. Vertex Expansion and Truncation

The effective action $\Gamma[\Phi]$ consists of all possible combinations of fields and their derivatives. Naturally, one wants to find a systematic expansion scheme for the effective action which allows for quantitative error control. One such scheme that is used throughout this work is the vertex expansion,

$$\Gamma[\Phi] = \sum_{n=1}^{\infty} \int \Gamma_{\Phi_1 \dots \Phi_n} \Phi_1 \dots \Phi_n \,, \tag{3.19}$$

where one expands the effective (average) action in terms of n-point correlation functions. For simplicity, momentum arguments in (3.19) were dropped.

Inserting (3.19) into the previously presented quantum master equations and taking functional derivatives, i.e. projecting onto the moments of the effective action, one can see that the functional equations yield an infinite tower of coupled equations and that the functional equation of an n-point function depends on vertices of order up to $n+2$.

The necessity to truncate the expansion (3.19) at some finite order $n_{\max}$ arises, thereby closing the finite number of remaining equation. This procedure introduces errors in the otherwise exact functional relations. By systematically improving the truncation, one aims at establishing convergence of the correlation functions.

Generally, one can expand an n-point correlation function in its tensor basis with appropriate scalar vertex dressings, $\lambda^{(i)}_{\Phi_1 \dots \Phi_n}(p_1, \dots, p_{n-1})$,

$$\Gamma_{\Phi_1 \dots \Phi_n}(p_1, \dots, p_{n-1}) = \sum_{i=1} \lambda^{(i)}_{\Phi_1 \dots \Phi_n}(p_1, \dots, p_{n-1}) \tau^{(i)}_{\Phi_1 \dots \Phi_n}(p_1, \dots, p_{n-1}) \,. \tag{3.20}$$

The choice of tensor basis is not unique. A minimal truncation in terms of tensor structures and vertices that are taken into account is including only the classical ones and dismiss subleading tensor structures and higher order vertices.

From the structure of the functional equations, one can already see that correlation functions of order $n+2 \geq 5$ only indirectly contribute to the functional equations of the propagators of the theory as they only enter as one-loop corrections into the functional equations of vertices of order n. Phenomenologically, higher order n-point functions are, loosely speaking, proportional to the n particle phase space and thus suppressed. Large densities and resonances in the interaction however can counteract this phase-space suppression. Within these restrictions truncating the effective action at some $n_{\max}$ is a commonly used approximation.

Another viable option is to use symmetry identities of the respective gauge theory to identify the dressing functions of the $(n+1)$- and $(n+2)$-point functions with those of lower order correlation functions instead of dropping them in the functional equations of the n-point correlator.

From (3.20) one can see that including the full momentum dependencies of the scalar dressing functions increases the computational effort tremendously. Reducing the full momentum structure to only one average momentum argument in the dressing functions is a commonly applied truncation.

The different truncations that were used throughout this work are described in more detail in the respective chapters and a quantitative investigation of different functional methods within a truncation can be found in Chapter 5.

3.3. Regulators

The fRG and mSTI master equations, (3.16) and (3.18), depend on a regulator insertion R^{ab} that acts as an infrared momentum regularisation which is chosen such that it fulfills the following properties:

(A) The suppression of infrared modes via,

$$\lim_{p^2/k^2\to 0} R^{ab}(p) > 0\,.$$

(B) The effective action goes to the physical limit for $k \to 0$,

$$\lim_{k\to 0} R^{ab}(p) = 0\,.$$

(C) The action has the classical UV limit,

$$\lim_{k\to\infty} R^{ab}(p) = \infty\,.$$

At vanishing cutoff the effective action $\Gamma[\Phi]$ should be independent of the choice of cutoff,

$$\frac{\delta\Gamma[\Phi]}{\delta R^{ab}(p)} = 0\,. \tag{3.21}$$

This is directly linked to the RG consistency condition and the renormalisation, for further details, see e.g. [145].

Within these restrictions, there is still a plethora of possible regulator functions. However, the effective action at $k = 0$ must be independent of the choice of regulator. For convenience one usually parametrises,

$$R^{ab}(p) = \Gamma^{ba}(p)\Big|_{m=0} r(y) \quad \text{with} \quad y = \frac{p^2}{k^2}\,, \tag{3.22}$$

where $r(p^2/k^2)$ is the regulator shape function. Standard choices of shape functions are

- the Litim-regulator shape function, [146, 147],

$$r(y) = \left(\frac{1}{y} - 1\right)\Theta(1 - \frac{1}{y})$$

- an exponential shape function with parameters a and b,

$$r(y) = \frac{a e^{y^{-b}}}{1 - e^{y^{-b}}}$$

The different shape functions and their derivatives are shown in Figure 3.1.

The regulator and shape functions that were used for numerical computations throughout this work are parametrised in Section B.2.2.

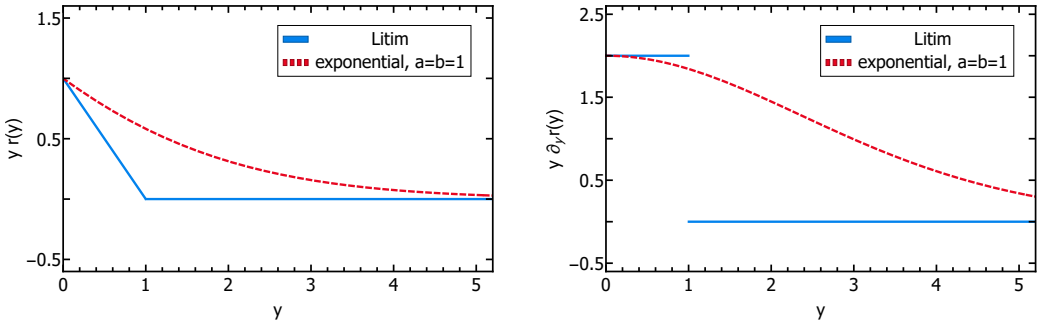

Figure 3.1.: Regulator, $yr(y)$ (left) and regulator derviative $y\partial_y r(y)$ (right), for different shape functions over y. The blue line corresponds to the Litim shape function and the red dashed line to the exponential regulator shape function with $a = b = 1$.

As briefly mentioned in Section 3.1.3, the introduction of a cutoff term breaks BRST symmetry explicitly. This leads to a modification of the Slavnov-Taylor identities at non-vanishing cutoff which manifests as a modification of the action at the cutoff,

$$\lim_{k\to\Lambda} \Gamma_k = S_\Lambda \neq S\,, \tag{3.23}$$

with arguments dropped for simplicity. To obtain gauge invariant observably one must therefore somehow restore BRST symmetry at $k = 0$. One approach is via gauge invariant flows, see e.g. [32, 148–162], these are however still in an early stage of development.

A more hands-on approach yielding an effective action at $k = 0$ that fulfills the STI, is by determining the modification of the action at the cutoff S_Λ. Technically this can either be done by additionally solving the mSTI at every RG-step and by fulfilling the mSTI at k inevitably fulfilling the STI at $k = 0$, or by choosing an ansatz for S_Λ with parameters that need to be finetuned such, that the STI is fulfilled at $k = 0$.

A comparison between both methods as well as a discussion of their limitations is presented in Chapter 5.

4. Deriving Symbolic Functional Equations

This chapter is based on [1].
To date, there are still only a few computer-algebraic tools for functional methods [163–174]. In this work, we present a package of *QMeS* (*Quantum Master equations: environment for numerical Solutions*), that can be used for the symbolic derivation of functional equations arising from a master equation. Relevant examples are Functional Renormalisation Group (fRG) Equations, Dyson-Schwinger Equation (DSE) or Slavnov-Taylor Identities (STI) and their modification in the presence of a cutoff, the modified STIs (mSTI). In most cases, the cutoff is an infrared cutoff, and hence the mSTI includes the STI as a special case for a vanishing cutoff.

The package is written in *Mathematica* and can be used to derive a functional equation such as fRGEs, DSEs, mSTIs from a given field content and, for the DSE, a given classical action. Then, symbolic equations for different n-point functions, i.e. the moments of the master equations, can be derived. Naturally, it works in a general field space, allowing for arbitrary theories and can include momentum routing for the diagrammatic/symbolic results. Its coherent implementation of conventions and handling of fermionic minus signs for diagrams allows for a simple and intuitive use. Due to its modular structure, it facilitates future extensions to other master equations and more complicated objects and truncations.

The main objects of functional approaches, i.e. quantum master equations as well as our condensed notation was introduced in Chapter 3. We proceed by describing the details of the package in Section 4.1, i.e. how the modules are connected via the interface, as well as the installation process. Then we give an overview of the input and output in *QMeS-Derivation*. Section 4.3 contains two examples: Yang-Mills and Yukawa theory ($N_f = 1$ and $N_f = 2$). For these example theories, we describe, how to derive different symbolic functional equations from an action. In Section 4.4 we summarise the main features of *QMeS-Derivation*.

4.1. Description

This section outlines the basic design and features of *QMeS*, i.e. its modules and how they are connected via the interface. Furthermore, we give instructions on how to install the package.

4.1.1. Modules and Interface

The code consists of four main modules - *getDSE.m*, *FunctionalDerivatives.m*, *SuperindexDiagrams.m* and *FullDiagrams.m* - which are connected by the interface *DeriveFunctionalEquation.m*.

The four modules correspond to the four output options described in Section 4.2.4. The workflow is depicted in Figure 4.1.

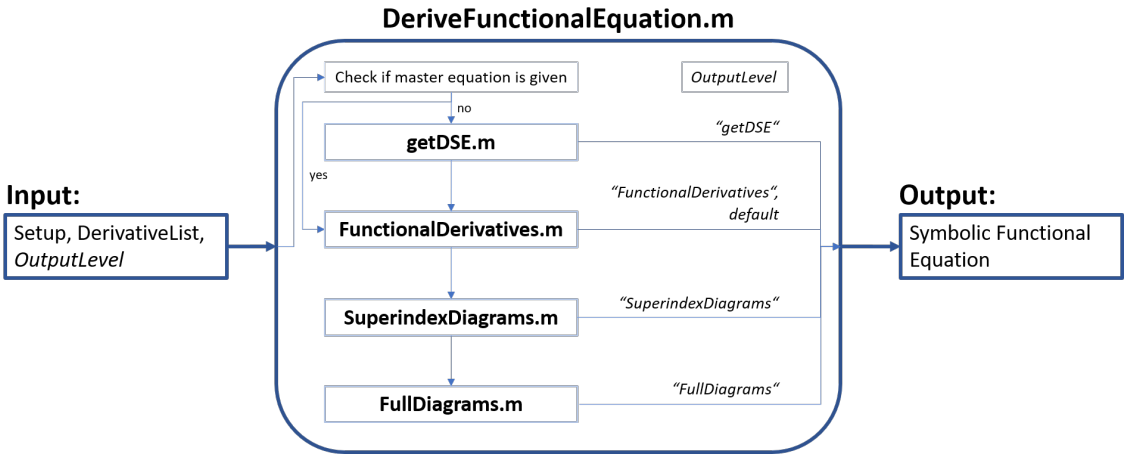

Figure 4.1.: Depiction of the workflow of *QMeS-Derivation* with its interface and modules.

The user is required to provide a setup that consists of either a master equation or an association indicating that *QMeS* first needs to derive the DSE for a given classical action.

Furthermore, the setup needs to contain a definition of the field space and a truncation, as well as a list of field derivatives. Specifying the preferred form of the output (i.e. `"OutputLevel"`) is optional.

Depending on whether or not a master equation was provided the interface calls the *FunctionalDerivatives.m* or first the *getDSE.m* module which then generates the Dyson-Schwinger equation of the theory, and passes it on to the *FunctionalDerivatives.m* module along with the setup and derivative list. Within this module, the (remaining) field derivatives of the master equation are performed and fields are set to zero.

In the interface, the output and user-provided input are again passed on to the *SuperindexDiagrams.m* module, where the trace in field space is performed, the field content of objects, like propagators, n-point functions, and regulator insertions, are sorted, prefactors are computed and the truncation is applied.

The result together with the initial input is then used by the *FullDiagrams.m* module to replace the superfield indices with physical indices and the objects are replaced by functions of indices.

If the user has specified an output option, the workflow is terminated after the corresponding module providing the user with the chosen output. The default output option is `"FunctionalDerivatives"`.

4.1.2. Requirements and Installation

Functionality of *QMeS-Derivation* is supported in *Mathematica* 12.0 or higher, although it may also work with older versions.

To install the package download the installer via:

```
Import["https://raw.githubusercontent.com/
QMeS-toolbox/QMeS-Derivation/main/QMeSInstaller.m"];
```

Other options are to either save a copy of the repository in the `"../Mathematica/Applications"` folder or append the path (`yourpath`) where the copy is saved to the list of paths where *Mathematica* searches for packages via:

```
AppendTo[$Path, "yourpath"];
```

Then the package can be loaded in Windows by calling the following or an equivalent path for Linux and MacOS:

```
<<"QMeS-Derivation\\DeriveFunctionalEquation.m"
```

4.2. Input, Functions and Options

To compute functional derivatives of a master equation one needs to define said equation as well as the theory one is working in. Both must be collected in an association.

```
Setup = <|"MasterEquation" -> masterEquation,
"FieldSpace" -> fields,
"Truncation" -> truncation|>;
```

If one first wants to derive a DSE of a given theory, the setup must be provided as,

```
SetupDSE = <|
"MasterEquation" -> <|"getDSE" -> "True",
"classicalAction" -> classicalAction|>,
"FieldSpace" -> fields,
"Truncation" -> truncation|>;
```

Note that one then needs a definition of the classical action via possible vertices.

4.2.1. Master Equations and Objects

Within the QMeS framework, a master equation is defined as a list of objects, the first being an overall prefactor. Each object is of a specific `"type"` (e.g. propagator, n-point function, regulator or regulator derivative). Furthermore, every object contains a list of `"indices"` that are superfield indices. For the fRG equation and the mSTI, the indices should be closed. We recall the fRG equation (3.16) as an example of a master equation,

$$\partial_t \Gamma = \frac{1}{2} \dot{R}^{ab} G_{ab} \,,$$

```
fRGEq = {"Prefactor" -> {1/2},
<|"type" -> "Regulatordot", "indices" -> {a, b}|>,
<|"type" -> "Propagator", "indices" -> {a, b}|>};
```

as well as the modified Slavnov-Taylor identity (mSTI) introduced in (3.18),

$$\frac{\delta \Gamma}{\delta Q^a} \frac{\delta \Gamma}{\delta \Phi_a} = R^{ab} G_{bc} \Gamma^c{}_{Q^a} \,.$$

The mSTI can be written as:

```
LHSmSTIEq = {"Prefactor" -> {1},
<|"type" -> "nPoint", "indices" -> {Q[a]}, "nPoint" -> 1, "spec" -> "BRST"|>,
<|"type" -> "nPoint", "indices" -> {a}, "nPoint" -> 1, "spec" -> "none"|>};

mSTIEq = {"Prefactor" -> {1},
<|"type" -> "Regulator", "indices" -> {a, b}|>,
<|"type" -> "Propagator", "indices" -> {b, c}|>,
<|"type" -> "nPoint", "indices" -> {c, Q[a]}, "nPoint" -> 2, "spec" -> "BRST"|>};
```

It is furthermore possible to derive the DSE of a given theory with the aforementioned setup. For further information see section Section 4.2.4. The superindices in the master equations should not coincide with the names of fields or any of their indices.

Prefactors

The first entry in every diagram is the `Prefactor`. It can contain numbers (1,−1,1/2,...) or a metric factor $(-1)^{ab}$. For example the prefactor

```
"Prefactor" -> {-1/2, {a,b}, {b,b}, {b,c}};
```

translates into

$$-\frac{1}{2}(-1)^{ab}(-1)^{bb}(-1)^{bc}\,, \tag{4.1}$$

where again the superfield index convention introduced in (3.4) is used.

Regulator and Regulator Derivative

```
<|"type" -> "Regulatordot", "indices" -> {a, b}|>;

<|"type" -> "Regulator", "indices" -> {a, b}|>;
```

A regulator R^{ab} or regulator derivative $\dot{R}^{ab}$ is an object with two superfield indices corresponding to the incoming and outgoing fields with their respective momenta and indices.

Propagator

```
<|"type" -> "Propagator", "indices" -> {a, b}|>;
```

A propagator G_{ab} is an object with two superfield indices corresponding to the fields and their indices. These are lower indices. Note that for fRG and mSTI equations the propagator is k-dependent whereas it is not for DSEs.

n-Point Functions

```
<|"type" -> "nPoint", "indices" -> {a, b, c, d},
"nPoint" -> 4, "spec" -> "none"|>;

<|"type" -> "nPoint", "indices" -> {a, b},
"nPoint" -> 2, "spec" -> "classical"|>;

<|"type" -> "nPoint", "indices" -> {a, b, Q[c]},
"nPoint" -> 3, "spec" -> "BRST"|>;
```

n-Point functions are field derivatives of the effective action. The value of `"nPoint"` indicates the number of derivatives, whereas the `"indices"` again represent the superfield indices. The specification `"spec"` implies whether the vertex is a BRST (`"BRST"`, $\Gamma^{ab}{}_{Q^c}$), a 1PI (`"none"`, Γ^{abcd}) or a classical (`"classical"`, S^{ab}) one. The superfield index of a BRST source needs to be written as `"Q[i]"` to indicate that this is a lower index belonging to the BRST source of a field `Q[field]` (for the notation, see Section 4.2.2.1). Again it is worth mentioning, that in case of fRG or mSTI equations the 1PI and BRST vertices are k-dependent objects.

Fields

```
<|"type" -> "Field", "indices" -> {a}|>;
```

Fields Φ_a are objects with one lower index. Note that after taking all functional derivatives, external fields, which are leftover, are set to zero.

4.2.2. Theory

The user is required to define a specific theory. This breaks down into two main parts: defining the fields with the respective indices and the truncation.

4.2.2.1. Fields with Indices

The fields of a theory are either fermionic or bosonic. Antifermion/fermion pairs must be combined in a list.

```
fields =
<|"bosonic" -> {A[p, {mu, a}], B[p]},

"fermionic" -> {{cbar[p, {a}], c[p, {a}]}, {af[p,{d}], f[p,{d}]}},

"BRSTsources" ->
{{Q[A], "fermionic"}, {Q[B], "fermionic"},
{Q[cbar], "bosonic"}, {Q[c], "bosonic"},
{Q[af], "bosonic"}, {Q[f], "bosonic"}}|>;
```

If a theory contains no fields of either bosonic or fermionic statistics, it is then required to assign an empty list.

When computing mSTIs one also needs to define the BRST charges of fields. They are indicated by `Q[field]` followed by the respective property of the charge (either `"fermionic"` or `"bosonic"`). For the computation of DSE or fRG equations, it is not necessary to define the BRST sources.

The respective indices are provided as arguments of the fields, where the momentum is always the first entry, followed by a list of further indices (e.g. group or Lorentz indices). Note that the names of the indices for different fields do not need to be unique. For better readability it is recommended to define the same kind of index with the same name: these names (e.g. `{mu, i}`) in combination with a unique number (e.g. `$8215`) will be used to create unique indices (e.g. `{mu$8215, i$8215}`) by *QMeS*.

4.2.2.2. Truncation and Classical Action

For the derivation of DSEs it is necessary to define the classical action via vertices. This is done by giving a list of combination of fields that appear as a classical vertex in the action,

```
classicalAction = {{A, A}, {c, cbar}, {A, A, A},
{A, A, A, A}, {A, c, cbar}};
```

Furthermore the truncation of the full theory is defined by specifying the truncation of 1PI and BRST vertices. It is worth mentioning that the user is also required to include the possible propagators in this list,

```
Truncation = {{A, A}, {c, cbar}, {A, A, A},
{A, A, A, A}, {A, c, cbar}, {A, A, c, cbar}};
```

The truncation may be similar or include more vertices than the classical action.

In both definitions the order of fields or vertices is irrelevant.

4.2.3. Derivative List

Lastly one needs to specify a list of field derivatives. Note that the last entry of the list will be the first derivative.

```
DerivativeList1 = {A, A};
DerivativeList2 = {A[a], A[b]};
DerivativeList3 = {A[-p, {mu, a}], A[p, {nu, b}]};
```

Generally one has three options: the first is to only provide the field names. This can be combined with the output options `"getDSE"` and `"FunctionalDerivatives"`. The second is to assign superindices to the fields, this input additionally works with `"SuperindexDiagrams"`. If one wants to obtain full diagrams with momentum routing (`"FullDiagrams"`), then one needs to assign indices and momenta to the fields.

4.2.4. Outputs

The main function takes two arguments: the setup and the list of field derivatives,

```
DeriveFunctionalEquation[Setup, DerivativeList];
```

The output is always a list of the diagrams that are produced. The specification of the diagrams can be altered with `options`.

Options are called via

```
DeriveFunctionalEquation[Setup, DerivativeList,
"OutputLevel" ->  options];
```

There are three options specifying the level of the output via `"OutputLevel"`:

getDSE

The first option is to simply derive the Dyson-Schwinger equation via `getDSE`. The user needs to specify the classical vertices as well as at least one field derivative $\frac{\delta}{\delta\phi}$. From this, the RHS of the DSE is computed according to the rules in Section A.2. This means the classical action (3.1) can be written as,

$$S[\phi] = S^{a_1 a_2}\phi_{a_1}\phi_{a_2} + S^{a_1 a_2 a_3}\phi_{a_1}\phi_{a_2}\phi_{a_3} + \cdots + S^{a_1 \ldots a_n}\phi_{a_1}\ldots\phi_{a_n}\,, \tag{4.2}$$

where only those orders appear that are given in the theory. All prefactors (and signs) should be contained in the definition of $S^{a_1\ldots a_m}$. Then the *getDSE* module computes

$$\left.\frac{\delta S}{\delta\phi_i}\right|_{\phi_i=\Phi_i+G_{ij}\frac{\delta}{\delta\Phi_j}}\,. \tag{4.3}$$

Terms that end with a field derivative are immediately dropped. One then gets the general diagrams that contribute to the DSE for a given classical action. If the field derivative list contains more than one entry, the last one is a field, whereas the others are processed as expectation values of fields.

```
DerivativeListDSE = {Phi[a], Phi[b], Phi[c], Phi[d]}
```

The list above thus produces

$$\Gamma^{abcd} = \frac{\delta^3}{\delta\Phi_a\Phi_b\Phi_c}\left(\frac{\delta S}{\delta\phi_d}\right)_{\phi_i=\Phi_i+G_{ij}\frac{\delta}{\delta\Phi_j}} . \tag{4.4}$$

FunctionalDerivatives

If the option is set to `"FunctionalDerivatives"` the user obtains a list of diagrams that are generated by taking functional derivatives of the quantum master equation. The trace over fields in the diagrams is however not taken. Therefore one gets symbolic diagrams with fields set to zero. When choosing this option with a given master equation, the user is not required to specify a truncation.

The default output level is equal to calling the `"FunctionalDerivatives"` option.

SuperindexDiagrams

The third option is called `"SuperindexDiagrams"`. If this is chosen, the trace over fields is taken, where only those diagrams remain that satisfy the truncation, and the fields in the objects are sorted canonically. This means that upper indices (eg. for regulators, regulator derivatives or vertices, including BRST-vertices) are sorted as (*bosonic*, *antifermionic*, *fermionic*) and lower fermionic indices in reverse order. If two indices have are of the same type, e.g. two bosonic fields, they are sorted alphabetically. Lastly, the prefactors are evaluated.

QMeS aims at generating outputs for general theories. For this reason, we refrain from symmetrization or identification procedures for diagrams.

FullDiagrams

For the last module one may call the main function with the option `"FullDiagrams"`, which means that in addition to the previous steps also the momentum routing is done for all 1-loop diagrams (i.e. fRG, mSTI, but not for all DSE diagrams). Superfield indices are replaced by physical indices and objects are transformed into functions of indices such that one can insert Feynman rules easily.

4.3. Examples

In this section, we give different examples of deriving symbolic functional equations with *QMeS*.

The first example is deriving functional equations (i.e. fRG, mSTI and DSE) within Yang-Mills theory which serves as a prerequisite for QCD. Studying QCD with functional methods is an ab initio approach to investigate the non-perturbative regime.

Then we derive fRG equations in $N_f = 1$ and $N_f = 2$ Yukawa theory. It illustrates and emphasizes how *QMeS* handles multiple fermions and sorts the vertices accordingly. Furthermore, a simple Yukawa model can already be used to describe nuclear forces between fermions which are mediated by pions thus approximating QCD with an effective field theory.

4.3.1. Yang-Mills Theory

In the following, we want to give the crucial steps one needs to take to compute functional equations in Yang-Mills theory (YM) with *QMeS*.

The theory we work in is SU(3) Yang-Mills theory, thus one has bosonic gauge fields $A^a_\mu(p)$, fermionic ghosts $c^a(p)$ and antighosts $\bar{c}^a(p)$. The classical Euclidean YM action including gauge fixing and ghost terms can be written as,

$$S = \int d^4x \left(\frac{1}{4} F^a_{\mu\nu} F^a_{\mu\nu} + \frac{1}{2\xi} \partial_\mu A^a_\mu \partial_\nu A^a_\nu + \partial_\mu \bar{c}^a \left(\partial_\mu c^a + g f^{abc} A^b_\mu c^c \right) \right) , \tag{4.5}$$

with $F^a_{\mu\nu} = \partial_\mu A^a_\nu - \partial_\nu A^a_\mu + g f^{abc} A^b_\mu A^c_\nu$. After Legendre transforming the classical action and introducing a regulator term one obtains the effective average action,

$$\begin{aligned} \Gamma =& \frac{1}{2}\Gamma^{AA} AA - \Gamma^{\bar{c}c}\bar{c}c - \Gamma^{A\bar{c}c} A\bar{c}c + \frac{1}{6}\Gamma^{AAA} AAA \\ &+ \frac{1}{24}\Gamma^{AAAA} AAAA - \frac{1}{2}\Gamma^{AA\bar{c}c} AA\bar{c}c + \frac{1}{4}\Gamma^{\bar{c}\bar{c}cc}\bar{c}\bar{c}cc \,, \end{aligned} \tag{4.6}$$

with indices suppressed. For a BRST-symmetric action one includes the source terms,

$$\Gamma_{BRST} = -\Gamma^{c}_{\ Q^A} cQ^A + \Gamma^{A}_{\ Q^{\bar{c}}} AQ^{\bar{c}} - \Gamma^{Ac}_{\ \ Q^A} AcQ^A - \frac{1}{2}\Gamma_{Q^c}^{\ \ cc} Q^c cc \,, \tag{4.7}$$

which relate to the BRST transformations,

$$\begin{aligned} \mathfrak{s} A^a_\mu &= \partial_\mu c^a + g f^{abc} A^b_\mu c^c \\ \mathfrak{s} c^a &= \frac{1}{2} g f^{abc} c^b c^c \\ \mathfrak{s} \bar{c}^a &= B^a \\ \mathfrak{s} B^a &= 0 \,. \end{aligned} \tag{4.8}$$

with the auxiliary Nakanishi-Lautrup field B^a and one the BRST operator is nilpotent, $\mathfrak{s}^2 = 0$. One can then proceed by integrating out the auxiliary field and arrives at the relation $\langle \mathfrak{s}\phi_a \rangle = -\frac{\delta\Gamma}{\delta Q^a}$. For more details see Section A.1.3 and Section A.1.4.

For pure Yang-Mills theory, we can define the fields in *QMeS* as,

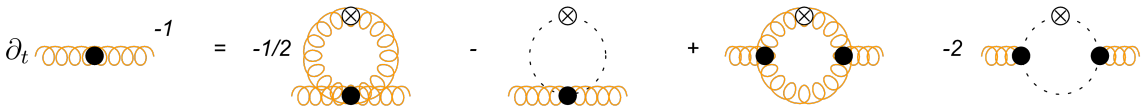

Figure 4.2.: Graphical representation of the flow equation of the gluon two-point function, explicitly given in (4.10). The dashed lines represent the ghost, curly orange lines the gluon. The black circles represent full vertices and the crossed circle represents the regulator derivative. The power -1 indicates a full two-point function.

```
fieldsYM = <|"bosonic" -> {A[p, {mu, a}]},
"fermionic" -> {{cbar[p, {a}], c[p, {a}]}}|>;
```

Note that fermions need to be defined as a pair of the antifermion and corresponding fermion.

Next, we specify the truncation for the effective average action without the BRST terms. It is important to also define the two-point functions in order to get the possible propagators.

```
TruncationYM = {{A, A}, {c, cbar}, {A, A, A},
{A, A, A, A}, {A, c, cbar}, {A, A, c, cbar},
{c, c, cbar, cbar}};
```

The classical Yang-Mills action is given by

```
classicalActionYM = {{A, A}, {c, cbar},
{A, A, A}, {A, A, A, A}, {A, c, cbar}};
```

Since we have a theory with ghosts c^a and color indices a, b, d, ..., we use i, j, m ... as superindices for the master equations.

4.3.1.1. Flow of the Gluon Two-Point Function

To compute the flow of the gluon two-point function we need to define the Quantum Master equation which is in this case the fRG equation (3.16). This translates to *QMeS* input as,

```
fRGEq = {"Prefactor" -> {1/2},
<|"type" -> "Regulatordot", "indices" -> {i, j}|>,
<|"type" -> "Propagator", "indices" -> {i, j}|>};
```

Now we can define the setup

```
SetupYMfRG = <|"MasterEquation" -> fRGEq,
"FieldSpace" -> fieldsYM,
"Truncation" -> TruncationYM|>;
```

The only thing that is missing is a specification of the field derivatives that we want to take:

```
DerivativeListAA = {A[-p, {mu, a}], A[p, {nu, b}]};
```

Now we can derive symbolic diagrams. In general we have different output options (see Section 4.2.4).

First we can take a look at the general structure of diagrams that are produced when taking two functional derivatives with respect to the superfields Φ_a and Φ_b by calling the *QMeS* command `DeriveFunctionalEquation` with the output option `"OutputLevel" -> "FunctionalDerivatives"`. We then obtain

$$\begin{aligned}\dot{\Gamma}^{ab} = &-\frac{1}{2}(-1)^{ia}(-1)^{ib}(-1)^{nn}\dot{R}^{ij}G_{im}\Gamma^{mabn}G_{nj}\\ &+\frac{1}{2}(-1)^{ia}(-1)^{ib}(-1)^{nn}(-1)^{n'n'}\\ &\dot{R}^{ij}G_{im}\Gamma^{man}G_{nm'}\Gamma^{m'bn'}G_{n'j}\\ &+\frac{1}{2}(-1)^{ia}(-1)^{ib}(-1)^{nn}(-1)^{n'n'}(-1)^{ab}\\ &\dot{R}^{ij}G_{im}\Gamma^{mbn}G_{nm'}\Gamma^{m'an'}G_{n'j}\,. \end{aligned} \tag{4.9}$$

One thus gets a tadpole diagram and two diagrams with two three-point vertices respectively. Next, we want to get the fully traced diagrams by evaluating

```
fRGDiagramsAA = DeriveFunctionalEquation[SetupYMfRG,
DerivativeListAA, "OutputLevel" -> "FullDiagrams"];
```

As a result we obtain in superindex notation where now $a \simeq (-p,\mu,a)$ and $b \simeq (p,\nu,b)$,

$$\begin{aligned}\dot{\Gamma}^{A_aA_b} = &-\dot{R}^{\bar{c}c}G_{c\bar{c}}\Gamma^{A_aA_b\bar{c}c}G_{c\bar{c}}\\ &-\frac{1}{2}\dot{R}^{AA}G_{AA}\Gamma^{AA_aA_bA}G_{AA}\\ &+\frac{1}{2}\dot{R}^{AA}G_{AA}\Gamma^{AA_aA}G_{AA}\Gamma^{AA_bA}G_{AA}\\ &+\frac{1}{2}\dot{R}^{AA}G_{AA}\Gamma^{AA_bA}G_{AA}\Gamma^{AA_aA}G_{AA}\\ &-\dot{R}^{\bar{c}c}G_{c\bar{c}}\Gamma^{A_a\bar{c}c}G_{c\bar{c}}\Gamma^{A_b\bar{c}c}G_{c\bar{c}}\\ &-\dot{R}^{\bar{c}c}G_{c\bar{c}}\Gamma^{A_b\bar{c}c}G_{c\bar{c}}\Gamma^{A_a\bar{c}c}G_{c\bar{c}}\,. \end{aligned} \tag{4.10}$$

The *QMeS* output is a list of different traced diagrams such that one can easily define and insert the Feynman rules for the different objects like propagators, regulators, or vertices. It can be found in Section A.3.1. A graphical representation of the flow can be found in Figure 4.2.

4.3.1.2. mSTI of Gluon Two-Point Function

To compute the mSTI of the gluon two-point function we need to alter our definition of fields and include the corresponding BRST sources.

```
fieldsYMmSTI = <|"bosonic" -> {A[p, {mu, a}]},
"fermionic" -> {{cbar[p, {a}], c[p, {a}]}},
"BRSTsources" -> {{Q[A], "fermionic"},
{Q[cbar], "bosonic"}, {Q[c], "bosonic"}}|>;
```

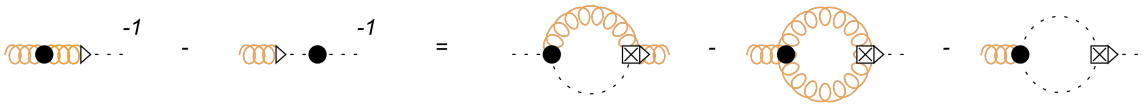

Figure 4.3.: Graphical representation of the mSTI of the gluon two-point function, explicitly given in (4.11). The dashed lines represent the ghost, curly orange lines the gluon. The black circles represent full vertices and the crossed square corresponds to a regulator and the triangle to a BRST vertex. The power -1 indicates a full two-point function.

The truncation then also changes. The vertices on the right-hand side of the mSTI are truncated as,

```
TruncationYMRHSmSTI = {{A, A}, {c, cbar},
{A, A, A}, {A, A, A, A}, {A, c, cbar},
{A, c, Q[A]}, {c, c, Q[c]}};
```

and for the left-hand side, we choose

```
TruncationYMLHSmSTI = {{A, A}, {c, cbar},
{A, A, A}, {A, A, A, A}, {A, c, cbar},
{A, Q[cbar]}, {c, Q[A]}, {A, c, Q[A]},
{c, c, Q[c]}};
```

Lastly we need to define the right- and left-hand side of the mSTI equation (3.18). In the *QMeS* formalism this is done by

```
mSTIRHS = {"Prefactor" -> {1},
<|"type" -> "Regulator", "indices" -> {i, j}|>,
<|"type" -> "Propagator", "indices" -> {j, m}|>,
<|"type" -> "nPoint",
"indices" -> {m, Q[i]}, "nPoint" -> 2, "spec" -> "BRST"|>};

mSTILHS = {"Prefactor" -> {1},
<|"type" -> "nPoint",
"indices" -> {Q[i]}, "nPoint" -> 1, "spec" -> "BRST"|>,
<|"type" -> "nPoint",
"indices" -> {i}, "nPoint" -> 1, "spec" -> "none"|>};
```

We define the two setups as,

```
SetupYMmSTIRHS = <|"MasterEquation" -> mSTIRHS,
"FieldSpace" -> fieldsYMmSTI,
"Truncation" -> TruncationYMRHSmSTI|>;

SetupYMmSTILHS = <|"MasterEquation" -> mSTILHS,
"FieldSpace" -> fieldsYMmSTI,
"Truncation" -> TruncationYMmSTILHS|>;
```

To obtain the mSTI of the gluon two-point function one needs to take derivatives with respect to the ghost and gluon field,

```
DerivativeListAAmSTI = {A[-p, {mu, a}], c[p, {b}]};
```

We obtain the full mSTI by evaluating

```
mSTIDiagramsAALHS = DeriveFunctionalEquation[SetupLHSmSTILHS,
DerivativeListmSTI, "OutputLevel" -> "FullDiagrams"];

mSTIDiagramsAARHS = DeriveFunctionalEquation[SetupmSTIRHS,
DerivativeListmSTI, "OutputLevel" -> "FullDiagrams"];
```

With the superindices $a \simeq (-p, \mu, a)$ and $b \simeq (p, b)$ the algebraic equations are then given as,

$$\begin{aligned}\Gamma^{c_b}_{\ Q^A}\Gamma^{AA_a} - \Gamma^{A_a}_{\ Q^{\bar{c}}}\Gamma^{\bar{c}c_b} &= R^{AA}G_{AA}\Gamma^{A\bar{c}c_b}G_{c\bar{c}}\Gamma^{A_a c}_{\ \ \ Q^A} \\ &- R^{AA}G_{AA}\Gamma^{AA_aA}G_{AA}\Gamma^{Ac_b}_{\ \ \ Q^A} \\ &- R^{\bar{c}c}G_{c\bar{c}}\Gamma^{A_a\bar{c}c}G_{c\bar{c}}\Gamma_{Q^c}^{\ \ cc_b}\,, \end{aligned} \tag{4.11}$$

where for the sake of brevity, indices and momenta are dropped. The output of *QMeS* is given in Section A.3.2. The diagrams that contribute to the mSTI can be found in Figure 4.3.

4.3.1.3. DSE of Ghost-Gluon Vertex

In this subsection, we derive the DSE for the ghost-gluon vertex. This can be done by taking functional derivatives of the action,

$$\Gamma^{A\bar{c}c} = \frac{\delta^2}{\delta A \delta \bar{c}} \left(\frac{\delta S}{\delta c}\right)_{\phi_a \to \Phi_a + G_{ab}\frac{\delta}{\delta \Phi_b}}\,. \tag{4.12}$$

We define the setup,

```
SetupYMDSE = <|"MasterEquation" ->
<|"getDSE" -> "True", "classicalAction" -> classicalActionYM|>,
"FieldSpace" -> fieldsYM,
"Truncation" -> TruncationYM|>;
```

We define the derivative list

```
DerivativeListAcbarcDSE =
{A[p1, {mu, a}], cbar[p2, {b}], c[-p1 - p2, {d}]};
```

We get the full result by using the command:

```
DSEDiagramsAcbarc = DeriveFunctionalEquation[SetupYMDSE,
DerivativeListAcbarcDSE, "OutputLevel" -> "FullDiagrams"];
```

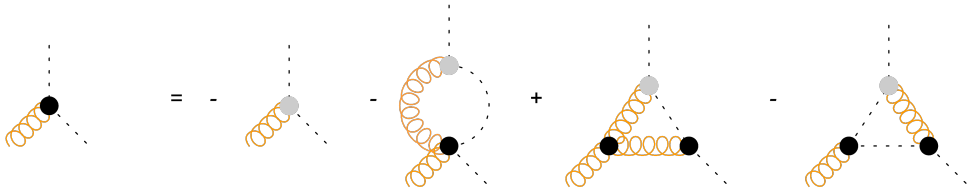

Figure 4.4.: Graphical representation of the DSE of the ghost-gluon vertex, explicitly given in (4.13). The dashed lines represent the ghost, curly orange lines the gluon. The black and grey circles represent full and classical vertices.

Diagrammatically the result is,

$$\begin{aligned}\Gamma^{A_a\bar{c}_b c_d} =& - S^{A_a\bar{c}_b c_d} \\ & - S^{A\bar{c}c_d} G_{AA} \Gamma^{AA_a\bar{c}_b c} G_{c\bar{c}} \\ & + S^{A\bar{c}c_d} G_{AA} \Gamma^{AAA_a} G_{AA} \Gamma^{A\bar{c}_b c} G_{c\bar{c}} \\ & - S^{A\bar{c}c_d} G_{AA} \Gamma^{A\bar{c}_b c} G_{c\bar{c}} \Gamma^{A_a\bar{c}c} G_{c\bar{c}}\,, \end{aligned} \tag{4.13}$$

where we have used the superindices $a \simeq (p1, \mu, a)$, $b \simeq (p2, b)$ and $d \simeq (-p1 - p2, d)$. The full equation can be found in Section A.3.3. The symbolic DSE can be found in Figure 4.4.

4.3.2. Yukawa Theory

In this example, we want to compute simple two-point flows in Yukawa theory. To further illustrate how *QMeS* handles multiple fermions we do this in $N_f = 1$ as well as $N_f = 2$. Generally, we can write the action of a Yukawa theory as,

$$\begin{aligned} S = & \int d^4x \Big(\frac{1}{2}\phi(-\partial^2 + m_\phi^2)\phi + \lambda\phi^4 \\ & + \bar{\psi}\left(\not{\partial} + m_\psi\right)\psi - g\phi\bar{\psi}\psi\Big)\,. \end{aligned} \tag{4.14}$$

The effective action contains

$$\begin{aligned}\Gamma =& \Gamma^{\phi\phi}\phi\phi + \Gamma^{\bar{\psi}\psi}\bar{\psi}\psi + \Gamma^{\phi\bar{\psi}\psi}\phi\bar{\psi}\psi \\ & + \Gamma^{\phi\phi\phi\phi}\phi\phi\phi\phi + \Gamma^{\bar{\psi}\bar{\psi}\psi\psi}\bar{\psi}\bar{\psi}\psi\psi\,. \end{aligned} \tag{4.15}$$

As a master equation, we again use the fRG equation,

```
fRGEq = {"Prefactor" -> {1/2},
<|"type" -> "Regulatordot", "indices" -> {i, j}|>,
<|"type" -> "Propagator", "indices" -> {i, j}|>};
```

4.3.2.1. $N_f = 1$

For $N_f = 1$ we only have one flavour of fermions and thus only one antifermion/fermion pair in the definition of fields. Furthermore, a Yukawa theory also contains a scalar field, which has bosonic statistics.

```
fieldsNf1 = <|"bosonic" -> {Phi[p]},
"fermionic" -> {{Psibar[p, {d}], Psi[p, {d}]}}|>;
```

The truncation is given as,

```
TruncationfRGNf1 = {{Phi, Phi}, {Psi, Psibar},
{Phi, Psi, Psibar}, {Phi, Phi, Phi, Phi},
{Psi, Psi, Psibar, Psibar}};
```

Thus we can summarize the setup,

```
SetupNf1 = <|"MasterEquation" -> fRGEq,
"FieldSpace" -> fieldsNf1,
"Truncation" -> TruncationfRGNf1|>;
```

Flow of the Scalar Two-Point Function

To compute the flow of the scalar two-point function we define the list of derivatives as,

```
DerivativeListScalarTwopoint = {Phi[-p], Phi[p]};
```

To get the full diagrams one has to run the command

```
fRGDiagramsPhiPhiNf1 = DeriveFunctionalEquation[SetupNf1,
DerivativeListScalarTwopoint, "OutputLevel" -> "FullDiagrams"];
```

The result with superindices $a \simeq (-p)$ and $b \simeq (p)$ is given as,

$$\begin{aligned}\dot{\Gamma}^{\phi_a\phi_b} = &-\frac{1}{2}R^{\phi\phi}G_{\phi\phi}\Gamma^{\phi\phi\phi_a\phi_b}G_{\phi\phi}\\ &- R^{\bar{\psi}\psi}G_{\psi\bar{\psi}}\Gamma^{\phi_a\bar{\psi}\psi}G_{\psi\bar{\psi}}\Gamma^{\phi_b\bar{\psi}\psi}G_{\psi\bar{\psi}}\\ &- R^{\bar{\psi}\psi}G_{\psi\bar{\psi}}\Gamma^{\phi_b\bar{\psi}\psi}G_{\psi\bar{\psi}}\Gamma^{\phi_a\bar{\psi}\psi}G_{\psi\bar{\psi}}\,.\end{aligned} \tag{4.16}$$

The full output of *QMeS* is given in Section A.3.4.

Flow of the Fermionic Two-Point Function

The derivative list for the flow of the fermionic two-point is

```
DerivativeListFermionTwopoint = {Psibar[-p, {d}], Psi[p, {e}]};
```

The full diagrams can be obtained with

```
fRGDiagramsPsibarPsiNf1 = DeriveFunctionalEquation[SetupNf1,
DerivativeListFermionTwopoint, "OutputLevel" -> "FullDiagrams"];
```

The result with superindices is then given as,

$$\begin{aligned}\dot{\Gamma}^{\bar{\psi}_d\psi_e} = &- R^{\bar{\psi}\psi} G_{\psi\bar{\psi}} \Gamma^{\bar{\psi}\bar{\psi}_d\psi_e\psi} G_{\psi\bar{\psi}} \\ &- \frac{1}{2} R^{\phi\phi} G_{\phi\phi} \Gamma^{\phi\bar{\psi}\psi_e} G_{\psi\bar{\psi}} \Gamma^{\phi\bar{\psi}_d\psi} G_{\phi\phi} \\ &- \frac{1}{2} R^{\phi\phi} G_{\phi\phi} \Gamma^{\phi\bar{\psi}_d\psi} G_{\psi\bar{\psi}} \Gamma^{\phi\bar{\psi}\psi_e} G_{\phi\phi} \\ &- \frac{1}{2} R^{\bar{\psi}\psi} G_{\psi\bar{\psi}} \Gamma^{\phi\bar{\psi}_d\psi} G_{\phi\phi} \Gamma^{\phi\bar{\psi}\psi_e} G_{\psi\bar{\psi}} \\ &- \frac{1}{2} R^{\bar{\psi}\psi} G_{\psi\bar{\psi}} \Gamma^{\phi\bar{\psi}\psi_e} G_{\phi\phi} \Gamma^{\phi\bar{\psi}_d\psi} G_{\psi\bar{\psi}} \,, \end{aligned} \tag{4.17}$$

where indices were again dropped. The full output of *QMeS* is given in Section A.3.4.

4.3.2.2. $N_f = 2$

Since we now want to include two flavours of fermions, we need to implement two anti-fermion/fermion pairs. For simplicity we call them $(\bar{\psi}_1, \psi_1)$ and $(\bar{\psi}_2, \psi_2)$.

```
fieldsNf2 = <|"bosonic" -> {Phi[p]},
"fermionic" -> {{Psibar1[p, {d}], Psi1[p, {d}]},
{Psibar2[p, {d}], Psi2[p, {d}]}}|>;
```

The truncation is then given by

```
TruncationfRGNf2 = {{Phi, Phi}, {Psi1, Psibar1},
{Psi2, Psibar2}, {Phi, Psi1, Psibar1},
{Phi, Psi2, Psibar2}, {Phi, Phi, Phi, Phi},
{Psi1, Psi1, Psibar1, Psibar1},
{Psi2, Psi2, Psibar2, Psibar2},
{Psi1, Psi2, Psibar1, Psibar2}};
```

The setup is then given as,

```
SetupNf2 = <|"MasterEquation" -> fRGEq,
"FieldSpace" -> fieldsNf2,
"Truncation" -> TruncationfRGNf2|>;
```

Flow of the Scalar Two-Point Function

As before we define the two scalar field derivatives as,

```
DerivativeListScalarTwopoint = {Phi[-p], Phi[p]};
```

To get the full diagrams one has to run the command

```
fRGDiagramsPhiPhiNf2 = DeriveFunctionalEquation[SetupNf2,
DerivativeListScalarTwopoint, "OutputLevel" -> "FullDiagrams"];
```

The result in superindex notation with $a \simeq (-p)$ and $b \simeq (p)$ is given as,

$$\begin{aligned}\dot{\Gamma}^{\phi_a\phi_b} = &-\frac{1}{2}R^{\phi\phi}G_{\phi\phi}\Gamma^{\phi\phi\phi_a\phi_b}G_{\phi\phi}\\ &- R^{\bar{\psi}_1\psi_1}G_{\psi_1\bar{\psi}_1}\Gamma^{\phi_a\bar{\psi}_1\psi_1}G_{\psi_1\bar{\psi}_1}\Gamma^{\phi_b\bar{\psi}_1\psi_1}G_{\psi_1\bar{\psi}_1}\\ &- R^{\bar{\psi}_1\psi_1}G_{\psi_1\bar{\psi}_1}\Gamma^{\phi_b\bar{\psi}_1\psi_1}G_{\psi_1\bar{\psi}_1}\Gamma^{\phi_a\bar{\psi}_1\psi_1}G_{\psi_1\bar{\psi}_1}\\ &- R^{\bar{\psi}_2\psi_2}G_{\psi_2\bar{\psi}_2}\Gamma^{\phi_a\bar{\psi}_2\psi_2}G_{\psi_2\bar{\psi}_2}\Gamma^{\phi_b\bar{\psi}_2\psi_2}G_{\psi_2\bar{\psi}_2}\\ &- R^{\bar{\psi}_2\psi_2}G_{\psi_2\bar{\psi}_2}\Gamma^{\phi_b\bar{\psi}_2\psi_2}G_{\psi_2\bar{\psi}_2}\Gamma^{\phi_a\bar{\psi}_2\psi_2}G_{\psi_2\bar{\psi}_2}\,. \end{aligned} \tag{4.18}$$

The full output of *QMeS* is given in Section A.3.5.

Flow of the Fermionic Two-Point Function

The derivatives with respect to the first antifermionic and fermionic fields is given as,

```
DerivativeListFermion1Twopoint = {Psibar1[-p, {d}], Psi1[p, {e}]};
```

The full diagrams can be obtained with

```
fRGDiagramsPsibar1Psi1Nf2 = DeriveFunctionalEquation[SetupNf2,
DerivativeListFermion1Twopoint, "OutputLevel" -> "FullDiagrams"];
```

The result in superindex notation is then

$$\begin{aligned}\dot{\Gamma}^{\bar{\psi}_{1d}\psi_{1e}} = &- R^{\bar{\psi}_1\psi_1}G_{\psi_1\bar{\psi}_1}\Gamma^{\bar{\psi}_1\bar{\psi}_{1d}\psi_{1e}\psi_1}G_{\psi_1\bar{\psi}_1}\\ &+ R^{\bar{\psi}_2\psi_2}G_{\psi_2\bar{\psi}_2}\Gamma^{\bar{\psi}_{1d}\bar{\psi}_2\psi_{1e}\psi_2}G_{\psi_2\bar{\psi}_2}\\ &- \frac{1}{2}R^{\phi\phi}G_{\phi\phi}\Gamma^{\phi\bar{\psi}_{1d}\psi_1}G_{\psi_1\bar{\psi}_1}\Gamma^{\phi\bar{\psi}_1\psi_{1e}}G_{\phi\phi}\\ &- \frac{1}{2}R^{\phi\phi}G_{\phi\phi}\Gamma^{\phi\bar{\psi}_1\psi_{1e}}G_{\psi_1\bar{\psi}_1}\Gamma^{\phi\bar{\psi}_{1d}\psi_1}G_{\phi\phi}\\ &- \frac{1}{2}R^{\bar{\psi}_1\psi_1}G_{\psi_1\bar{\psi}_1}\Gamma^{\phi\bar{\psi}_{1d}\psi_1}G_{\phi\phi}\Gamma^{\phi\bar{\psi}_1\psi_{1e}}G_{\psi_1\bar{\psi}_1}\\ &- \frac{1}{2}R^{\bar{\psi}_1\psi_1}G_{\psi_1\bar{\psi}_1}\Gamma^{\phi\bar{\psi}_1\psi_{1e}}G_{\phi\phi}\Gamma^{\phi\bar{\psi}_{1d}\psi_1}G_{\psi_1\bar{\psi}_1}\,. \end{aligned} \tag{4.19}$$

Here one can see how the canonical sorting of fields in vertices is followed by an alphabetical one. The full output of *QMeS* is given in Section A.3.5.

4.4. Conclusion

In this work we have introduced the *Mathematica* package *QMeS-Derivation*. It allows deriving symbolic functional equations from a master equation (fRG, mSTI, DSE). This includes taking functional derivatives, tracing in field space, and a momentum routing for 1-loop diagrams. One of the most notable features is that during this process *QMeS* is able to deal with fermionic signs effectively and consistently. Special emphasis is put on the modular structure of the code which allows for future extensions like for example the extension of the momentum routing to higher loop order diagrams.

We elucidated the usage of the package by computing different functional equations in $SU(3)$ Yang-Mills and $N_f = 1$ and $N_f = 2$ Yukawa theory starting from an action S.

5. On Gauge Invariance in Gauge-Fixed Yang-Mills Theory

This chapter is based on [3].

Infrared QCD is a strongly correlated system and is governed by confinement and spontaneous chiral symmetry breaking, whose understanding and resolution require numerical non-perturbative first principle approaches. Functional diagrammatic approaches such as the functional renormalisation group (fRG) and Dyson-Schwinger equations (DSE), or n-particle irreducible approaches (nPI) potentially offer both, analytic access to the mechanisms behind the infrared dynamics of QCD as well as its quantitative numerical resolution, for literature on the fRG and DSE approaches in QCD see the recent reviews [59, 64] and references therein.

The diagrammatic nature of functional approaches is best implemented within gauge fixed QCD, for a recent discussion of gauge invariant alternatives see [64] and references therein. A specifically well-suited gauge fixing is the Landau gauge, in particular for numerical applications. The latter require truncations to the infinite hierarchy of coupled loop equations for correlation functions in functional approaches. Naturally, the strongly correlated nature of infrared QCD begs the question of whether the truncations commonly used for explicit numerical solutions transport the underlying gauge symmetry of QCD: are the correlation functions computed *gauge consistent*. Naturally, the gauge consistency of the correlation functions is essential for confinement, both its manifestation in gauge-fixed approaches as well as its understanding.

In the present work, we put forward a systematic approach towards the evaluation of the above question: First, one computes transverse and longitudinal correlation functions in QCD with functional approaches. Then, the gauge consistency of the results is tested by inserting them into the Slavnov-Taylor identities (STIs). The STIs encode the changes of gauge-fixed correlation functions under gauge or BRST-transformations. However, the evaluation of the latter test comes with an intricacy. The STIs also constitute a set of functional relations for correlation functions. These relations can be derived from the BRST identity of the effective action, the BRST master equation, similarly to deriving functional relations from the fRG-flow of the effective action or the functional DSE for the latter. In the case of the STIs, longitudinal correlation functions are related to combinations of transverse and longitudinal correlation functions. In summary, fRG equations, DSEs, and STIs represent different resummation schemes for correlation functions and while their respective solutions agree in exact solutions, at a finite orders of an expansion the solutions will deviate. To exemplify this situation, let us emphasise that one can easily guarantee the STIs for a finite set of correlation functions in a given order of the truncation if simply using the STIs for the computation of the longitudinal correlation functions. Evidently, this resolution of the STIs does not guarantee the gauge consistency of the transverse correlation functions. This is best seen in the Landau gauge, where the set of functional relations for transverse correlation functions is decoupled from the system of longitudinal ones. Instead, gauge consistency should rather be evaluated by the *smallness* of the de-

viations of correlation functions within *all* functional relations at hand: fRG equations, DSEs, STIs and nPI-relations. For a detailed discussion of these subtleties, we refer to [35, 64].

In the present work, we study Landau gauge Yang-Mills theory within a systematic vertex expansion with the functional renormalisation group. Longitudinal correlation functions are also computed from the respective Slavnov-Taylor identities, that follow from the BRST master equation for the effective action. We use an advanced truncation level for these computations, even though fully quantitative computations are still more advanced, for comparison see [37, 39]. The respective results are also compared with the corresponding lattice results. In Section 5.2 we then discuss the consequences for the gauge consistency of the present results as well as extensions of the current computations.

5.1. Slavnov-Taylor Identities in Functional Approaches

We consider $SU(N_c)$ Yang-Mills theory in Euclidean space-time within the Landau gauge. The explicit results are obtained in the physical (QCD) case $N_c = 3$, but they readily extend the general N_c. The gauge-fixed classical action, including the ghost term and BRST source terms, is given by

$$\begin{aligned} S = \int_x \Big[& \frac{1}{4} F^a_{\mu\nu} F^a_{\mu\nu} + \partial_\mu \bar{c}^a D^{ab}_\mu c^b + B^a \partial_\mu A^a_\mu - \frac{\xi}{2} B^a B^a \\ & - Q^a_{A,\mu} D^{ab}_\mu c^b - \frac{1}{2} g f^{abc} Q^a_c c^b c^c + \frac{1}{\xi} Q_{\bar{c}} \partial_\mu A^a_\mu \Big] . \end{aligned} \tag{5.1}$$

The Landau gauge is implemented with $\xi \to 0$, and we have introduced the shorthand notation $\int_x = \int d^4x$. The covariant derivative D in the adjoint representation and field strength tensor are defined as,

$$\begin{aligned} D^{ab}_\mu c^b &= \partial_\mu c^a + g f^{acb} A^c_\mu c^b \,, \\ F^a_{\mu\nu} &= \partial_\mu A^a_\nu - \partial_\nu A^a_\mu + g f^{abc} A^b_\mu A^c_\nu \,. \end{aligned} \tag{5.2}$$

The gauge-fixed Yang-Mills action in (5.1) still carries gauge invariance in terms of BRST-symmetry (Becchi, Rouet, Stora, Tyutin) [110, 111]. The respective transformations are given by

$$\begin{aligned} \mathfrak{s} A^a_\mu &= D^{ab}_\mu c^b \\ \mathfrak{s} c^a &= \frac{1}{2} g f^{abc} c^b c^c \\ \mathfrak{s} \bar{c}^a &= B^a \\ \mathfrak{s} B^a &= 0 \,, \end{aligned} \tag{5.3}$$

with the Nakanishi-Lautrup field B^a and with the BRST transformation of the field ϕ_a, $\delta_{\mathrm{BRST}} \phi_a = \mathfrak{s}\phi_a \delta\lambda$. In (5.1) we have already added BRST source terms with the currents

$Q = (Q_A, Q_c, Q_{\bar{c}})$ are coupled to the respective BRST transformations of the fields. Evidently, we do not need Q_B as the respective BRST transformation vanishes identically. Moreover, with $\mathfrak{s}^2 = 0$ these additional terms are also BRST invariant. Our general convention and notation follows [1].

5.1.1. Functional Renormalisation Group

In the functional renormalisation group approach, an infrared cutoff is introduced by adding momentum-dependent mass terms ΔS_k to the classical action S in the path integral representation of the generating functional $Z[J, Q]$. Here, the super-current J includes currents for all component fields $J = (J_A, J_c, J_{\bar{c}}, J_B)$, and the BRST current Q is defined above (5.3). The regulator terms read

$$\Delta S_k = \int \left(\frac{1}{2} (R_A)^{ab}_{\mu\nu} \, A^a_\mu A^b_\nu + (R_c)^{ab} \, \bar{c}^a c^b \right) , \tag{5.4}$$

with the infrared cutoff scale k. The regulators $R = (R_A, R_c)$ suppress quantum fluctuations for momenta $p^2 \lesssim k^2$ for the respective fields, and vanishes for $p^2 \gtrsim k^2$. The specific form of the regulators used in the present work can be found in Section B.2.2.

The functional flow equation is derived for the scale-dependent effective action

$$\Gamma_k[\Phi, Q] = \int J \cdot \Phi - \log Z[J, Q] - \Delta S_k[\Phi] \, , \tag{5.5}$$

with the superfield

$$\Phi = (A_\mu, c, \bar{c}, B) \, . \tag{5.6}$$

Equation (5.5) is the modified Legendre transform of the Schwinger functional $\log Z$, where the regulator term has been separated for computational convenience. Its logarithmic scale derivative provides us with the one-loop exact fRG equation,

$$\partial_t \Gamma_k = \int \left(\frac{1}{2} (\dot{R}_A)^{ab}_{\mu\nu} \, (G_{AA})^{ab}_{\mu\nu} - (\dot{R}_c)^{ab} (G_{c\bar{c}})^{ab} \right) , \tag{5.7}$$

with $\dot{R} = \partial_t R$, the (negative) RG time $t = \ln(k/\Lambda)$, and the full ghost and gluon propagators

$$G_{AA} = \left[\frac{1}{\Gamma^{(2)} + R} \right]_{AA} , \qquad G_{c\bar{c}} = \left[\frac{1}{\Gamma^{(2)} + R} \right]_{c\bar{c}} . \tag{5.8}$$

Here, Λ is a reference scale, typically chosen to be the initial cutoff scale deep in the ultraviolet (UV). If the initial scale is chosen sufficiently large, the effective action tends towards the local UV effective action Γ_Λ that consists out of all UV-relevant terms. For Yang-Mills theory this UV effective action includes all terms in the classical action as well as a mass term for the gluon. The latter term originates in the breaking of gauge invariance via the regulator term for $k \neq 0$. In turn, for $k \to 0$, this breaking disappears and we are left with the full BRST invariant effective action. For a full derivation and further discussions, see e.g. [1, 64, 94, 115].

We close this section with a remark on some implicit assumptions within the derivation of the flow equation (5.7): it implies that the only k-dependence of the *renormalised*

generating functional originates in the cutoff term. Then, in particular, the renormalisation procedure is assumed to be k-independent, for a detailed discussion see e.g. [115, 120]. While the self-consistency of this assumptions is readily shown for the wave function renormalisations and vertices, the absence of a mass renormalisation for the gluon is less trivial and is of utmost importance for the interpretation of Yang-Mills theory in the presence of the infrared cutoff term as a deformation of Yang-Mills theory, rather than massive Yang-Mills theory (Curci-Ferrari (CF) model), see e.g. [175–178]. While this seemingly is only of formal interest, the massless limit of the CF model is an intricate one as it defines a flow in theory space. Instead, the removal of the momentum-local infrared regulator in Yang-Mills theory is smooth, as the cutoff term can be interpreted as the local deformation of Yang-Mills theory.

5.1.2. STI & mSTI

Classical BRST symmetry with the infinitesimal transformations (5.3) leads to symmetry identities on the quantum level, that can be formulated in terms of a master equation, see e.g. [179, 180],

$$\int_x \left(\frac{\delta\Gamma}{\delta Q^a_{A,\mu}} \frac{\delta\Gamma}{\delta A^a_\mu} + \frac{\delta\Gamma}{\delta Q^a_c} \frac{\delta\Gamma}{\delta c^a} + \frac{\delta\Gamma}{\delta Q^a_{\bar{c}}} \frac{\delta\Gamma}{\delta \bar{c}^a} \right) = 0 \,. \tag{5.9}$$

By integrating out the Nakanishi-Lautrup field leads to

$$\int_x \left(\frac{\delta\Gamma}{\delta Q^a_{A,\mu}} \frac{\delta\Gamma}{\delta A^a_\mu} + \frac{\delta\Gamma}{\delta Q^a_c} \frac{\delta\Gamma}{\delta c^a} - \frac{1}{\xi} (\partial_\nu A^a_\nu) \partial_\mu \frac{\delta\Gamma}{\delta Q^a_{A,\mu}} \right) = 0 \,. \tag{5.10}$$

In the derivation of (5.10), one also uses the fact that the anti-ghost field only appears linearly in the action.

Finally, the introduction of the cutoff term, (5.4), leads to a modification of the symmetry identity (5.11), the *modified Slavnov-Taylor identity* (mSTI). It can be derived similarly to the flow equation which can be interpreted as the equation which governs the violation of scale invariance. For the mSTI, the additional term in comparison to (5.10) originates from the lack of BRST invariance of the regulator term. As for the flow equation, it is a one-loop exact equation. In the presence of the Nakanishi-Lautrup field B, the mSTI takes the concise form,

$$\int_x \Gamma_{Q_i} \Gamma_{\Phi_i} = \int_{x,y} (R\,G)_{\Phi_i \Phi_j} \, \Gamma_{Q_j \Phi_i} \tag{5.11}$$

with the notation

$$\Gamma_{Q_1 \cdots Q_n \Phi_{n+1} \cdots \Phi_{n+m}} = \frac{\delta\Gamma[\Phi, Q]}{\delta Q_1 \cdots \delta Q_n \delta\Phi_{n+1} \cdots \delta\Phi_{n+m}} \,, \tag{5.12}$$

for mixed derivatives of the effective action with respect to BRST currents and fields. The integral $\int_{x,y}$ on the right-hand side of (5.11) constitutes a space-time trace of the product of operators $(R\,G)(x,y)$ and $\Gamma_{Q\Phi}(y,x)$. On both sides of (5.11), a sum over species of fields as well as internal and Lorentz indices is implied. For example, the left-hand side of (5.11) is simply that of (5.9), if re-instating all indices.

The right-hand side originates in the breaking of BRST invariance by the regulator term, similarly to the right-hand side of the flow equation, which manifests the breaking of scale invariance by the regulator term. We emphasise, that (5.11) is derived with the same implicitly assumption of the independence of the UV renormalisation procedure of the cutoff term. We will discuss the self-consistency of this assumption in Section 5.1.4.

For $k \to 0$ the mSTI reduces to the STI. Thus, satisfying the mSTI at all scales k, guarantees gauge invariance of observables at $k = 0$. A full derivation can be found e.g. in [1, 94] and references therein.

5.1.3. Vertex Expansion and Truncations

We expand the effective action in terms of Φ and Q vertices. At vanishing BRST current, $Q = 0$, this entails,

$$\Gamma_k[\Phi, 0] = \sum_{n=1}^{\infty} \int \Gamma_{\Phi_1 \dots \Phi_n} \Phi_1 \dots \Phi_n \,, \tag{5.13}$$

with the superfield Φ in (5.6), the 1PI correlation functions $\Gamma_{\Phi_1 \dots \Phi_n}$, and the normalisation $\Gamma_k[0, 0] = 0$. Including BRST and mixed vertices is done analogously. Inserting the vertex expansion (5.13) into the fRG equation (5.7), one sees readily, that a full solution of the theory requires the complete set of 1PI correlation functions. Specifically, the flow of $\Gamma_{\Phi_1 \dots \Phi_n}$ depends on correlation functions $\Gamma_{\Phi_1 \dots \Phi_m}$ with $2 \leq m \leq n + 2$. This leads to an infinite tower of coupled integro-differential equations. For most practical purposes this tower has to be truncated. Similar considerations apply to all closed functional master equations and in particular to the set of DSEs, whose towers of coupled integral equations also satisfy $2 \leq m \leq n + 2$.

For this work, we restrict ourselves to the truncation shown in Figure B.6. The gluon and ghost propagators are obtained from their respective two-point functions via (5.8),

$$\begin{aligned} \Gamma^{ab}_{AA,\mu\nu}(p) &= \Pi^{\perp}_{\mu\nu}(p) Z_A(p) p^2 \delta^{ab} + \Pi^{\parallel}_{\mu\nu}(p) \Gamma^{\parallel}_{AA}(p) \delta^{ab} \,, \\ \Gamma^{ab}_{\bar{c}c}(p) &= Z_c(p) p^2 \delta^{ab} \,, \end{aligned} \tag{5.14}$$

the transverse and longitudinal projection operators,

$$\begin{aligned} \Pi^{\perp}_{\mu\nu}(p) &= \left(\delta_{\mu\nu} - \frac{p_\mu p_\nu}{p^2} \right) \,, \\ \Pi^{\parallel}_{\mu\nu}(p) &= \frac{p_\mu p_\nu}{p^2} \,. \end{aligned} \tag{5.15}$$

The longitudinal scalar part $\Gamma^{\parallel}_{AA}$ in (5.14) contains the gauge fixing part that diverges in the Landau gauge limit $\xi \to 0$ and a regular contribution, that originates from the breaking of BRST invariance for finite k and vanishes in the limit $k \to 0$. We have

$$\Gamma^{\parallel}_{AA}(p) = \frac{1}{\xi} p^2 + \Gamma^{\parallel}_{AA,\mathrm{reg}} \,. \tag{5.16}$$

We remark that in the Landau gauge limit the propagator is transverse and does not depend on $\Gamma^{\parallel}_{AA,\mathrm{reg}}$, even though the latter contribution does not vanish. This is one of

the properties that single out the Landau gauge not only as the technically least difficult Lorenz gauge, but also suggests the best convergence of the results for correlation functions in a systematic vertex expansions: for any other choice of ξ the regular part $\Gamma^{\parallel}_{AA,\mathrm{reg}}$ feeds back into the dynamics of the system, even though its integrated impact has to vanish at vanishing cutoff scale. A more detailed discussion including the consistency of different functional relations (fRG, DSE, mSTI) is discussed in Section 5.1.4.

With the projection operators we can split correlation functions into their transverse and longitudinal parts,

$$\Gamma_{\Phi_1\cdots\Phi_n} = \Gamma^{\perp}_{\Phi_1\cdots\Phi_n} + \Gamma^{\parallel}_{\Phi_1\cdots\Phi_n}\,, \tag{5.17}$$

where $\Gamma^{\perp}_{\Phi_1\cdots\Phi_n}$ is the completely transverse part of the correlation function, structurally given by $\Gamma^{\perp}_{\Phi_1\cdots\Phi_n} = (\Pi^{\perp})^n\Gamma_{\Phi_1\cdots\Phi_n}$. The longitudinal part simply is the complement, and hence is built up from correlation functions with at least one longitudinal leg.

We will explain this splitting at the example of the ghost-gluon vertex. Its complete basis is spanned by only two tensor structures: the classical one, proportional to the anti-ghost momentum, and a longitudinal non-classical one, which is proportional to the gluon momentum,

$$\Gamma^{abc}_{A\bar{c}c,\mu}(p,q) = if^{abc}\Big(\lambda_{A\bar{c}c,\mathrm{cl}}(p,q)q_\mu + \lambda_{A\bar{c}c,\mathrm{ncl}}(p,q)p_\mu\Big)\,. \tag{5.18}$$

However, we can rewrite this in terms of the projection operators defined in (5.15), which are longitudinal and transverse in the gluon momentum p,

$$\Gamma^{abc}_{A\bar{c}c,\mu}(p,q) = if^{abc}\Big(\lambda_{A\bar{c}c}(p,q)\,\Pi^{\perp}_{\mu\nu}(p)q_\nu + \bar{\lambda}_{A\bar{c}c,1}(p,q)\,p_\mu\Big)\,, \tag{5.19}$$

with

$$\begin{aligned}\lambda_{A\bar{c}c}(p,q) &= \lambda_{A\bar{c}c,\mathrm{cl}}(p,q)\,,\\ \bar{\lambda}_{A\bar{c}c,1}(p,q) &= \frac{p\cdot q}{p^2}\lambda_{A\bar{c}c,\mathrm{cl}}(p,q) + \lambda_{A\bar{c}c,\mathrm{ncl}}(p,q)\,.\end{aligned} \tag{5.20}$$

The singularity of such a split with projection operators at $p=0$ is reflected in the prefactor $p\cdot q/p^2$ of the classical dressing in $\bar{\lambda}_{A\bar{c}c,1}(p,q)$. It is matched by the respective one in the transverse projection operator multiplying $\lambda_{A\bar{c}c}(p,q)$. Therefore, for non-singular dressings in (5.18) we only have a parameterisation singularity.

In the present work, we consider relations between the dressings at the symmetric point $p^2 = q^2 = -2p\cdot q$. In the ultraviolet limit, the non-classical dressing vanishes and we are left with the classical one. Hence, for the present purpose it is convenient to simply use the longitudinal projection of the classical tensor structure, $\Pi^{\parallel}_{\mu\nu}(p)q_\nu$, for the longitudinal part. This leads us to,

$$\Gamma^{abc}_{A\bar{c}c,\mu}(p,q) = \Big(\lambda_{A\bar{c}c}(p,q)\,\Pi^{\perp}_{\mu\nu}(p) + \lambda_{A\bar{c}c,1}(p,q)\,\Pi^{\parallel}_{\mu\nu}(p)\Big)\; if^{abc}q_\mu\,, \tag{5.21}$$

see also [37]. The dressing $\lambda_{A\bar{c}c,1}$ is given by

$$\lambda_{A\bar{c}c,1}(p,q) = \lambda_{A\bar{c}c,\mathrm{cl}}(p,q) + \frac{p^2}{p\cdot q}\lambda_{A\bar{c}c,\mathrm{ncl}}(p,q)\,, \tag{5.22}$$

and we have in particular $\bar{\lambda}_{A\bar{c}c,1}(p,q) = -2\lambda_{A\bar{c}c,1}(p,q)$ at the symmetric point. Moreover, for all momenta except those with $p\cdot q = 0$, the dressing in (5.22) has the ultraviolet limit $\lambda_{A\bar{c}c,1} \to \lambda_{A\bar{c}c,\mathrm{cl}}$ which facilitates the following discussions, while $\bar{\lambda}_{A\bar{c}c,1} \to (p\cdot q)/p^2\lambda_{A\bar{c}c,\mathrm{cl}}$. In conclusion, the transverse ghost-gluon dressing is equivalent to the classical one, whereas the longitudinal dressing is a combination of the classical and non-classical dressing. For a comparison of the dressings, see Figure 5.4 and Figure B.2.

We now proceed by parametrising the BRST and gluonic vertices in terms of transverse and longitudinal projections analogously to the parameterisation of the ghost-gluon vertex discussed above. With the anti-ghost shift symmetry of the effective action, we can relate the BRST vertices $\Gamma^{c}_{\ Q_A}$ and $\Gamma^{Ac}_{\ \ Q_A}$ to the ghost two-point and the ghost-gluon vertex. A derivation thereof can be found in Section B.2.5,

$$\Gamma^{ab}_{cQ_A,\mu}(p) = -iZ_c(p)p_\mu\delta^{ab}\,,$$

$$\Gamma^{abc}_{AcQ_A,\mu\nu}(p,q) = -f^{abc}\Big(\Pi^{\perp}_{\mu\nu}(p)\lambda_{A\bar{c}c}(p,-q-p) + \Pi^{\parallel}_{\mu\nu}(p)\lambda_{A\bar{c}c,1}(p,-q-p)\Big)\,. \tag{5.23}$$

Notably, this identity even holds diagramatically for the flows of the dressings. The other BRST two-point function and vertex are parameterised as,

$$\Gamma^{ab}_{AQ_{\bar{c}},\mu}(p) = -ip_\mu\frac{1}{\xi}\delta^{ab}\,,$$

$$\Gamma^{abc}_{ccQ_c}(p,q) = -if^{abc}\lambda_{Q_ccc}(p,q)\,. \tag{5.24}$$

In the present work we approximate the three- and four-gluon vertices with their fully dressed classical tensor structures, noted as $\tau_{A^3,\mathrm{cl}}$ and $\tau_{A^4,\mathrm{cl}}$. The purely transverse part is obtained by contracting the classical tensor structure with three and four transverse projection operators respectively. The complements now contain mixed vertices with longitudinal and transverse legs as well as a purely longitudinal part. The parts with at least three longitudinal legs do not contribute since they do not feed back into the diagrams and are therefore not included in our truncation. Thus we parameterise the gluonic vertices as,

$$\Gamma_{A^3}(p,q) = \left(\lambda_{A^3}\left(\Pi^{\perp}\right)^3 + \lambda_{A^3,1}\left(\Pi^{\perp}\right)^2\Pi^{\parallel} + \lambda_{A^3,2}\Pi^{\perp}\left(\Pi^{\parallel}\right)^2\right)\tau_{A^3,\mathrm{cl}} + \cdots$$

$$\Gamma_{A^4}(p,q,r) = \left(\lambda_{A^4}\left(\Pi^{\perp}\right)^4 + \lambda_{A^4,1}\left(\Pi^{\perp}\right)^3\Pi^{\parallel} + \lambda_{A^4,2}\left(\Pi^{\perp}\right)^2\left(\Pi^{\parallel}\right)^2\right)\tau_{A^4,\mathrm{cl}} + \cdots \tag{5.25}$$

where indices and momenta are dropped and the permutations are implicitly assumed for simplicity. The dots indicate terms with $(\Pi^{\parallel})^n\tau_{A^3,\mathrm{cl}}$ and $(\Pi^{\parallel})^n\tau_{A^4,\mathrm{cl}}$ with $n \geq 3$ as well as projections of further (non-classical) tensor structures. We emphasise that for $p\cdot q = 0$ or $p\cdot r = 0$ the parameterisation in (5.25) may lead to parameterisation singularities for the dressings, that are then seen in the respective projections of the diagrams in the functional relations. For further details on the parameterisation, see Section B.2.1. The longitudinal four-gluon vertices are approximated by their STI-values, see (5.46).

The remaining dressings are obtained from their respective fRG equations that are depicted in Figure B.6 at the symmetric point for three(four)-point functions,

$$p_i\cdot p_j = \begin{cases} p^2 & \text{for } i=j, \\ -\frac{1}{n-1} & \text{otherwise, where } n = 3(4). \end{cases} \tag{5.26}$$

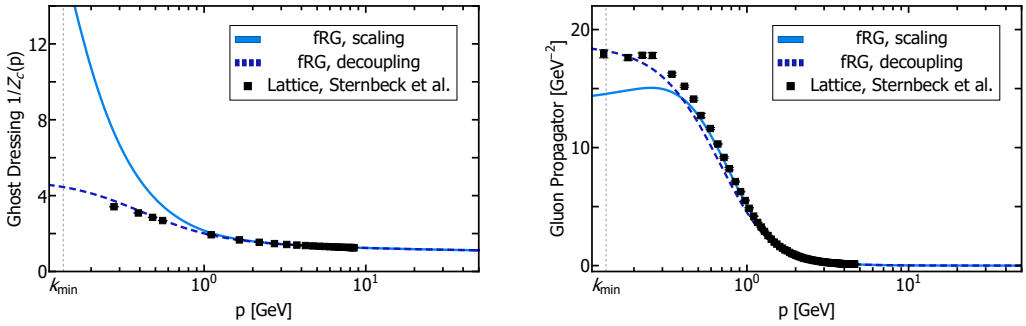

Figure 5.1.: Ghost, $1/Z_c(p)$, (left) and gluon, $1/Z_A(p)$ (right) dressing in comparison to the lattice result (dots) from [149]. The global normalization of the lattice results was fixed by our scaling solution, c.f. Section B.2.3.

For simplicity, the vertex dressings feeding back into the fRG equations are evaluated at the average momentum configuration $\lambda_i(\bar{p})$ with,

$$\bar{p}^2 = \frac{1}{n}\sum_{i=1}^{n} p_i^2 \,, \tag{5.27}$$

which has been shown to be a good approximation, see e.g. [181]. From the transverse dressings we can derive momentum dependent running couplings,

$$\alpha_{A\bar{c}c}(p) = \frac{1}{4\pi}\frac{\lambda_{A\bar{c}c}(p)^2}{Z_A(p)Z_c(p)^2} \,,$$

$$\alpha_{A^3}(p) = \frac{1}{4\pi}\frac{\lambda_{A^3}(p)^2}{Z_A(p)^3} \,,$$

$$\alpha_{A^4}(p) = \frac{1}{4\pi}\frac{\lambda_{A^4}(p)}{Z_A(p)^2} \,. \tag{5.28}$$

These vertex couplings are perturbatively two-loop degenerate, which can also be seen in our truncation, see Figure 5.2.

5.1.4. Functional Relations and Consistency Constraints

For the computation of functional relations, our choice of the Landau gauge is very efficient, since in Landau gauge Yang-Mills theory the set of all transverse functional relations is closed, i.e.

$$\Gamma^{\perp}_{(n)} = \mathrm{funRel}^{\perp}_{(n)}[\{\Gamma^{\perp}_{(m\leq n+2)}\}] \,, \tag{5.29a}$$

where $\{\Gamma^{\perp}_{(m\leq n+2)}\}$ indicates the set of all transverse correlation functions with $2 \leq m \leq n+2$. In contradistinction, the longitudinal correlation functions satisfy

$$\Gamma^{\parallel}_{(n)} = \mathrm{funRel}^{\parallel}_{(n)}[\{\Gamma^{\parallel}_{(2<m\leq n+2)}\}, \{\Gamma^{\perp}_{(m\leq n+1)}\}] \,, \tag{5.29b}$$

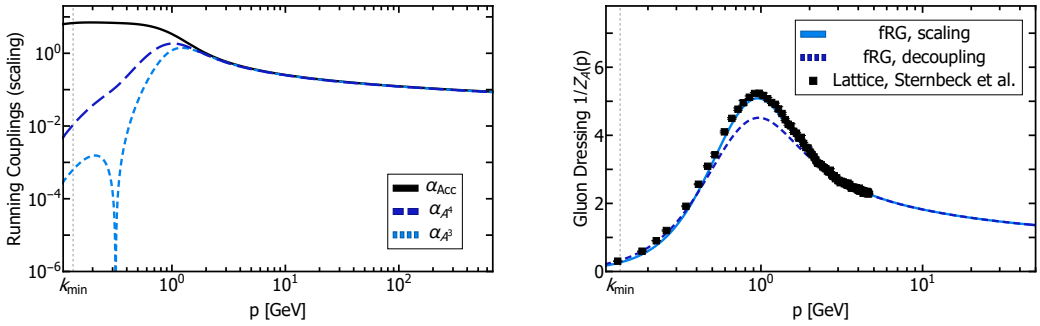

Figure 5.2.: Left: Running couplings as defined in (5.28) obtained from different Yang-Mills vertex dressings. Right: Scaling and decoupling gluon propagator in comparison to the lattice result from [149]. The global normalization of the lattice results was fixed by our scaling solution, c.f. Section B.2.3.

Equation (5.29a) follows from the fact that the gluon propagator G_A as well as $(G\,\dot{R}\,G)_{AA}$ are transverse in the Landau gauge and hence so are all internal legs. Also, the propagator only depends on $\Gamma^{\perp}_{(2)}$. The structure (5.29) applies to fRG equations and DSEs, for more details see [35, 37, 64, 94].

The mSTIs in (5.11) involve longitudinal and transverse correlation functions, and they are similar to (5.29b) with,

$$\Gamma^{\parallel}_{(n)} = \mathrm{mSTI}_{(n)}[\{\Gamma^{\parallel}_{(2<m\leq n+2)}\},\{\Gamma^{\perp}_{(m\leq n+1)}\}]\,. \tag{5.30}$$

Note that (5.30) constitutes yet another tower of functional relations for longitudinal correlation functions. Naturally, as for truncated towers of fRG equations and DSEs its solution for a given truncation will in general differ from both, the solution of the longitudinal fRG equations and the longitudinal DSEs (or any other tower of longitudinal functional relations). Moreover, for a finite set of longitudinal and transverse correlation functions, one may simply use the (m)STI for computing the longitudinal correlation functions. Such a scheme trivially builds in gauge consistency by construction. Naturally, the longitudinal correlation functions will then in general not satisfy the respective fRG equations or DSEs. In conclusion, it is not the violation of the mSTI alone, which comprises the information about gauge consistency, but the combination of all functions relations.

However, even though (5.30) is very similar to the fRG equations and DSEs for the longitudinal dressings, there is an important structural difference which is most apparent in the Landau gauge limit: while (5.29a) and (5.29b) only depend on the transverse part of the regulator, the mSTI (5.30) depends on the longitudinal part for regulators whose longitudinal part diverges with $1/\xi$. A natural class of regulators with this property are *RG-adapted* or spectrally adapted regulators, see [115, 182]. In this case, the regulators are proportional to the full dispersion of the respective field, which is detailed in Section B.2.2. This choice ensures, that the effective action in the presence of the regulator has the underlying RG-invariance of the full theory at vanishing regulator, hence the name *RG-adapted*. Specifically, the longitudinal part of the gluon regulator reads

$$(R_A)^{\parallel,ab}_{\mu\nu}(p) = \delta^{ab}\Pi^{\parallel}_{\mu\nu}(p)\Gamma^{\parallel}_{AA}(p)\,r\left(\frac{p^2}{k^2}\right)\,. \tag{5.31}$$

The class of regulators with (5.31) leads to

$$\lim_{\xi\to 0} p_\mu (G_{AA} R_A)_{\mu\nu} = p_\nu \frac{r_A}{1+r_A}(p^2/k^2)\,, \tag{5.32}$$

and hence one of the internal lines in the mSTI diagrams has a longitudinal part. In turn, for gluon regulators with a regular longitudinal part we have

$$p_\mu (G_{AA} R_A)_{\mu\nu} \propto \xi p_\nu\,, \tag{5.33}$$

and hence all internal lines are transverse in the Landau gauge. Then, the mSTI has the same structure as (5.29b) in terms of contributing correlation functions.

Interestingly, the fRG equations and DSEs (in the presence of a regulator), (5.29), are the same in the Landau gauge limit for regulators with either (5.32) or (5.33). However, it can be shown, that the contributions of the longitudinal part of the propagator (5.32) do not cancel in the mSTI. In particular, the gluon mass m_k^2 from the STI only receives contributions from the longitudinal part of $(R_k G)_{AA}$. In conclusion, only for gluon regulators whose longitudinal part contains the gauge fixing term $1/\xi p^2 r(p^2/k^2)$, the mSTI gluon mass and that from the fRG flow equation or DSE agree, and the implicit assumption of k-independence of the renormalisation procedure is self-consistent. This intricacy emphasises the importance of gauge consistency of the regularisation procedure. The comparison of functional mSTI and fRG/DSE always allows us to choose a longitudinal regulator $R_A^{\parallel}$ such that all functional relations are compatible. However, this also implies that gauge consistency of truncated fRG flows or DSEs should rather be checked with a set of correlation functions and not a single one.

In summary, throughout this work we will use *RG-adapted* regulators (5.31), which are also *gauge consistent*, as discussed above. A more detailed study of this intricacy and the general regulator (shape) dependence is still under investigation and will be published elsewhere.

We conclude this section with two remarks. Firstly, for regular correlation functions, one can use the STIs for also extracting a part of the respective transverse correlation functions. Loosely speaking, regularity implies

$$|\partial_{p_i} \Gamma_{(n)}| < \infty\,, \tag{5.34}$$

in which case the longitudinal and transverse parts are linked. However, in the present case of Yang-Mills theories, it can be shown that regular correlation functions are at odds with confinement. In turn, in perturbation theory, one can show that the regularity assumption holds true. Indeed, it is also related to the identification of running couplings (5.28). This adds yet another layer of complexity to the current situation: for perturbative and semi-perturbative momenta regularity holds true and we should see the respective relations between longitudinal and transverse correlation functions.

In summary, this leaves us with the necessity as well as a large variety of non-trivial consistency checks. We also emphasise that great care is needed in the interpretation of violations of the mSTI or alternatively of other functional relations for longitudinal correlation functions within truncations.

5.1.5. Confinement

Confinement describes the effect that no coloured particles can be detected directly by experiments, i.e. the absence of coloured states from the physical asymptotic spectrum

of our theory. It is fundamentally linked to the non-abelian gauge group of QCD. Thus first investigations thereof may already be carried out in Yang-Mills theory. One possible mechanism for confinement has been proposed by Kugo and Ojima [183].

The Kugo-Ojima confinement scenario can generally be broken down into three criteria. First, if we have a global, non-perturbative BRST charge, i.e. unbroken BRST symmetry, it can be used to construct the physical state space $\mathcal{H}_{phys}$. Second, if the global colour charge is unbroken, $\mathcal{H}_{phys}$ only contains colourless states. And third, the cluster decomposition principle has to be violated in the total state space $\mathcal{H}$, but not in $\mathcal{H}_{phys}$.

For the latter, it has already been argued in [184] that this is indeed fulfilled in the covariant operator formulation of QCD.

From the second criterion, we can deduce direct implications for our infrared (IR) Green's functions. It can be shown that this requires an IR enhancement of the ghost propagator. This yields a unique IR renormalization condition. We shall refer to this as the *scaling* solution. This enhancement is accompanied by a dynamical creation of a gluon mass,

$$\lim_{p\to 0} Z_c(p^2) \propto (p^2)^{\kappa}\,,$$
$$\lim_{p\to 0} Z_A(p^2) \propto (p^2)^{-2\kappa}\,, \tag{5.35}$$

with $1/2 < \kappa < 1$.

There are furthermore two other solutions that are studied in this work: the *decoupling* solution, which is the confining solution with the smallest dynamically created gluon mass $m^2_{\perp,k_{min}}$, and massive solutions to which we will also refer to as *Higgs* solutions. The Higgs solutions exhibit an explicit gluon mass and break global color symmetry. Both, Higgs and the decoupling solution break BRST symmetry, [35, 185]. An investigation of the different solutions within our setup can be found in Section 5.2.5. The full range of solutions, in terms of the mass value $m^2_{\perp,k_{\min}}$, can be found in Figure 5.5, where also our choice of scaling and decoupling and the Higgs solution that was investigated is indicated.

The IR behaviour of the decoupling and Higgs solution is characterized by

$$\lim_{p\to 0} Z_c(p^2) \propto 1\,,$$
$$\lim_{p\to 0} Z_A(p^2) \propto (p^2)^{-1}\,. \tag{5.36}$$

The scaling exponents obtained from our results can be found in (B.17).

More details on confinement in general and on the investigation of the different solutions can be found in [37, 71].

5.2. Numerical Results

In this work, we solve the transverse sector of Yang-Mills correlation functions self-consistently in Landau gauge. In addition to that, we compute the longitudinal and BRST dressings from the fRG and from the mSTI. We proceed by comparing the results obtained with both approaches. All momentum-dependent equations are computed at the symmetric point.

5.2.1. Solving the Transverse Sector from the fRG

As stated in Section 5.1.4, the transverse sector of Yang-Mills theory is closed in Landau gauge. Thus, we have a closed system of momentum-dependent self-consistent coupled differential equations that can be solved.

The mSTI requires a non-zero gluon mass $m^2_{\perp,\Lambda}$ at the cutoff. The exact value is uniquely fixed by demanding a scaling or decoupling type solution.

The constant initial values of the vertex dressings are tuned such that the respective couplings are perturbatively degenerate at $k = k_{min}$, i.e. fulfill the two-loop exact relation from (5.28) thus rendering only the initial value of the ghost-gluon dressing a free parameter. It is chosen to be $\lambda_{A\bar{c}c,\Lambda}(p) = 1$ at the cutoff.

The vertex dressings of the three(four)-point functions generally depend on two(three) momentum variables. To reduce the numerical effort we approximate the momentum dependencies of the dressings to one variable, which we chose to be the average momentum $\bar{p}$ at the symmetric point, see (5.27). The symbolic equations for these quantities can be found in figure Figure B.6 and were derived with *QMeS-Derivation* [1, 2].

The explicit form of the projection operators utilized to project onto the transverse, classical tensor structures are given in Section B.2.1. However, it is worth mentioning, that even after projecting, other tensor structures still enter the diagrammatic equations and thus contribute to the functional equations. We approximate their dressing functions with the transverse, classical dressing.

The results for the transverse correlation functions obtained from this setup are shown in Figure 5.1 and Figure 5.2. The scale was set using the shown lattice computation and more details regarding the scale setting and global normalization can be found in Section B.2.3.

One can see that the couplings are degenerate for scales $2 \ll p \ll \Lambda$ GeV. In this region, the correlation functions from the scaling and decoupling solution also agree very well with the lattice result. At smaller momenta, the results are not comparable due to the different gauge fixing procedures on the lattice and in functional computations, see e.g. [186**?**]. When comparing the gluon propagator dressing in Figure 5.2 however, one can see that the scaling solution matches the lattice results at intermediate scales $p \approx 1\,\text{GeV}$ much better than the decoupling solution.

5.2.2. BRST and Longitudinal Yang-Mills Sector from the fRG

The BRST symmetric Yang-Mills action additionally contains source terms Q_i coupled to the respective BRST transformations of the fields. These vertices are fully dressed objects, see Section 5.1.3. BRST symmetry, and thus the mSTIs, relate the longitudinal parts of vertex functions to themselves and the transverse parts, see (5.30).

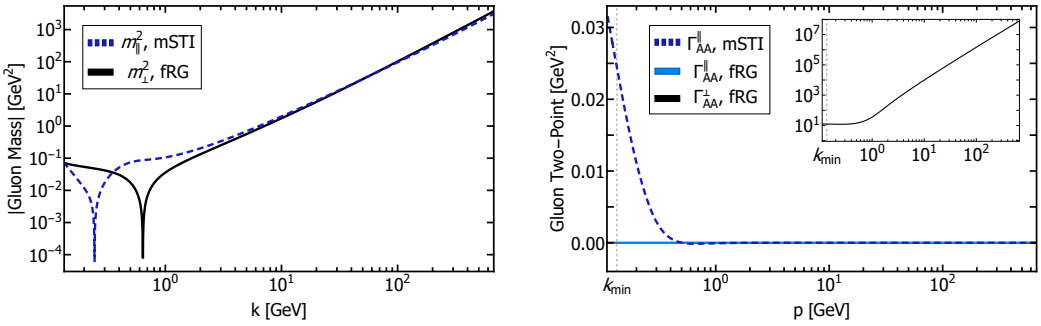

Figure 5.3.: Left: Transverse (solid black) and longitudinal (solid green) gluon mass from the fRG and longitudinal (dashed dark green) gluon mass from the mSTI over k. Right: Transverse (solid black) and longitudinal (solid green) gluon two-point from the fRG and longitudinal (dahsed dark green) gluon two-point from the mSTI at $k = k_{min}$ over p.

Thus for a self-consistent check of the (m)STIs we also need to compute the longitudinal and BRST dressings from the fRG. The symbolic equations were also derived using *QMeS-Derivation* and can be found in Figure B.6. Again, the average momentum approximation at the symmetric point (5.27) was used to simplify the momentum-dependence of the vertex dressings.

Diagrammatically, the fRG equations of the transverse and longitudinal quantities are identical, the vertices contributing in the diagrams are however different. As an illustrative example of how the vertex contributions differ, see Section B.3.1, where we derive the transverse and longitudinal one-loop gluon mass from the fRG and mSTI.

The projection procedure for the derivation of longitudinal fRG equations can be found in Section B.2.1.

We can immediately see that the three-gluon dressing with one longitudinal leg vanishes at the symmetric point,

$$\dot{\lambda}_{A^3,1} \propto \mathcal{P}^{abc}_{A^3,1,\mu\nu\rho}(p,q)\dot{\Gamma}^{abc}_{A^3,\mu\nu\rho}(p,q) = 0\,, \tag{5.37}$$

rendering this dressing RG-invariant, $\lambda_{A^3,1,k}(p) \equiv \lambda_{A^3,1,\Lambda} \equiv \lambda_{A^3,\Lambda}$. We use the same initial values for the longitudinal dressings as for the transverse ones. As the longitudinal gluon two-point function does not feed back into the flows, its initial value is chosen as, $\Gamma^{\parallel}_{AA,k_{min}}(p) = 0$.

Generally, the longitudinal fRG equations are coupled to the transverse sector and to themselves, see Section 5.1.4. However, due to the non-running of the three-gluon vertex dressing with one longitudinal leg, the equations decouple hierarchically and we can solve them successively. Explicitly (and omitting the transverse sector) one can write,

$$\begin{aligned}
\dot{\lambda}_{A\bar{c}c,1}(p) &= \mathrm{fRG}\left[\lambda_{A\bar{c}c,1}, \lambda_{A^3,1}\right]\,, \\
\dot{\lambda}_{A^3,2}(p) &= \mathrm{fRG}\left[\lambda_{A\bar{c}c,1}, \lambda_{A^3,1}, \lambda_{A^4,1}, \lambda_{A^4,2}\right]\,, \\
\dot{\Gamma}^{\parallel}_{AA}(p) &= \mathrm{fRG}\left[\lambda_{A\bar{c}c,1}, \lambda_{A^3,1}, \lambda_{A^4,2}\right]\,,
\end{aligned} \tag{5.38}$$

with momentum arguments on the right-hand side dropped for simplicity.

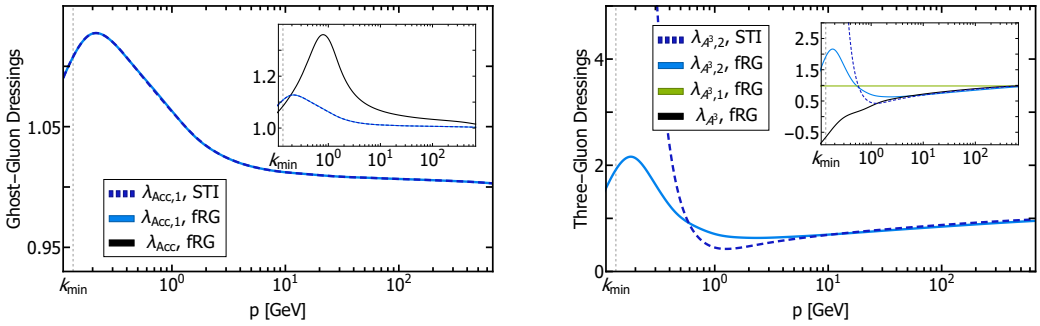

Figure 5.4.: Left: Transverse (solid black) and longitudinal (solid blue) ghost-gluon dressings from the fRG and longitudinal (dashed dark blue) ghost-gluon dressing from the STI at $k = k_{min}$ over p. Right: Transveral (solid black) and longitudinal (solid blue) three-gluon dressings from the fRG and longitudinal (dashed dark blue) three-gluon dressing from the STI at $k = k_{min}$ over p.

One can see that the longitudinal two-point function does not feed back into the flows.

We solve the above system self-consistently while using the STI expressions (5.46) for the longitudinal four-gluon dressings.

With this at hand, we obtain the longitudinal fRG dressings that are shown in Figure 5.3 and Figure 5.4. A discussion thereof can be found in Section 5.2.4.

We furthermore compute the BRST dressings from the fRG. Due to the shift symmetry identity that allows for the identification of the Z_{cQ_A} and λ_{AcQ_A} with the ghost and ghost-gluon dressing, see Section B.2.5, one is only left with one dressing, λ_{Q_ccc}. We show in Section 5.2.3.2 that this dressing is also related to the longitudinal ghost-gluon dressing.

5.2.3. Modified Slavnov-Taylor Identitites

We proceed by inserting the fRG results into the (m)STI equations. This gives us a non-trivial consistency check of our solution.

Numerically, it is not feasible to integrate the equations down to exactly zero, rendering a small, yet finite cutoff $k_{\min} = 0.135\,\mathrm{GeV}$. Consequently, we must not check the consistency of our results with the STIs but rather with the mSTIs. In the following we will refer to expressions of the general form $STI - Diagrams \stackrel{!}{=} 0$ as mSTIs, where the $Diagrams$ are the one-loop diagrammatic corrections of the STI due to the BRST symmetry breaking cutoff terms (5.11). The symbolic equations can be found in Figure B.7.

In this section, we will present the STIs within our truncation. For the derivation procedure and the diagrammatic contributions, see Section B.3.

All (m)STIs are evaluated at the symmetric point (5.26) and the dressings are computed on the average momentum configuration (5.27).

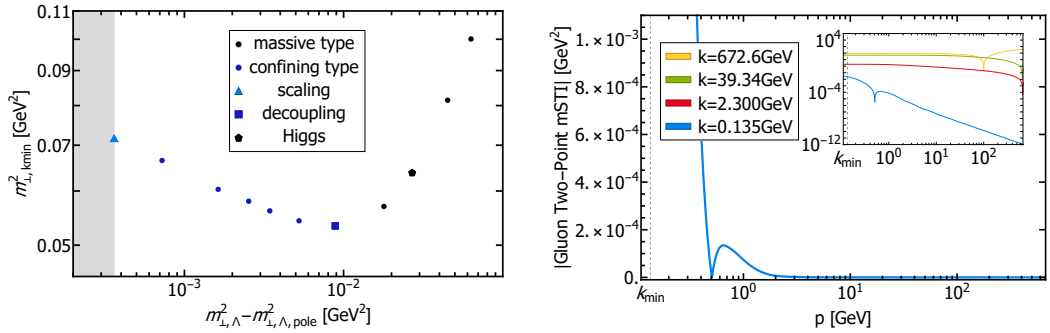

Figure 5.5.: Left: Gluon Mass $m^2_\perp$ at $k = k_{min}$ from different fRG solutions. The black markers correspond to Higgs type and the blue markers to confining solutions, where the lighter blue triangle indicates the scaling solution and the dark blue circle the decoupling solution that were used for further investigations throughout this work. The definition of the gluon mass is given in Section B.2.2. The grey area indicates the unphysical region characterised by Landau-pole-like singularities. Right: Absolute value of the gluon two-point mSTI for different values of k over p.

5.2.3.1. Gluon Two-Point and Gluon Mass STI

The STI for the longitudinal gluon two-point function is,

$$\Gamma^{\parallel}_{AA,\mathrm{reg}}(p) = 0\,. \tag{5.39}$$

This also renders the longitudinal gluon mass zero,

$$m^2_{\parallel} = \Gamma^{\parallel}_{AA}(p=0) = 0\,. \tag{5.40}$$

A few more technical details can be found in Section B.2.2 and the quantities are shown in Figure 5.3.

5.2.3.2. Ghost-Gluon STI

The STI for the ghost-gluon vertex relates the longitudinal part of ghost-gluon vertex to the BRST projected vertex $Q_c cc$. The relation in our truncation reads,

$$2p_\mu \Gamma_{A\bar{c}c,\mu}(p,q) Z_c(p) + q^2 \Gamma_{ccQ_c}(p,-p-q) Z_c(q) = 0\,. \tag{5.41}$$

Thus we can derive the STI for the respective dressings at the symmetric point,

$$\lambda_{A\bar{c}c,1}(p) - \lambda_{Q_c cc}(p) = 0\,. \tag{5.42}$$

A formulation of the ghost-gluon STI in terms of the classical and non-classical tensor basis is presented in Section B.3.2. The respective dressings are depicted in Figure 5.4 and Figure B.2.

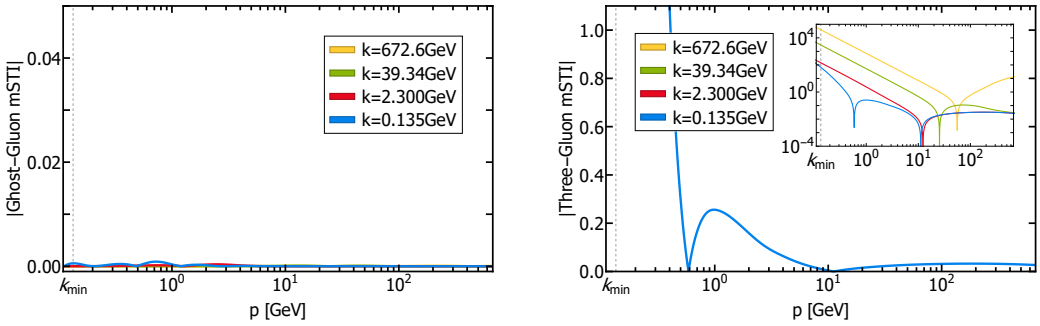

Figure 5.6.: Left: Absolute value of the ghost-gluon mSTI measure for different values of k over p. Right: Absolute value of the three-gluon mSTI measure for different values of k over p.

5.2.3.3. Three-Gluon STI

The STI for the three-gluon vertex with two longitudinal legs is,

$$\lambda_{A^3,2}(p) - \frac{Z_A(p)}{Z_c(p)}\lambda_{Q_c cc}(p) = 0\,. \tag{5.43}$$

After applying the ghost-gluon STI and dividing by propagator dressings, one obtains the well-known perturbative relation for the couplings,

$$\frac{\lambda^2_{A^3,2}(p)}{4\pi Z^3_A(p)} = \frac{\lambda^2_{A\bar{c}c,1}(p)}{4\pi Z_A(p) Z^2_c(p)}\,. \tag{5.44}$$

This is a valid approximation as is shown in Section 5.2.4.3 and Figure 5.6.

For the three gluon vertex with only one longitudinal leg, there exits no STI, since this projection has no overlap with the classical tensor structure. The dressings are shown in Figure 5.4.

5.2.3.4. Four-Gluon STI

The four-gluon STI relates different longitudinal four-gluon dressings to longitudinal and transverse three-gluon and ghost-gluon dressings. We have again used the ghost-gluon STI (5.42) and obtain at the symmetric point,

$$\lambda_{A^4,1}(p) - \frac{1}{Z_c(p)}\lambda_{A\bar{c}c}(\frac{\sqrt{10}}{3}p)\lambda_{A^3}(\frac{\sqrt{10}}{3}p) = 0\,, \tag{5.45}$$

$$\lambda_{A^4,2}(p) - \frac{32}{33Z_c(p)}\lambda_{A\bar{c}c,1}(\frac{\sqrt{10}}{3}p)\lambda_{A^3}(\frac{\sqrt{10}}{3}p) - \frac{1}{33Z_c(p)}\lambda_{A\bar{c}c}(\frac{\sqrt{10}}{3}p)\lambda_{A^3,1}(\frac{\sqrt{10}}{3}p) = 0\,.$$

It is worth mentioning that the STIs at the symmetric point are quite different from the ones usually present in the literature, as e.g. in (5.28).

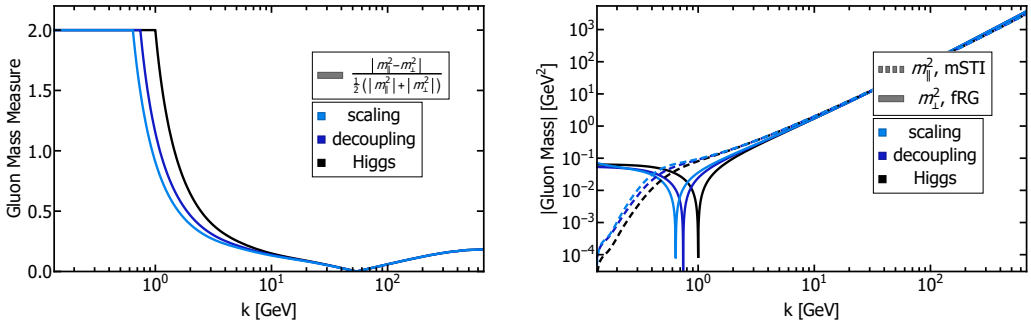

Figure 5.7.: Left: Gluon mass measure for the longitudinal mass from the mSTI the transverse mass from the fRG for different solutions over k. Right: Transverse (solid lines) gluon mass from the fRG and longitudinal (dashed lines) gluon mass from the mSTI for different solutions over k.

5.2.4. Discussion

We can now proceed by comparing the longitudinal results of different correlation functions obtained from the fRG and mSTI approach.

5.2.4.1. Longitudinal Gluon Mass

The longitudinal mSTI mass, $m_{\parallel}^2$, and the transverse fRG mass, $m_{\perp}^2$ exhibit the same running for large k which is shown in Figure 5.3. This is in good agreement with the one-loop running, which is the same for both masses, for further details, see Section B.3.1. At the scale $k \approx 5\,\text{GeV}$ however, they split, which is most likely due to the difference in the IR of the longitudinal and transverse vertices, cf. Figure 5.4. For $k = k_{min}$ the value of both masses agrees again, meaning the longitudinal mass shows the same scaling behaviour as the transverse mass. The STI, (5.40), however, should render the longitudinal gluon mass zero. This deviation therefore might stem from our truncation in the vertex sector in the fRG equations, more precisely in the pure gluon sector, see Section 5.2.4.2. Another plausible explanation would be IR cutoff effects, however, differentiating the two is currently not feasible.

5.2.4.2. Longitudinal Gluon Two-Point Function

The solution of the longitudinal two-point fRG equation constitutes the simplest case possible since neither the longitudinal two-point nor the longitudinal propagator does anyhow feed back into the diagrams in Landau gauge. This means that a solution can be obtained by simply integrating the equation over the cutoff k and choosing the initial condition for $\Gamma^{\parallel}_{AA,\mu\nu,\text{reg},\Lambda}(p)$ such, that one obtains zero for the evaluated integral. Thereby one not only solves the fRG equation but also satisfies the (m)STI at k_{min}.

By comparing the longitudinal gluon two-point from the fRG and from the mSTI, one can see that they do not agree well on all scales k, see Figure 5.3 and Figure 5.5. They are only identical at $k = k_{min}$ for $p \gtrsim 0.5\,\text{GeV}$. For small momenta one can see a deviation of order $\mathcal{O}(10^{-}2\,\text{GeV}^2)$. Albeit small, the deviation is qualitatively similar to the deviation in the three-gluon mSTI, Figure 5.6. Since the longitudinal three-gluon dressing enters the mSTI equation for the gluonic two-point, but not vice versa, one can therefore conclude,

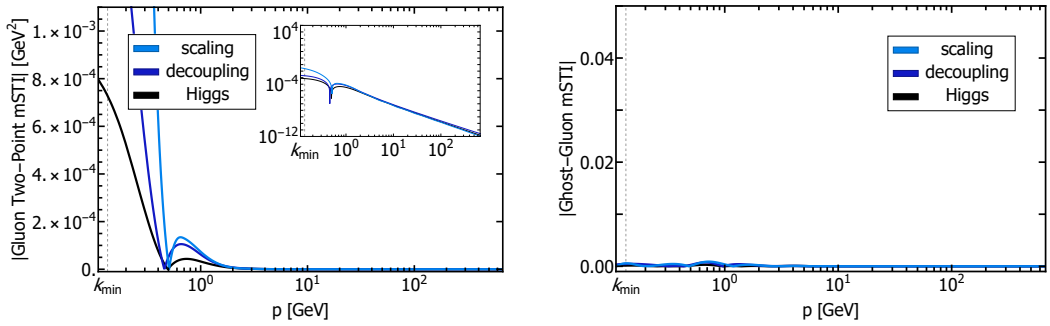

Figure 5.8.: Left: Absolute value of the two-gluon mSTI measure for different solutions over p. Right: Absolute value of the ghost-gluon mSTI measure for different solutions over p.

that both deviations are due to the truncation of the fRG equation for the longitudinal three-gluon and four-gluon dressing.

5.2.4.3. Longitudinal Ghost-Gluon Dressing

In a general covariant gauge, only $\lambda_{A\bar{c}c}$ requires renormalisation. The non-classical dressing $\lambda_{A\bar{c}c,ncl}$ vanishes for large momenta. The non-classical dressing obtained from the fRG and mSTI is depicted in Figure B.2.

We can see that our results fulfill this property perturbatively since the non-classical dressing is approximately zero for large momenta, $p \gg 5\,\mathrm{GeV}$. In the infrared, it is however non-trivial. It is worth mentioning that the longitudinal and transverse ghost-gluon dressings do not agree well at any momentum scale p. From Figure 5.4, Figure 5.6 and Figure B.2 we can see that the mSTI and fRG dressing agree perfectly for all momenta p implying that there is a non-trivial cancellation of diagrams within the two functional approaches. Indeed, Figure 5.6 merely depicts the numerical accuracy of our computation. The (m)STI already holds true at the level of fRG equations, c.f. Figure B.6: The diagrams contributing to the flow of the longitudinal ghost-gluon dressing that contain three-gluon vertices cancel non-trivially. The remaining diagrams are equivalent if the ghost-gluon STI is fulfilled at the cutoff $k = \Lambda$.

This non-trivial result implies BRST symmetry being conserved by the respective fRG computation and thus strongly hints at gauge invariance of our setup.

5.2.4.4. Longitudinal Three-Gluon Dressing

The results for the different three-gluon dressings are shown in Figure 5.4. As demonstrated in (5.37) the three-gluon dressing with one longitudinal leg, $\lambda_{A^3,1}$, does not run. One can see that the dressing with two longitudinal legs from the fRG agrees with the transverse fRG dressing, λ_{A^3}, and the longitudinal STI dressing for large momenta $p \gg 5\,\mathrm{GeV}$. The longitudinal STI dressing and the transverse fRG dressing however agree up to even smaller scales $p \gg 1.5\,\mathrm{GeV}$. In the infrared one can observe that the general behaviour of the longitudinal fRG and STI dressings agree. The STI dressing diverges for $p \to 0$ whereas the fRG dressing forms a maximum at $p \approx 0.2\,\mathrm{GeV}$. The minimum of both dressings is given at approximately the same momentum, $p \approx 1\,\mathrm{GeV}$.

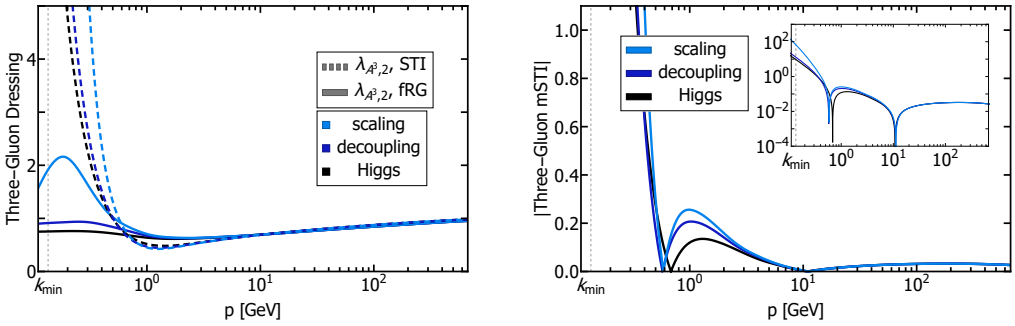

Figure 5.9.: Left: Longitudinal three-gluon dressing $\lambda_{AAA,2}(p)$ from the fRG (solid lines) and from the STI (dashed lines) for different solutions. Right: Absolute value of the three-gluon mSTI measure for different solutions over p.

In contrast to that, the transverse dressing gets smaller and even becomes negative for $p \to 0$. Thus we can observe a clear splitting between the transverse and longitudinal sector in both approaches which is due to the different contributions of longitudinal and transverse vertices in transverse and longitudinal functional equations.

The slight deviation in the UV can be explained by the logarithmic finetuning procedure: we have chosen the same initial values for the longitudinal and transverse dressings. The contributions on the level of correlation functions to the flows are however different. By choosing different (constant) initial values for the longitudinal dressings at the cutoff it is nevertheless possible to generate a better agreement of the dressings in the UV at $k = k_{min}$.

As stated in the previous section, the three-gluon mSTI shows a deviation at $p \approx 5\,\text{GeV}$. This might be due to the fact that we did not include a full tensor basis of the gluonic sector and even approximated the longitudinal four-gluon dressings with their STI values in the fRG equation of the three-gluon vertex.

For momenta $p > 5\,\text{GeV}$, the three-gluon mSTI is however fulfilled, where the small deviation for very large momenta stems from the tuning procedure, as described before.

5.2.5. Discussion of Different Solutions

In this section, we present a comparison of the mSTIs for different types of solutions, i.e. the scaling, decoupling, and a Higgs type solution, that are highlighted amongst the range of solutions in figure Figure 5.5.

Studying the gluon mass measure in Figure 5.7,

$$\frac{|m_\parallel^2 - m_\perp^2|}{\frac{1}{2}(|m_\parallel^2| + |m_\perp^2|)}\,, \tag{5.46}$$

where the longitudinal mass is obtained from the mSTI and the transverse mass from the fRG, one can see that all three solutions fulfill the measure equally well up until $p \approx 20\,\text{GeV}$. There, the Higgs solution starts to deviate. It is expected that for a more massive Higgs solution, the deviation starts at an even larger momentum scale p. Vice versa, the scaling solution fulfills the measure up to smaller scales than the decoupling solution.

The ghost-gluon mSTI is fulfilled for all three types of solutions, the small deviations shown in Figure 5.8 simply depict the numerical precision in the computation.

Generally, we do not expect the mSTIs to be fulfilled for scales $p \ll 1\,\mathrm{GeV}$, since non-classical vertices and tensor structures that were not taken into account in our truncation, contribute significantly in this regime. We furthermore expect IR cutoff effects contributing below this scale, being within one order of magnitude of k_{min}.

However, we can clearly see a divergence in the gluon two-point, Figure 5.8, and three-point mSTI, Figure 5.9, for momenta $p \ll 1\,\mathrm{GeV}$. This singularity could be related to resonances and is most distinct in the scaling solution.

Comparing the longitudinal three-gluon dressing $\lambda_{A^3,2}$ from the fRG and from the STI for different types of solutions, one can see that the scaling solution yields the best qualitative agreement of the dressings.

5.3. Conclusion

We have studied gauge symmetry in Landau gauge Yang-Mills theory with functional methods where gauge invariance was implemented via BRST symmetry. We have self-consistently computed a set of momentum-dependent transverse and longitudinal correlation functions from the functional Renormalisation Group (fRG) for different (non-) confining solutions and compared the transverse results to lattice and Dyson-Schwinger computations. We have furthermore computed longitudinal correlation functions from the (modified) Slavnov-Taylor identities (mSTI) on the basis of the above results. They show good agreement with the respective longitudinal fRG results hinting at gauge consistency of our setup.

6. Glueball Masses from the fRG

This section is based on the work that will be presented in [4].
An interesting consequence of the non-Abelian nature of Yang-Mills theory is the existence of hadronic states that consist of gluons only. The masses of the different so-called glueballs have been studied extensively in lattice computations [187–191]. First computations of glueball masses with functional methods, especially Dyson-Schwinger equations (DSE), have been made possible with the treatment of bound states via Bethe-Salpeter equations (BSE) [45, 46], see e.g. [192–196]. An overview of the topic is given in e.g. [68, 197]. For approaches with other methods, see e.g. [198–208].

In the following, we put forward a self-consistent approach of extracting the scalar ($J^{PC} = 0^{++}$) and pseudo-scalar ($J^{PC} = 0^{-+}$) glueball mass from a Euclidean fRG computation in Landau gauge Yang-Mills theory, based on the results presented in the previous Chapter 5. We obtain the glueball spectral functions via Padé approximants [209, 210] and via Gaussian Process Regression (GPR) [211] of the Euclidean correlator data. For a review of the latter, see e.g. [212].

In Section 6.1 we introduce the spectral representation of Euclidean dressing functions, as well as Padé approximants (Section 6.2) and GPR (Section 6.3), and discuss the preliminary spectral functions from both approaches in Section 6.4 where we also compare the reconstructed dressings to the fRG dressing. The thereby obtained preliminary scalar and pseudo-scalar glueball masses are then compared to lattice computations, DSE-BSE results as well as results from other approaches. We conclude in Section 6.5 by summing up our findings and hinting at future improvements of the procedure. Chapter C contains additional details on the numerical computation.

6.1. Spectral Representation

In the previous chapter, we have solved truncated Yang-Mills theory in Euclidean space-time. To have access to quantities like transport coefficients, pole masses, and decay rates, it is however necessary to access Minkowski space. This can be either done by solving the (functional) equations directly in real-time formalism, as was put forward by, e.g. [213, 214], via the Schwinger-Keldysh closed time-path in the fRG [162, 215], or by finding a spectral representation of the correlation functions obtained in Euclidean space-time, see e.g. [216, 217] for examples in QCD. The existence of such a spectral representation follows as a direct consequence of locality of the underlying quantum field theory [218–220].

The latter approach and different methods to obtain the spectral density will be discussed in the following chapters.

6.1.1. Källén-Lehmann Spectral Representation

The relation between a general Euclidean propagator $G(p)$ and its spectral function $\rho(\omega)$ is given by the Källén-Lehmann representation [221, 222],

$$G(p_0, |\vec{p}|) = \int_0^\infty \frac{d\lambda}{\pi} \frac{\lambda \rho(\lambda, |\vec{p}|)}{p_0^2 + \lambda^2} \,. \tag{6.1}$$

The existence of a spectral function fulfilling (6.1) consequently constrains all non-analyticities of the propagator to the real momentum axis. Therefore one can obtain the spectral function by evaluating the propagator at real frequencies,

$$\rho(\omega) = 2 \lim_{\epsilon \to 0^+} \text{Im } G(-i(\omega + i\epsilon)) \,, \tag{6.2}$$

where the spatial momentum was set to zero, since in the vacuum, one can restore the full phase space from Lorentz symmetry.

On the level of propagators, the spectral function contains the energy spectrum of the theory, as the Källén-Lehmann representation (6.1) can be derived from the sum over energy eigenstates, see e.g. [92].

6.1.2. Spectral Representation of the Four-Gluon Vertex Dressing

Spectral representations of higher order n-point functions, with $n > 2$ are not uniquely defined, due to the dependence of the dressings on $n - 1$ momenta. However for single (momentum) exchange channels one can find a representation similar to (6.1),

$$\lambda_{A^4}(p) = \lambda_{A^4,\Lambda} + \int_\lambda \frac{\lambda \rho_{A^4}(\lambda)}{p^2 + \lambda^2} \,, \tag{6.3}$$

where $\int_\lambda = \int_0^\infty \frac{d\lambda}{\pi}$ and where we have split the full four-gluon vertex as,

$$\Gamma^{abc}_{A^4,\mu\nu\rho\sigma}(p, p, -p, -p) = \sum_i \tau^{(i),abc}_{A^4,\mu\nu\rho\sigma}(p, p, -p, -p) \lambda^{(i)}_{A^4}(p) \,, \tag{6.4}$$

with dimensionless tensor structures $\tau^{(i),abc}_{A^4,\mu\nu\rho\sigma}(p, p, -p, -p)$ and where the dressing is evaluated at the average momentum configuration, see Section C.1.2 for details.

The constant part $\lambda_{A^4,\Lambda}$ has to be separated since it does not have a spectral representation.

This is in accordance with a Hubbard-Stratonovich [223, 224] transformation, where the channel is treated in analogue to an exchange of a particle, i.e. a propagator.

Then the relation between the full vertex and the spectral function is,

$$\rho_{A^4}(\omega) = 2 \lim_{\epsilon \to 0^+} \text{Im } \lambda_{A^4}(-i(\omega + i\epsilon)) \,. \tag{6.5}$$

Thus the four-gluon dressing in an s-channel approximation contains information about the exchange of a glueball.

6.1.3. Ill-Conditioning of the Analytic Continuation

Without further assumptions about the complex structure the analytic continuation in (6.2) and (6.5) is ill-conditioned [225, 226]. Technically the Euclidean correlation functions are given as numerical data, i.e. with finite numerical precision and accuracy and usually over a discretized momentum grid p_i with $i = 1, \ldots, N$.

Generally, different spectral functions may fulfill the Källén-Lehmann representation (6.1) of the Euclidean correlator point-wise on the momentum grid p_i.

This ambiguity of different spectral representations leading to equivalent Euclidean correlation functions. This range of possible spectral functions can be reduced by implementing further constraints on the spectral function, like the asymptotic behavior or normalization and positivity of spectral representations of asymptotic states.

Different approaches suitable for the numerical solution of inverse problems have been used to obtain a spectral representation, such as Bayesian inference techniques [216, 227–229], neural networks [230–235], and others approaches, see e.g. [236–245].

The approach via Padé approximants has been used in e.g. [225, 246–248] and a first application of GPR to inverse problems has been put forward in [249] and a computation of spectral functions in Yang-Mills propagators was presented in [217].

6.2. Padé Approximants

Obtaining a spectral representation of Euclidean correlation functions via Padé approximants [209, 210] is based on expressing the correlator in terms of a rational function [225],

$$R_{n,m}(p) = \frac{P_n(p)}{Q_m(p)} \tag{6.6}$$

where $P_n(p)$ and $Q_m(p)$ are polynomials of order n and m in the Euclidean frequency p_0. One then obtains the spectral function by analytically continuing the rational function via (6.2).

To obtain a stable analytic continuation, one chooses the order of polynomials as either, (n, n) or $(n-1, n)$. For the reconstruction of data via N data points one therefore chooses a rational function of order $(\frac{N-1}{2}, \frac{N-1}{2})$ if N is an odd number, or $(\frac{N}{2}-1, \frac{N}{2})$ if N is even.

For the Padé approach to yield meaningful results, the Euclidean data must not have any non-analyticities like divergences, the data must be of high enough accuracy and the number of data points must be large enough [226]. Both can be checked by reconstructing the Euclidean correlator via the Källen-Lehmann representation, (6.1), and comparing it to the original data.

Usually, the reconstructed data from a Padé spectral function only agree with the original data in a specific momentum regime. In other regimes, the deviation is usually large and even the qualitative behavior of the reconstructed data is often quite different [216], as we will also see in Section 6.4.

However, one is usually still able to see the main features of the lowest-lying state, i.e. its position but for example not its width or any information about higher states, see e.g. [216, 247, 250].

6.3. Gaussian Process Regression

In the following, we present the main aspects of GPR relevant for the spectral reconstruction that was developed by [249]. For introductions reviews see e.g. [212, 251–254].

If a function $f(x)$ can be described by a Gaussian Process (GP), one writes,

$$f(x) \sim \mathcal{GP}\left(\mu(x), k(x,x')\right) , \tag{6.7}$$

where $\mu(x) = \langle f(x) \rangle$ is the statistical mean and $k(x,x')$ the statistical covariance function of the process,

$$k(x,x') = \left\langle \left(f(x) \left\langle f(x) \right\rangle\right) \left(f(x') \left\langle f(x') \right\rangle\right) \right\rangle . \tag{6.8}$$

The covariance matrix gives the correlation of uncertainties between different sample points.

Now by definition we can write for any set of sample points x_i,

$$\begin{pmatrix} f(x_1) \\ f(x_2) \\ \vdots \\ f(x_N) \end{pmatrix} \sim \mathcal{N}\left(\begin{pmatrix} \mu(x_1) \\ \mu(x_2) \\ \vdots \\ \mu(x_N) \end{pmatrix}, \begin{pmatrix} k(x_1,x_1) & k(x_1,x_2) & \dots & k(x_1,x_N) \\ k(x_2,x_1) & k(x_1,x_2) & \dots & k(x_1,x_N) \\ \vdots & \vdots & \ddots & \vdots \\ k(x_N,x_1) & k(x_N,x_2) & \dots & k(x_N,x_N) \end{pmatrix} \right) , \tag{6.9}$$

where $\mathcal{N}(\mu, \mathbf{\Sigma})$ is a multivariate normal distribution.

Generally the values of the function $y_i \equiv f(x_i)$ at the sample points x_i are computed or measured within uncertainties, see the discussion in Section 6.1.3.

Assuming these can be described by a Gaussian with covariance matrix $\mathbf{C_d}$ and zero mean value, one can then predict the function at other values x,

$$\begin{pmatrix} f(x) \\ \hat{\mathbf{y}} \end{pmatrix} \sim \mathcal{N}\left(\begin{pmatrix} \mu(x) \\ \hat{\boldsymbol{\mu}} \end{pmatrix}, \begin{pmatrix} k(x,x) & \hat{\mathbf{k}}^\top(x) \\ \hat{\mathbf{k}}(x) & \hat{\mathbf{K}} + \mathbf{C_d} \end{pmatrix} \right) , \tag{6.10}$$

where we have defined the quantities,

$$\begin{aligned} \mu_i &= \mu(x_i) \, , \\ \hat{k}_i(x) &= k(x_i, x) \, , \\ \hat{K}_{ij} &= k(x_i, x_j) \, . \end{aligned} \tag{6.11}$$

Thus our knowledge of $f(x)$ from the sampling points x_i with the function values y_i is,

$$\begin{aligned} f(x)|\hat{\mathbf{y}} \sim \mathcal{N} \Big(& \mu(x) + \hat{\mathbf{k}}^\top(x) \left(\hat{\mathbf{K}} + \mathbf{C_d}\right)^{-1} (\hat{\mathbf{y}} - \hat{\boldsymbol{\mu}}) \, , \\ & k(x,x) - \hat{\mathbf{k}}^\top(x) \left(\hat{\mathbf{K}} + \mathbf{C_d}\right)^{-1} \hat{\mathbf{k}}(x) \Big) \, . \end{aligned} \tag{6.12}$$

6.3.1. Mean and Covariance Functions

From the above, one can see that the defining functions of any GP are the mean and covariance function. Usually one does not know these functions from measurements or

computations, but one has to model them. The mean function can be chosen according to the general behavior of the data as e.g. a constant or linear function. For the covariance function one commonly uses one of the following options:

$$k_D(x,x') = \sigma_1^2 \delta(d(x,x'))\,,$$

$$k_G(x,x') = \sigma_1^2 \exp\left(-\frac{d(x,x')^2}{2\sigma_2^2}\right)\,,$$

$$k_M(x,x') = \sigma_1^2 \frac{2^{1-\nu}}{\Gamma(\nu)} \left(\frac{\sqrt{2\nu}d(x,x')}{\sigma_2}\right)^{\nu} K_\nu \left(\frac{\sqrt{2\nu}d(x,x')}{\sigma_2}\right)\,, \tag{6.13}$$

where $d(x,x')$ is a measure between the two points, e.g. $d(x,x') = (x-x')$, $\Gamma(v)$ the Gamma function and K_ν a modified Bessel function.

The Gaussian kernel is related to the Matérn-kernel via $\nu \to \infty$, and to the Delta-kernel via $\sigma_2 \to 0$. σ_1 describes the amplitude and σ_2 the typical length scale. We can summarize both in the hyperparameter $\boldsymbol{\alpha} = (\sigma_1, \sigma_2)$.

6.3.2. Gaussian Processing with Indirect Data

Generally, the computed or measured data points d_i can be indirectly related to the underlying function $f(x)$ via,

$$d_i = \int w_i(x) f(x) dx \tag{6.14}$$

where $w_i(x)$ is an integration kernel, relating the data points to a function. One can already see that the Källén-Lehmann representation (6.1) satisfies (6.14). Since integrations preserve Gaussian statistics one can conclude, that if $f(x)$ can be described by a Gaussian process, also the data d_i form a multivariate normal distribution,

$$d_i \sim \mathcal{N}\left(\int w_i(x)\mu(x)dx, \int\int w_i(x)k(x,x')w_i(x')dxdx'\right)\,. \tag{6.15}$$

Thus the function $f(x)$ and the N data points d_i form a Gaussian process,

$$\begin{pmatrix} f(x) \\ d_i \\ \vdots \\ d_N \end{pmatrix} \sim \mathcal{N}\left(\begin{pmatrix} \mu(x) \\ \hat{\boldsymbol{\omega}} \end{pmatrix}, \begin{pmatrix} k(x,x) & \hat{\mathbf{w}}^\top(\mathbf{x}) \\ \hat{\mathbf{w}}(\mathbf{x}) & \hat{\mathbf{W}} + \mathbf{C_d} \end{pmatrix}\right) \tag{6.16}$$

with

$$\hat{\omega}_i = \int w_i(u)\mu(u)du\,,$$

$$\hat{w}_i(x) = \int w_i(u)k(u,x)du\,,$$

$$\hat{W}_{ij} = \int\int w_i(u)k(u,v)w_j(v)dudv\,. \tag{6.17}$$

Thus the function $f(x)$ based on the data d_i is then given as,

$$f(x)|\hat{\mathbf{d}} \sim \mathcal{GP}\left(\mu(x) + \hat{\mathbf{w}}^\top(\mathbf{x})\left(\hat{\mathbf{W}} + \mathbf{C_d}\right)^{-1}\left(\hat{\mathbf{d}} - \hat{\boldsymbol{\omega}}\right), \right.$$
$$\left. k(x,x) - \hat{\mathbf{w}}^\top(\mathbf{x})\left(\hat{\mathbf{W}} + \mathbf{C_d}\right)^{-1}\hat{\mathbf{w}}(x)\right) \tag{6.18}$$

6.3.3. Optimization of Parameters

As introduced in (6.13) one can choose different covariance functions with a variable hyperparameter $\boldsymbol{\sigma}$ describing amplitude and correlation length. One can obtain optimal values for the hyperparameter by maximizing the associated likelihood [217, 252],

$$\mathbb{P}(\hat{\mathbf{y}}|\boldsymbol{\alpha}) = \frac{1}{\sqrt{(2\pi)^N|\hat{\mathbf{K}} + \mathbf{C_d}|}} \exp\left(-\frac{1}{2}(\hat{\mathbf{y}} - \hat{\boldsymbol{\mu}})^\top\left(\hat{\mathbf{K}} + \mathbf{C_d}\right)^{-1}(\hat{\mathbf{y}} - \hat{\boldsymbol{\mu}})\right). \tag{6.19}$$

For convenience one usually maximizes the log likelihood with respect to α,

$$\log\mathbb{P}(\hat{\mathbf{y}}|\boldsymbol{\alpha}) = -\frac{1}{2}(\hat{\mathbf{y}} - \hat{\boldsymbol{\mu}})^\top\left(\hat{\mathbf{K}} + \mathbf{C_d}\right)^{-1}(\hat{\mathbf{y}} - \hat{\boldsymbol{\mu}}) - \frac{1}{2}\log|\hat{\mathbf{K}} + \mathbf{C_d}| - \frac{N}{2}\log 2\pi\,. \tag{6.20}$$

The optimized parameters that were used throughout this work, as well as further details related to the optimization procedure can be found in Section C.2.2.

6.4. Numerical Results

While the author of this thesis was involved in all stages of obtaining the results that are presented in this section, the fRG dressings and GP results were obtained by other collaborators of [4].

In this section, we present results for the scalar and pseudoscalar glueball spectral function via GPR and via Padé approximants. We obtain the full vertex dressing from an fRG computation on the results presented in Chapter 5. Further details on the computation can be found in Chapter C. As described in Section 6.1.2, the full dressing contains information about bound-states, where each one is suppressed as $\propto e^{-m}$ with the respective glueball mass m, see e.g. the discussion in [255, 256]. Thus we can directly extract the spectral function of the scalar ($J^{PC} = 0^{++}$) glueball from the classical transverse four-gluon vertex dressing. To this end, we use the respective projection operator in the s-channel,

$$\mathcal{P}^{abcd}_{s,\mu\nu\rho\sigma}(p,p,-p) = \frac{\left[\Pi^{\perp}(p)\Pi^{\perp}(p)\Pi^{\perp}(p)\Pi^{\perp}(p)\tau_{A^4,cl}(p,p,-p)\right]^{abcd}_{\mu\nu\rho\sigma}}{\Pi^{\perp}(p)\Pi^{\perp}(p)\Pi^{\perp}(p)\Pi^{\perp}(p)\tau_{A^4,cl}(p,p,-p)\tau_{A^4,cl}(p,p,-p)}\,, \tag{6.21}$$

where indices are suppressed for simplicity. The classical four-gluon vertex tensor structure is,

$$\begin{aligned}\tau^{abcd}_{A^4,cl,\mu\nu\rho\sigma}(p_1,p_2,p_3) = {} & f^{abe}f^{cde}\left(\delta_{\mu\rho}\delta_{\nu\sigma} - \delta_{\mu\sigma}\delta_{\nu\rho}\right) \\ & + f^{ace}f^{bde}\left(\delta_{\mu\nu}\delta_{\rho\sigma} - \delta_{\mu\sigma}\delta_{\nu\rho}\right) \\ & + f^{ade}f^{bce}\left(\delta_{\mu\nu}\delta_{\rho\sigma} - \delta_{\mu\rho}\delta_{\nu\sigma}\right)\,,\end{aligned} \tag{6.22}$$

and the transverse projection operator is defined as,

$$\Pi^{\perp}_{\mu\nu}(p) = \delta_{\mu\nu} - \frac{p_\mu p_\nu}{p^2}\,. \tag{6.23}$$

Due to the exponential suppression of heavier states, we need to find a projection operator for the four-gluon vertex, that excludes all scalar particle exchanges. We know that the pseudoscalar ($J^{PC} = 0^{-+}$) glueball has a Lorentz tensor structure proportional to [196],

$$\tau_{A^4,ps,\mu\nu}(p,P) = \epsilon_{\mu\nu\alpha\beta}p^T_\alpha P_\beta\,, \tag{6.24}$$

where P and p are the total and relative momenta, T indicates transverse with respect to P, and $\epsilon_{\mu\nu\alpha\beta}$ is the anti-symmetric tensor. In the s-channel approximation there exists no relative momenta thus we have chosen the transverse momentum such that $p^T_\mu p^T_\mu = p^2$, $p^T_\mu P_\mu = 0$. The parametrisation of the momenta is given in Section C.1.4.

From this, we construct the pseudo-scalar projection operator in the s-channel,

$$\mathcal{P}^{abcd}_{ps,\mu\nu\rho\sigma}(p,p,-p) = \frac{\left[\Pi^{\perp}(p)\Pi^{\perp}(p)\Pi^{\perp}(p)\Pi^{\perp}(p)\tau_{A^4,ps}(p,2p)\tau_{A^4,ps}(p,-2p)\right]^{abcd}_{\mu\nu\rho\sigma}}{\Pi^{\perp}(p)\Pi^{\perp}(p)\Pi^{\perp}(p)\Pi^{\perp}(p)\tau^2_{A^4,ps}(p,2p)\tau^2_{A^4,ps}(p,-2p)} \tag{6.25}$$

Note that this does not project onto a dressing but rather onto the full four-point function. For a full four-gluon vertex tensor basis, see e.g. [257].

Projecting the fRG equation for the four-gluon vertex with both projection operators, one obtains equations for the scalar dressings $\lambda_{A^4,s}$ and the pseudo-scalar dressing $\lambda_{A^4,ps}$.

The diagrammatic equations are shown in Figure C.1. It is worth mentioning that in general there are diagrams with ghost loops contributing to the four-gluon dressing fRG equation. Due to the s-channel approximation they vanish here.

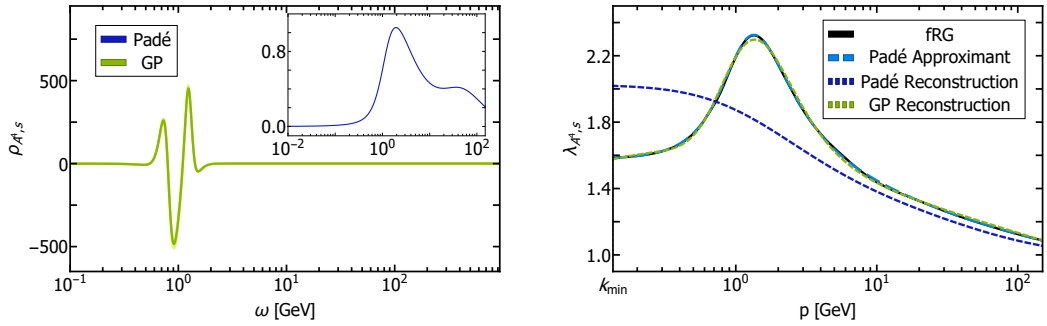

Figure 6.1.: Left: Scalar spectral function $\rho_{A^4,ps}$ over frequency ω obtained from Padé approximants (dark blue line) and from GP (green line). The light green band represents the standard deviation. Right: Pseudo-scalar Euclidean dressing $\lambda_{A^4,ps}$ from the fRG (black solid line) in comparison to reconstructions thereof from the Padé (dotted dark blue) and the GP (dotted green) spectral functions and in comparison to the Padé approximant (dashed light blue).

6.4.1. Discussion

We proceed by presenting the scalar and pseudo-scalar spectral function obtained from Padé approximants and via a GP approach.

The spectral function for the scalar four-gluon vertex dressing and the fRG dressing as well as the reconstructed dressing from both methods can be found in Figure 6.1. The respective pseudo-scalar results are presented in Figure 6.2.

One can immediately see that both approaches yield very different spectral functions for both, the scalar and pseudo-scalar projection.

Generally, the scalar and pseudo-scalar spectral functions via Padé look very different in comparison to their GP counterparts which can be accounted for by the failure of the Padé method, see the discussion below. The respective spectral function has a distinct positive peak at $\omega = 1.933\,\text{GeV}$ for the scalar and at $\omega = 1.843\,\text{GeV}$ for the pseudo-scalar projection.

When comparing the reconstructed dressings from the spectral functions with the fRG dressing, one can see that for both projections the reconstructed dressing via Padé only agrees qualitatively well with the respective scalar and pseudo-scalar fRG dressing for momenta $p \geq 10\,\text{GeV}$. The deviations for very large momenta can be associated with UV cutoff effects. For smaller momenta, the reconstructed dressings do not even show the same qualitative behavior as the fRG dressing. This failure of the approach to reproduce the Euclidean data is explained when one further investigates the Padé approximants. Both approximants show poles in the Euclidean momentum range, see Figure C.2.

A qualitatively similar result was presented in [216] for the gluon propagator spectral function and reconstructed dressing via Padé approximants. It was argued there, that the approach does violate the holomorphicity of the dressing and therefore the spectral function via Padé approximants does not reproduce the dressing. For a more detailed discussion, see Section C.2.1. Due to the failure of the reconstruction, we refrain from relating the peaks in the Padé spectral function to a potential glueball mass.

The reconstructed dressings via GP generally agree better with the fRG dressing. From the reconstructed scalar dressing, we can see that it agrees very well with the fRG dressing for large momenta, only slight deviations thereof can be seen in the regime $4 \leq p \leq 7\,\text{GeV}$.

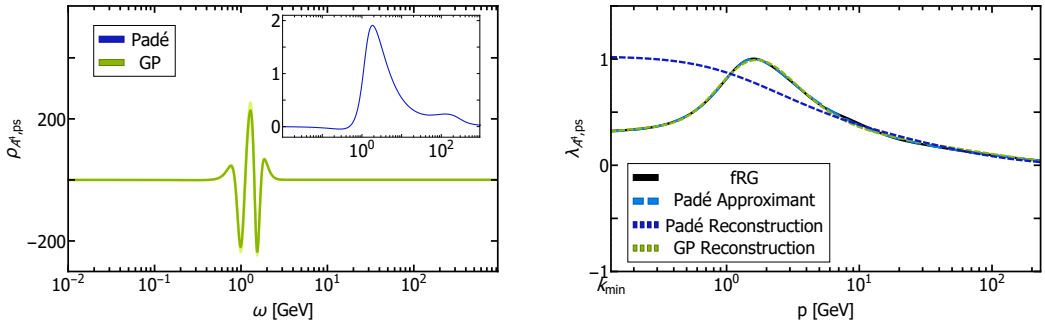

Figure 6.2.: Left: Pseudo-scalar spectral function $\rho_{A^4,ps}$ over frequency ω obtained from Padé approximants (dark blue line) and from GP (green line). The light green band represents the standard deviation. Right: Pseudo-scalar Euclidean dressing $\lambda_{A^4,ps}$ from the fRG (black solid line) in comparison to reconstructions thereof from the Padé (dotted dark blue) and the GP (dotted green) spectral functions and in comparison to the Padé approximant (dashed light blue).

For momenta between $0.8 \leq p \leq 2\,\text{GeV}$, i.e. around the peak, the deviation is larger.

The same holds true for the reconstructed pseudo-scalar dressing. However, it is worth mentioning that the peak structure of the pseudo-scalar fRG dressing for momenta $1 \leq p \leq 3\,\text{GeV}$ is very well reproduced by the GP. Larger deviations are only visible in the momentum regime between $5 \leq p \leq 15\,\text{GeV}$. Generally, the agreement of the reconstructed dressings with the Euclidean fRG dressing is well within our numerical precision.

Both, the scalar and pseudo-scalar spectral functions from GP exhibit a rich peak structure which persists under modifications of the procedure. The connection thereof to physical bound states however is questionable and a further investigation of the system is necessary. The appearance of many peaks or oscillations in the spectral function can usually be accounted for by the ill-conditioning of the procedure, see e.g. [216]. A promising approach, that might enhance the bound-state structure in the spectral function, is to compute spectral functions of the respective couplings, defined as,

$$\alpha_{A^4,s/ps} = \frac{\lambda_{A^4,s/ps}(p)}{4\pi Z_A(p)^2}\,, \tag{6.26}$$

from the scalar and pseudo-scalar dressing and the gluon propagator dressing $Z_A(p)$.

Furthermore, adding more prior knowledge about the spectral function, such as the UV and IR asymptotic behavior which can be extracted from the Euclidean dressing, should improve the overall procedure and results.

6.4.1.1. Glueball Masses

For a preliminary study of the glueball masses extracted from the spectral functions of the projected four-gluon vertex dressings, we read off the position of the largest peak (in terms of absolute value) in the respective spectral functions.

We obtain $\omega_{\text{peak,s}} = 0.911\,\text{GeV}$ and $\omega_{\text{peak,ps}} = 1.287\,\text{GeV}$ for the scalar and pseudo-scalar peak respectively. As we work within an s-channel approximation, the position of

	Masses [MeV]				
J^{PC}	lattice	Hamiltonian/ Regge theory	consitutent models	DSE-BSE	this work (preliminary)
0^{++}	1760(50) [187] 1740(50) [189] 1651(23) [191]	1980 [204] 1580 [201]	1710 [200] 1855 [198, 199]	1850(130) [196] 1640 [193]	1822 (GP)
0^{-+}	2640(40) [187] 2610(40) [189] 2600(40) [191]	2220 [204] 2560 [201]	2610 [200] 2492 [198, 199]	2580(180) [196] 4530 [193]	2574 (GP)

Table 6.1.: Comparison of masses for the scalar ($J^{PC} = 0^{++}$) and pseudoscalar ($J^{PC} = 0^{-+}$) glueball from different methods. The errors for [187, 189] are a combination of statistical error and of the use of an anisotropic lattice, whereas the errors in [191] are statical errors only. The errors in [196] come from the extrapolation method. In [198, 199] we compare to the results obtained from Model B.

the peak correspond to half the glueball mass $\omega_{\text{peak,s/ps}} = \frac{m_{s/ps}}{2}$. The results are shown in Table 6.1.

We can immediately see that the scalar and pseudo-scalar glueball mass extracted from the respective four-gluon dressings agree very well with the lattice and DSE-BSE results.

We postpone a further discussion and comparison of results to later work, where we aim at improving the GP method with the aforementioned approaches.

6.5. Conclusion

We have presented a self-consistent approach for extracting bound state information from a Euclidean four-gluon vertex dressing function within an fRG computation. The dressing has been computed on the results presented in Chapter 5. By appropriately projecting out tensor structures contributing to lighter bound states we have gained access to the scalar and pseudo-scalar dressing function. We have obtained spectral functions of the dressings via Padé approximants and via Gaussian Process Regression. While the latter leads to reconstructed dressings that agree well with the respective fRG dressings, the former does not even qualitatively reproduce the dressings for non-perturbative and semi-perturbative momenta. The failure of a simple and naïve Padé approach within this context is no surprise, as the approximant shows poles in the analytic half-plane. The masses obtained via Padé are therefore not reliable and not stated here. The scalar and pseudo-scalar glueball mass via GPR were obtained as 1822 MeV, and 2574 MeV respectively, and agree well with the values from lattice and DSE-BSE computations. For a quantitative statement about the spectral function within both projections, an improvement of the GP is necessary which could consist of extrapolating the Euclidean data in the IR and UV according to analytic relations or studying spectral functions of quantities like couplings rather than dressing.

7. Phase Structure of QCD

This chapter is based on [5].
The QCD phase diagram is subject to many experimental and theoretical studies. It provides insight into the evolution of the early universe as well as into the underlying processes in heavy-ion collisions [59, 130, 258–265]. While it is widely accepted that there exists a crossover between the hadronic (confined) phase and the deconfined quark-gluon plasma for $T \approx 155\,\mathrm{MeV}$ [22, 23] at low chemical potential, the relation of this confinement-deconfinement phase transition to chiral symmetry breaking is still under investigation. For larger chemical potentials, the phase transition is of first order and the existence of a critical endpoint at finite temperature and chemical potential is highly conjectured. Employing functional methods allows for a study of the whole phase diagram. For recent results see e.g. [58–67]. For corresponding lattice QCD studies at small chemical potential, see e.g. [25, 266–272].

In this work, we access the QCD phase structure via thermal correlation functions for $2+1$-flavor QCD at finite chemical potential within a self-consistent Dyson-Schwinger (DSE) approach. Special emphasis is put on the computation of the thermally split quark-gluon vertex feeding back into the quark gap equation. This is a first step in systematically improving the truncation that was presented in previous works, see e.g. [65, 66]. This approach allows for a study of the chiral phase structure and a potential critical end point in the QCD phase diagram, where the only input parameters are the fundamental strong coupling and the current quark masses at the renormalisation scale.

In Section 7.1 we present the setup for this work, followed by a discussion of the input parameters and how we extract the chiral transition temperature $T_c(\mu_B)$ in Section 7.2. In Section 7.3 we present preliminary results of the light quark mass dressing and the leading dressing of the quark-gluon vertex and conclude our results in Section 7.4.

7.1. Setup

The classical QCD action in Euclidean space-time is given as,

$$S_{\mathrm{QCD}}[q,\bar{q},A,c,\bar{c}] = \int_x \Big(\frac{1}{4} F^a_{\mu\nu} F^a_{\mu\nu} + \frac{1}{2\xi} \partial_\mu A^a_\mu \partial_\nu A^a_\nu \\ - \bar{c}^a \partial_\mu D^{ab}_\mu c^b + \bar{q}(\not{D} + m_q) q \Big) , \tag{7.1}$$

where ξ is the gauge fixing parameter and $\int_x = \int d^4x$. The definitions of the covariant derivative and the field strength tensor can be found in Chapter 2.

In this work we choose an approach with Dyson-Schwinger equations to obtain the effective action $\Gamma[\Phi]$ in terms of correlation functions.

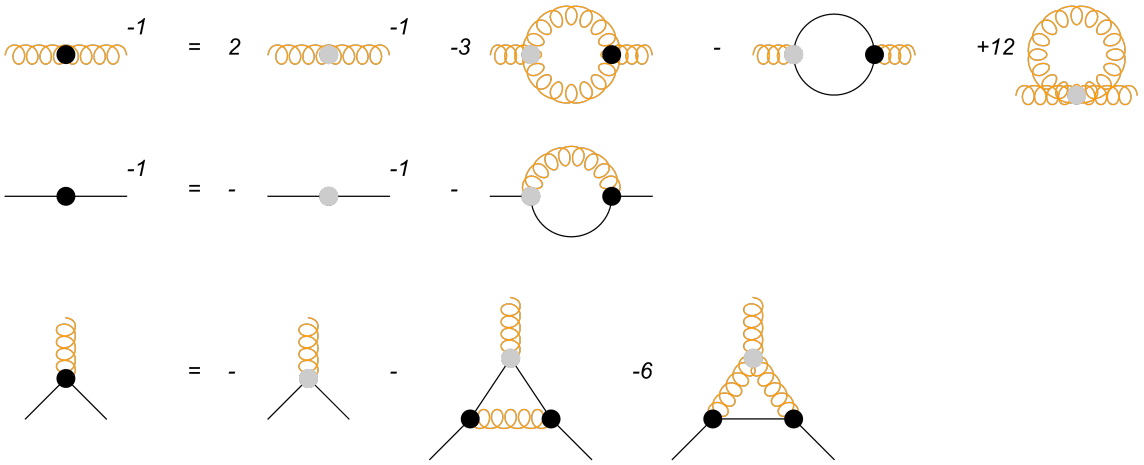

Figure 7.1.: Graphical representation of the DSEs that were solved for this work. The solid lines represent the quarks, curly orange lines the gluon. All propagators are fully dressed. The black and grey circles represent full and classical vertices.

The Dyson-Schwinger equation is (3.15),

$$\frac{\delta\Gamma[\Phi]}{\delta\Phi_a} = \frac{\delta S[\phi]}{\delta\phi_a}\bigg|_{\phi_b=\Phi_b+G_{bc}\frac{\delta}{\delta\Phi_c}} . \tag{7.2}$$

with the superfield $\Phi = \{q, \bar{q}, A_\mu, c, \bar{c}\}$ in QCD. The form of (7.2) relates the full correlators of order n to a $n-2$-loop exact equation containing full vertices and full propagators as well as a classical vertex. By choosing an appropriate ansatz for the classical action, one can obtain the full correlation function by interatively solving the respective DSEs. Thereby one gains insights into the non-perturbative regime of QCD.

7.1.1. Vertex Expansion and Truncation

We write the effective action in terms of a vertex expansion as (3.19),

$$\Gamma[\Phi] = \sum_{n=1}^{\infty} \int \Gamma_{\Phi_1\dots\Phi_n} \Phi_1 \dots \Phi_n \, . \tag{7.3}$$

Generally, this represents an expansion about a solution to the equations of motion in the vacuum. At finite temperature, this expansion has already been proven to be a viable scheme in, e.g. [69] and was employed at finite temperature and chemical potential in e.g. [66]. We include the vertices that are shown in the diagrams in Figure 7.1, where we neglect the ghost contributions to the gluon propagator, as they are small.

At finite temperature the vacuum $O(4)$ symmetry is replaced by $\mathbb{Z}_2 \times O(3)$. Thus, one obtains a split into two components, a magnetic and electric one. The former is transverse, the latter longitudinal to the heat bath. This split is introduced into the correlators via

the projection operators,

$$\Pi^M_{\mu\nu}(p) = \delta_{\mu\nu} - \frac{(p_\mu - p_0\delta_{\mu 0})(p_\nu - p_0\delta_{\nu 0})}{\vec{p}^2} - \delta_{0\mu}\delta_{0\nu}\,,$$

$$\begin{aligned}\Pi^E_{\mu\nu}(p) &= \Pi^\perp_{\mu\nu}(p) - \Pi^M_{\mu\nu}(p) \\ &= \delta_{0\mu}\delta_{0\nu} - \frac{p_\mu p_\nu}{p^2} + \frac{(p_\mu - p_0\delta_{\mu 0})(p_\nu - p_0\delta_{\nu 0})}{\vec{p}^2}\,.\end{aligned} \tag{7.4}$$

We then have

$$\Pi^M_{\mu\nu}(p) p_0 p_\nu = 0\,,$$

$$\Pi^E_{\mu\nu}(p) p_i p_\nu = 0\,, \tag{7.5}$$

where $i = (1,2,3)$. We furthermore decompose four-vectors into,

$$p = \begin{pmatrix} \tilde{\omega}_n \\ \vec{p} \end{pmatrix}\,, \tag{7.6}$$

where $\tilde{\omega}_n = 2\pi T n$ for gluons and $\tilde{\omega}_n = 2\pi T(n+1/2) - i\mu_B/3$ for quarks, $n \in \mathbb{Z}$ are the discrete Matsubara modes and μ_B the chemical potential. The full parametrisation of external and loop momenta that was used here can be found in Section D.4.

We therefore have the split in the propagators,

$$G^{ab}_{AA,\mu\nu}(p) = \delta^{ab}\frac{1}{p^2}\left(\frac{1}{Z_M(p)}\Pi^M_{\mu\nu}(p) + \frac{1}{Z_E(p)}\Pi^E_{\mu\nu}(p)\right)$$

$$G^{ab,ij,f_1f_2}_{q\bar{q}}(p) = \delta^{ab}\delta^{f_1f_2}\frac{\frac{Z_{q,\parallel}(p)}{Z_q(p)}(i\gamma_0^{ij}p_0 + m_q(p)) + i(\gamma_\mu^{ij}p_\mu - \gamma_0^{ij}p_0)}{Z_{q,\parallel}(p)(p_0^2 + m_q(p)^2) + \vec{p}^2 Z_q(p)}\,. \tag{7.7}$$

In the propagators, entering the quark-gluon vertex equation, the thermal split is however not applied, as this has been proven to be a good approximation, see e.g. [66]. There we use the $\mathcal{O}(4)$ symmetric propagators,

$$G^{ab}_{AA,\mu\nu}(p) = \Pi^\perp_{\mu\nu}(p)\delta^{ab}\frac{1}{Z_A(p)p^2}\,,$$

$$G^{ab,ij,f_1f_2}_{q\bar{q}}(p) = \delta^{ab}\delta^{f_1f_2}\frac{(m_q(p)\delta^{ij} + i\gamma_\mu^{ij}p_\mu)}{Z_q(p)(m_q(p)^2 + p^2)}\,, \tag{7.8}$$

and thus identify $Z_A = Z_M$, $\frac{Z_{q,\parallel}}{Z_q} \approx 1$ and $\lambda^{(i)}_{A\bar{q}q} \approx \lambda^{(i)}_{A\bar{q}q,M}$ with momentum arguments dropped for simplicity.

With this setup we derive Dyson-Schwinger equations for the electric and magnetic gluon and quark dressings, the quark mass and the leading electric and magnetic quark-gluon vertex dressings. The symbolic equations can be found in Figure 7.1.

For the quark-gluon vertex we only take into account the leading dressing functions,

$$\tau^{(1)}_\mu(p,q) = -i\gamma_\mu\,, \qquad \tau^{(4)}_\mu(p,q) = (\not{p} + \not{q})\gamma_\mu$$

$$\tau^{(7)}_\mu(p,q) = \frac{i}{2}\left[\not{p},\not{q}\right]\gamma_\mu\,, \tag{7.9}$$

where p is the anti-quark and q the quark momentum and where we apply a thermal split into electric and magnetic components. The full tensor basis as well as the procedure of applying the thermal split in the vertex is described in Section D.3. The symbolic equations can be found in Figure 7.1.

Here we have included the classical tensor $\tau^{(1)}$, a chirally symmetric tensor $\tau^{(7)}$, and a chiral symmetry breaking tensor $\tau^{(4)}$. It has been shown in previous studies in the vacuum that these are the only quanitatively important tensor structures, see e.g. [69, 91].

We approximate all vertex dressings feeding back into the equations at the symmetric point, $\lambda^{(n)}(\bar{p})$, with

$$\bar{p}^2 = \frac{1}{n}\sum_{i=1}^{n}(\tilde{\omega}_{n_i} + \vec{p}_i^2)\,. \tag{7.10}$$

For the wave function renormalisations Z_i with $i = (A,\, q,\, (q, \|))$ as well as the quark mass function feeding back we use,

$$\begin{aligned} Z(\tilde{\omega}_n, \vec{p}) &\approx Z(0, \sqrt{\tilde{\omega}_n^2 + \vec{p}^2})\,, \\ m_q(\tilde{\omega}_n, \vec{p}) &= m_q(\sqrt{\tilde{\omega}_n^2 + \vec{p}^2}) \end{aligned} \tag{7.11}$$

We only compute the zeroth, first and second mode of the propagator and vertex dressings and approximate the higher Matsubara frequencies with the above. This leaves us with equations for

$$\begin{aligned} &Z_A(\tilde{\omega}_n, \vec{p})\,, && m_q(\tilde{\omega}_n, \vec{p})\,, \\ &Z_q(\tilde{\omega}_n, \vec{p})\,, && Z_{q,\|}(\tilde{\omega}_n, \vec{p})\,, \\ &\lambda^{(i)}_{A\bar{q}q,E}(\tilde{\omega}_n, \bar{\vec{p}})\,, && \lambda^{(i)}_{A\bar{q}q,M}(\tilde{\omega}_n, \bar{\vec{p}})\,, \end{aligned}$$

with $n = \{0,\, 1,\, 2\}$, $i = \{1,\, 4,\, 7\}$ and $\bar{\vec{p}}^2 = \frac{1}{n}\sum_{i=1}^{n}\vec{p}_i^2$.

7.2. Chiral Condensate

The quark gap equation, i.e. the DSEs for Z_q, $Z_{q,\|}$, m_q carry the information of chiral symmetry breaking and the phase transition. They are therefore the quantities of main interest in our investigation.

We fix the renormalisation scale to $\mu = 40\,\mathrm{GeV}$, where the strong coupling is then given as $\alpha_s(\mu) = 0.1666$. The isospin symmetric light quark masses are determined via the physical pion mass $m_\pi(\mu) = 138\,\mathrm{MeV}$ as $m_q^0 = m_{u/d}(\mu) = 2.5\,\mathrm{MeV}$. We fix the ratio of strange to light quarks as, $m_s^0/m_q^0 \approx 27$. Thereby all parameters are fixed and no further input is required.

We begin the discussion with the quark mass dressing m_q. For high momenta, corresponding to the (approximate) chirally symmetric phase, the dressing m_q is fixed by the current quark mass m_q^0. At smaller energy scales, chiral symmetry is dynamically broken, the quark mass dressing increases to the constituent quark mass.

The chiral transition temperature $T(\mu_B)$ can be derived from the chiral susceptibility $\partial_T \Delta_{l,R}$ of the renormalised light chiral condensate $\Delta_{l,R}$ [65, 66, 90],

$$\Delta_{l,R} = \frac{1}{2\mathcal{N}_R} \sum_{\text{quarks}} \left[\Delta_q(T,\mu_B) - \Delta_q(0,0)\right] , \tag{7.12}$$

where $\mathcal{N}_R = m_\pi^4$ is a normalization factor and the quark condensate is given as,

$$\Delta_q \simeq -m_q^0 T \sum_{n\in\mathbb{Z}} \int \frac{d^3p}{(2\pi)^3}\, \mathrm{Tr}\, G_{q\bar{q}}(p)\,. \tag{7.13}$$

We expect from previous results, e.g. [66], that for increasing μ_B, the crossover in the renormalised light condensate over temperature steepens, leading to a second order critical endpoint and finally a first order phase transition.

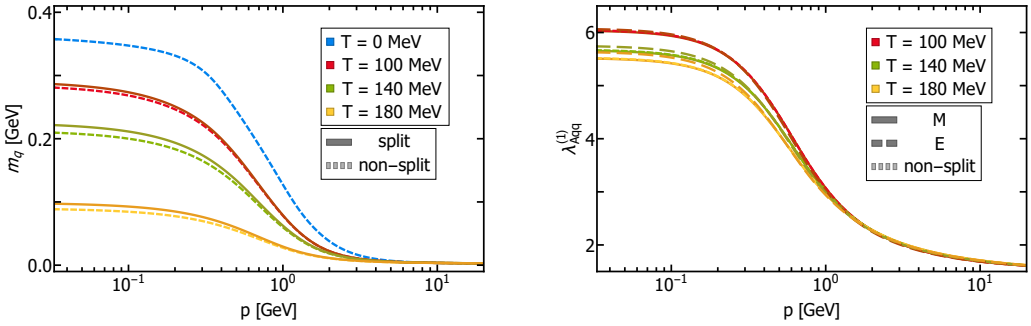

Figure 7.2.: Left: Light quark mass dressing m_q in GeV for different temperatures, where the (non-)split quark-gluon vertex enters the propagator equation. Right: Leading quark-gluon vertex dressing $\lambda^{(1)}_{A\bar{q}q}$ in comparison to the split dressings $\lambda^{(1)}_{A\bar{q}q,E}$ and $\lambda^{(1)}_{A\bar{q}q,M}$ for different temperatures.

7.3. Numerical Results

While the setup and the Dyson-Schwinger equations were provided by the author of this thesis, the iterative solution of the equations was performed by other collaborators of [5]. We present preliminary results for the quark mass dressing m_q and the leading quark-gluon vertex dressing $\lambda^{(1)}_{A\bar{q}q}$ in Figure 7.2.

The quark mass dressing m_q is shown for different truncations and different temperatures T, where 'split' refers to a thermal split in the quark-gluon vertex entering the quark gap equation as defined in Section D.3.

One can see that for all temperatures and momenta, the mass dressing obtained with the non-split quark-gluon vertex, i.e. where no thermal split was employed, are smaller than the results obtained with the split. Finally, this leads to an increase of the phase transition temperature. Overall, the deviation is however very small and the qualitative behavior of the dressing function is not affected by the split. The deviation of the results with the thermal split seems to be the largest around the phase transition temperature and decreases for higher temperatures. Generally, increasing the temperature leads to a decrease in the running of the quark mass dressing function.

Comparing the electric and magnetic, i.e. the split leading quark-gluon dressings $\lambda^{(1)}_{A\bar{q}q,E}$ and $\lambda^{(1)}_{A\bar{q}q,M}$ with the non-split dressing $\lambda^{(1)}_{A\bar{q}q}$ one can see that the overall deviation affiliated with the thermal split is small. One can even see that the magnetic and the non-split dressing agree perfectly for temperatures smaller and larger than the phase transition temperature, only for temperatures around the phase transition the magnetic dressing is slightly smaller than the non-split quark-gluon dressing. Overall, the electric dressing is larger than the magnetic and non-split one, the difference however becomes larger with increasing temperature although the running of the dressings becomes smaller. All in all one can conclude that the introduction of the thermal split does not significantly alter the leading quark-gluon dressing.

In conclusion one can see that the improvement of the truncation by introducing a thermal split in the quark-gluon vertex does not have a large influence on the running of the dressing functions hinting at apparent convergence of results.

7.4. Conclusion

We have presented a setup for the investigation of the chiral phase structure of $N_f = 2+1$ QCD solving a self-consistent set of Dyson-Schwinger equations where the only input parameters are the strong coupling at the renormalisation scale, the light current quark masses from the pion mass, and the ratio between light and strange current quark mass. The truncation is a qualitative improvement to the one presented in [66] as we apply the thermal split in the quark-gluon vertex that feeds into the equations of the propagators. We have obtained preliminary results for the quark mass dressing and the leading quark-gluon vertex dressing at vanishing chemical potential and finite temperature. We have shown that employing the thermal split leads to a small increase in the quark mass dressing and therefore to a small increase of the phase transition temperature. Overall, the running of the dressings does not show a big dependence on the introduction of the split hinting at apparent convergence of the results. A study of all the relevant dressings, also at finite chemical potential, and a computation of the chiral condensate, the phase transition temperature and a potential critical endpoint is deferred to later work.

8. Summary & Conclusion

With this work, we have paved the way for a quantitative and qualitative understanding of infrared QCD correlation functions with functional methods.

We have presented the *Mathematica* package *QMeS-Derivation* which allows the derivation of symbolic functional equations starting from a quantum master equation such as the fRG, DSE, or mSTI. This task was broken down into independent modules, explicitly taking functional derivatives, tracing in field space, and applying a momentum routing for one-loop diagrams. Its most remarkable features are the effective and consistent handling of fermionic minus signs, its theory-independent superfield formulation, and its implementation via a very small number of rules. This allows for simple future extensions and a flexible use also for theories and models unrelated to QCD. We have elucidated this by deriving different functional equations in $SU(3)$ Yang-Mills theory, and $N_f = 1$ and $N_f = 2$ Yukawa theory.

We have proceeded by studying gauge invariance in $SU(3)$ Landau gauge Yang-Mills theory with functional methods by using *QMeS* to derive fRG and (m)STI equations for the correlation functions. The (modified) Slavnov-Taylor identities carry the underlying gauge invariance of the system in a gauge-fixed setting. The conservation thereof within numerical computations that require truncations to the infinite tower of coupled functional equations is essential for the understanding of confinement and infrared gluon dynamics. We have studied this gauge consistency by solving the system of coupled momentum-dependent equations for the ghost and gluon propagator, the ghost-gluon, and the three- and four-gluon vertex self-consistently by feeding these quantities back into the loop equations. A comparison of the different (non-)confining results for the longitudinal correlation functions has shown good agreement between both functional approaches, i.e. the fRG and mSTI, although they represent different resummation schemes. This agreement hints at gauge consistency of the setup.

Furthermore, we have put forward a self-consistent approach to extract bound state information from a correlation function within the fRG. Explicitly, we have presented a procedure to obtain the scalar and pseudo-scalar glueball mass by contracting the four-gluon vertex fRG equation with the respective projection operators that eliminate the contributions from lower-lying bound states. The resulting equations were solved on the previously presented pure Yang-Mills results, rendering a Euclidean scalar and pseudo-scalar four-gluon vertex dressing. We have found spectral representations of these dressings by analytically continuing the Euclidean dressing via Padé approximants and by applying Gaussian Process Regression. The extracted preliminary values for the scalar and pseudo-scalar glueball mass from the respective spectral functions agree well with the corresponding values that were obtained within other frameworks and computations. Finally, we have given an outlook on possible improvements of both methods.

Lastly, we have presented a setup that allows studying the phase structure of QCD with functional methods. To this end, we have presented a set of DSEs for thermal correlation functions of $N_f = 2+1$ QCD at finite chemical potential, where we have improved existing truncations by introducing the thermal split in the quark-gluon vertex entering the propa-

gator equations. The only input parameters are the strong coupling at the renormalisation scale, the light current quark masses from the pion mass, and the ratio between light and strange current quark mass. This setup allows us to obtain the chiral phase structure and, potentially, the critical end point. We have presented preliminary results of the quark mass dressing and the leading quark-gluon dressing function for different temperatures and in different truncations. A full investigation of the system and the resulting phase structure is still in preparation.

All in all, we have made significant progress towards improving and understanding the whole workflow connected with obtaining infrared QCD correlation functions with functional methods. Particularly, by introducing *QMeS-Derivation*, a computer-algebraic tool for the derivation of functional equations, which we then applied to Yang-Mills theory to broaden our understanding of gauge invariance within functional methods. Equipped with these technical insights, we have extracted bound state masses from the correlation functions and presented a set of thermal correlation functions for a study of the phase diagram of QCD. Utilizing these developments, quantitative predictions of the chiral phase transition and of a potential critical endpoint from functional methods are feasible objectives. First results thereof are expected in the foreseeable future demonstrating the power of functional methods as a tool to study QCD from first principles.

A. Additional material: Deriving Symbolic Functional Equations

A.1. Derivation of Master Equations

In the following we want to outline the basic steps in deriving the *Dyson-Schwinger* and *Functional Renormalisation Group* equations, as well as *(modified) Slavnov-Taylor Identities* that were introduced in Section 3.1.

A.1.1. Derivation of the Dyson-Schwinger Equation

One can derive the *Dyson-Schwinger equation* (DSE) for 1PI Greens functions by taking a total derivative of the integral (3.6)

$$\begin{aligned} 0 &= \int D\phi \frac{\delta}{\delta\phi_a} \exp\left(-S[\phi] + J^a\phi_a\right) \\ &= \int D\phi \left(-\frac{\delta S}{\delta\phi_a} + (-1)^{aa} J^a\right) \exp\left(-S[\phi] + J^a\phi_a\right) \\ &= \left(-\frac{\delta S}{\delta\phi_a} + (-1)^{aa} J^a\right)_{\phi_b = \frac{\delta}{\delta J^b}} Z[J]\,. \end{aligned} \tag{A.1}$$

When pulling the derivative term the source out of the integral one has to replace the field ϕ with a derivative with respect to the source.
Using the relation,

$$e^{-W[J]} \left(\frac{\delta}{\delta J^a}\right) e^{W[J]} = \frac{\delta W[J]}{\delta J^a} + \frac{\delta}{\delta J^a}\,. \tag{A.2}$$

one obtains the DSE for connected Greens functions

$$\left.-\frac{\delta S[\phi]}{\delta\phi_a}\right|_{\phi_b = \frac{\delta W[J]}{\delta J^b} + \frac{\delta}{\delta J^b}} + (-1)^{aa} J^a = 0\,. \tag{A.3}$$

By rewriting the derivative with respect to J as and using the definition of the propagator $W_{ab} = G_{ab}$,

$$\begin{aligned} \frac{\delta}{\delta J^a} &= \frac{\delta\Phi_b}{\delta J^a}\frac{\delta}{\delta\Phi_b} \\ &= \frac{\delta}{\delta J^a}\frac{\delta W[J]}{\delta J^b}\frac{\delta}{\delta\Phi_b} \\ &= G_{ab}\frac{\delta}{\delta\Phi_b}\,, \end{aligned} \tag{A.4}$$

one can express the DSE in terms of the effective action

$$\frac{\delta\Gamma[\Phi]}{\delta\Phi_a} = \left.\frac{\delta S[\phi]}{\delta\phi_a}\right|_{\phi_b=\Phi_b+G_{bc}\frac{\delta}{\delta\Phi_c}} . \tag{A.5}$$

The generalized DSE for quantum symmetries can be derived by inserting a generic function $\Psi[\phi]$ in the derivation of equation (A.1),

$$\frac{1}{Z[J]}\int D\phi \frac{\delta}{\delta\phi_a}\left(\Psi[\phi]\exp\left(-S[\phi]+J^a\phi_a\right)\right) , \tag{A.6}$$

thus yielding

$$\langle\Psi[\phi]\rangle\frac{\delta\Gamma[\Phi]}{\delta\Phi_a} = \left\langle\Psi[\phi]\frac{\delta S[\phi]}{\delta\phi_a}\right\rangle - \left\langle\frac{\delta\Psi[\phi]}{\delta\phi_a}\right\rangle . \tag{A.7}$$

A.1.2. Derivation of the fRG Equation

Since one introduces an (infrared) momentum-regularisation one modifies the Schwinger functional by

$$Z[J,R] = e^{W[J,R]} = e^{-\Delta S[\phi,R]}e^{W[J]} , \tag{A.8}$$

with the so-called regulator insertion,

$$\Delta S[\phi,R] = \frac{1}{2}R^{ab}\phi_a\phi_b . \tag{A.9}$$

The flow of the generating functional can be written as,

$$\begin{aligned} k\partial_k Z[J,R] &= -\left(k\partial_k\Delta S[\phi,R]\right)Z_k[J,R] \\ &= -\frac{1}{2}\left(k\partial_k R^{ab}\right)\frac{\delta^2 Z[J,R]}{\delta J^a\delta J^b} . \end{aligned} \tag{A.10}$$

Using the relation,

$$\frac{1}{Z[J,R]}\frac{\delta^2 Z[J,R]}{\delta J^a J^b} = W_{ab} + W_a W_b , \tag{A.11}$$

the flow equation in terms of the Schwinger functional is

$$k\partial_k W = -\frac{1}{2}\left(k\partial_k R^{ab}\right)\left(W_{ab}+W_aW_b\right) , \tag{A.12}$$

where W is a function of J and R.

One can define the propagator as,

$$\begin{aligned} G_{ac}\left(\Gamma+\Delta S\right)^{cb} &= \gamma^b{}_a , \\ \leftrightarrow G_{ac}\left(\Gamma^{cb}+R^{bc}\right) &= \gamma^b{}_a . \end{aligned} \tag{A.13}$$

After a Legendre transformation one obtains the effective average action

$$\Gamma[\Phi,R] = \sup_J\left(J^a\Phi_a - W[J,R] - \Delta S[\Phi,R]\right) . \tag{A.14}$$

Again the relations between the fields and sources in terms of the effective average action are given as,

$$\frac{\delta(\Gamma[\Phi,R]+\Delta S[\Phi,R])}{\delta\Phi_a} = (-1)^{aa}J^a\,,$$
$$\frac{\delta W[J,R]}{\delta J^a} = \Phi_a\,. \tag{A.15}$$

By switching to the RG-time $t = ln(k/\Lambda)$ with $\partial_t = k\partial_k$ one can write

$$\begin{aligned}\partial_t\Gamma &= -\partial_t W - \partial_t\Delta S \\ &\quad - \partial_t J^a\left(\Phi_a - \frac{\delta W}{\delta J^a}\right) \\ &= \frac{1}{2}\left(\partial_t R^{ab}\right)(W_{ab}+W_aW_b) - \partial_t\Delta S \\ &= \frac{1}{2}\left(\partial_t R_k^{ab}\right)W_{ab} + \partial_t\Delta S - \partial_t\Delta S \\ &= \frac{1}{2}\dot{R}^{ab}G_{ab}\,.\end{aligned} \tag{A.16}$$

where $\Gamma \equiv \Gamma[\Phi]$, $W \equiv W[J,R]$, $\Delta S \equiv \Delta S[\Phi,R]$ and we have used equation (A.12) as well as

$$\begin{aligned}\frac{1}{2}\left(\partial_t R^{ab}\right)\frac{\delta W}{\delta J^a}\frac{\delta W}{\delta J^b} &= \frac{1}{2}\left(\partial_t R^{ab}\right)\Phi_a\Phi_b \\ &= \partial_t\Delta S\,.\end{aligned} \tag{A.17}$$

Note that the superfield index notation above implies the summation and thus trace over all fields and integration over space-time.

A.1.3. Derivation of the Slavnov-Taylor Identity

The classical Yang-Mills action of non-Abelian gauge theories is gauge invariant, but neither the ghost nor the gauge fixed action are,

$$\delta^a_{gauge}e^{-S_A} = \delta^a_{gauge}\left(S_{gf}+S_{gh}\right), \tag{A.18}$$

where δ^a_{gauge} is the generator of a gauge transformation. Additionally it has the form of an operator in the generalized DSE (A.7) with $\delta/\delta\phi_a\Psi[\phi] = \delta^a_{gauge}$ which means that:

$$\begin{aligned}&\frac{1}{Z[J]}\int D\phi\;\delta^a_{gauge}\left(\exp(-S_A[\phi]+J^a\phi_a)\right) \\ &= \left\langle J^a(\delta^a_{gauge}\phi_a) - \delta^a_{gauge}(S_{gf}+S_{gh})\right\rangle = 0\,.\end{aligned} \tag{A.19}$$

Carrying out the expectation value leads to the Slavnov-Taylor identities (STI) of the theory. These identities guarantee the gauge invariance of observables.

Since δ^a_{gauge} is not a symmetry of the underlying classical theory we would like to find a transformation that is. This is satisfied by the BRST transformation

$$\delta_{\mathrm{BRST}}\phi_a = \mathfrak{s}\phi_a\delta\lambda\,, \tag{A.20}$$

where the infinitesimal parameter $\delta\lambda$ as well as the BRST generator $\mathfrak{s}$ are Grassmannian.

The action is invariant under BRST transformations

$$\mathfrak{s}S_A[\phi] = 0\,. \tag{A.21}$$

Again with $\mathfrak{s}$ as an operator the generalized DSE can be written as,

$$\frac{1}{Z[J]}\int D\phi\;\mathfrak{s}\left(\exp(-S_A[\phi] + J^a\phi_a)\right) = 0\,. \tag{A.22}$$

Thus the expectation value vanishes,

$$(-1)^{aa}\left\langle J^a\mathfrak{s}\phi_a\right\rangle = 0\,. \tag{A.23}$$

Note that the prefactor $(-1)^{aa}$ is due to the grassmannian nature of $\mathfrak{s}$.

$$\mathfrak{s}J^a\phi_a = (-1)^{aa}J^a\mathfrak{s}\phi_a\,. \tag{A.24}$$

Since the BRST transformations of fields are usually quadratic in the fields, it seems as if one looses the algebraic nature of the symmetry on quantum level. To resolve this one may introduce additional source terms Q^a for the BRST transformations of the fields,

$$Z[J,Q] = \int D\phi\exp(-S_A[\phi] + J^a\phi_a + Q^a\mathfrak{s}\phi_a)\,. \tag{A.25}$$

Since $\mathfrak{s}^2 = 0$, this does not change (A.23).

Then one can write the STI takes again algebraic form as

$$\left\langle\mathfrak{s}\phi_a\right\rangle = \frac{1}{Z[J,Q]}\frac{\delta Z[J,Q]}{\delta Q^a}\,. \tag{A.26}$$

By Legendre transforming the Schwinger functional $\ln Z[J,Q]$ one obtains the effective action in the presence of source terms for the BRST transformation,

$$\Gamma[\Phi,Q] = J^a\Phi_a - \ln Z[J,Q]\,. \tag{A.27}$$

We can directly see that

$$\left\langle\mathfrak{s}\phi_a\right\rangle = -\frac{\delta\Gamma[\Phi,Q]}{\delta Q^a} = \frac{1}{Z[J,Q]}\frac{\delta Z[J,Q]}{\delta Q^a}\,. \tag{A.28}$$

Rewriting the expectation value (A.23) yields the STI

$$\frac{\delta\Gamma}{\delta Q^a}\frac{\delta\Gamma}{\delta\Phi_a} = 0\,. \tag{A.29}$$

Fulfilling this relation guarantees gauge invariance of observables.

A.1.4. Derivation of the Modified Slavnov-Taylor Identity

Due to the presence of the cutoff (A.9) in the effective average action, gauge and hence BRST symmetry are broken, which means that we need to introduce *modified Slavnov-Taylor identities* (mSTIs) at a non-vanishing momentum scale k that become the usual STIs for $k = 0$.

Starting from the generating functional with the cutoff term $\Delta S[\phi, R]$ one can derive the mSTIs,

$$Z[J, Q] = \int D\phi \exp\left(-S[\phi] - \Delta S[\phi, R]\right) \exp\left(J^a \phi_a + Q^a \mathfrak{s}\phi_a\right). \tag{A.30}$$

Note that either the BRST charge or the field itself is of grassmanian nature. Thus the expectation value (A.23) changes to

$$(-1)^{aa} \left\langle J^a \mathfrak{s}\phi_a \right\rangle = \left\langle \mathfrak{s}\Delta S[\phi, R] \right\rangle . \tag{A.31}$$

After Legendre transforming the momentum scale dependent Schwinger functional one obtains the following relation:

$$\left\langle \mathfrak{s}\phi_a \right\rangle = \frac{\delta W[J, Q, R]}{\delta Q^a} = -\frac{\delta \Gamma[\Phi, Q, R]}{\delta Q^a} . \tag{A.32}$$

Rewriting the sources J^a in terms of the effective average action (A.15) one is left with,

$$\frac{\delta \Gamma}{\delta Q^a} \frac{\delta \left(\Gamma + \Delta S\right)}{\delta \Phi_a} = \left\langle \mathfrak{s}\Delta S[\phi, R] \right\rangle . \tag{A.33}$$

Moving all terms that contain ΔS to the right, one can further simplify by using relation (A.32),

$$\begin{aligned} &\left\langle \mathfrak{s}\Delta S[\phi, R] \right\rangle - \frac{\delta \Delta S[\Phi, R]}{\delta \Phi_a} \frac{\delta \Gamma[\Phi, Q, R]}{\delta Q^a} \\ &= \left\langle \mathfrak{s}\Delta S[\phi, R] \right\rangle + \mathfrak{s}\Delta S[\Phi, R] . \end{aligned} \tag{A.34}$$

Inserting the cutoff term (A.9) one arrives at,

$$\begin{aligned} \left\langle R^{ab}(\mathfrak{s}\phi_a)\phi_b \right\rangle + R^{ab}(\mathfrak{s}\Phi_a)\Phi_b & \\ &= -R^{ab} \frac{\delta}{\delta J^b} \frac{\delta}{\delta Q^a} W[J, Q, R] \\ &= R^{ab} \frac{\delta}{\delta J^b} \frac{\delta \Gamma[\Phi, Q, R]}{\delta Q^a} \\ &= R^{ab} G_{bc} \Gamma^c{}_{Q^a} . \end{aligned} \tag{A.35}$$

Thus the full mSTI reads

$$\frac{\delta \Gamma}{\delta Q^a} \frac{\delta \Gamma}{\delta \Phi_a} = R^{ab} G_{bc} \Gamma^c{}_{Q^a} . \tag{A.36}$$

Satisfying the mSTI at each momentum scale k ensures gauge invariance of observables at $k = 0$.

A.2. Summary of Derivative Rules used by QMeS

The relevant derivative and sign rules that are used in *QMeS* can be summarized as

$$R^{ab} = (-1)^{ab} R^{ba}\,, \qquad G_{ab} = (-1)^{ab} G_{ba}\,, \qquad \Gamma^{ab} = (-1)^{ab} \Gamma^{ba}\,,$$
$$\tfrac{\delta}{\delta\Phi_a}\tfrac{\delta}{\delta\Phi_b} O = (-1)^{ab} \tfrac{\delta}{\delta\Phi_b}\tfrac{\delta}{\delta\Phi_a} O\,,$$

$$\tfrac{\delta}{\delta\phi_a} R^{bc} = 0\,, \qquad \tfrac{\delta}{\delta\phi_a}\phi_b = \delta_{ab}\,, \qquad \tfrac{\delta}{\delta\phi_a} S^{bcd} = 0\,,$$
$$\tfrac{\delta}{\delta\Phi_a} R^{bc} = 0\,, \qquad \tfrac{\delta}{\delta\Phi_a}\Phi_b = \delta_{ab}\,, \qquad \tfrac{\delta}{\delta\Phi_a} S^{bcd} = 0\,,$$

$$\tfrac{\delta}{\delta\Phi_a}\Gamma^{b\ldots n} = \Gamma^{ab\ldots n}\,, \qquad \tfrac{\delta}{\delta\Phi_a} G_{bc} = (-1)(-1)^{ab}(-1)^{ee} G_{bd}\Gamma^{dae} G_{ec}\,.$$

A.3. Results for the Examples

In this section we give the *QMeS* output for the examples in Section 4.3.

A.3.1. YM: Flow of Gluon Two-Point Function

The full diagrams of the flow of the gluon two-point function with all indices are

```
DeriveFunctionalEquation[SetupYMFRG, DerivativeListAA, "OutputLevel" → "FullDiagrams"]
```

$$\Big\{\Big\{\frac{1}{2}\,\mathrm{GAA}[\{-p-q,\ mu\$8215,\ i\$8215,\ p+q,\ mu\$8210,\ i\$8210\}]\times\mathrm{GAA}[\{-q,\ mu\$8204,\ i\$8204,\ q,\ mu\$8197,\ i\$8197\}]\times\mathrm{GAA}[\{q,\ mu\$8221,\ i\$8221,\ -q,\ mu\$8200,\ i\$8200\}]\times$$
$$\mathrm{RdotAA}[\{q,\ mu\$8197,\ i\$8197,\ -q,\ mu\$8200,\ i\$8200\}]\times\Gamma\mathrm{AAA}[\{-p-q,\ mu\$8215,\ i\$8215,\ q,\ mu\$8221,\ i\$8221,\ p,\ nu,\ n\}]\times\Gamma\mathrm{AAA}[\{-q,\ mu\$8204,\ i\$8204,\ p+q,\ mu\$8210,\ i\$8210,\ -p,\ mu,\ m\}]\Big\},$$
$$\Big\{-\frac{1}{2}\,\mathrm{Gccbar}[\{q,\ i\$8258,\ -q,\ i\$8263\}]\times\mathrm{Gccbar}[\{q,\ i\$8280,\ -q,\ i\$8255\}]\times\mathrm{Gccbar}[\{p+q,\ i\$8269,\ -p-q,\ i\$8274\}]\times\mathrm{Rdotcbarc}[\{-q,\ i\$8255,\ q,\ i\$8258\}]\times$$
$$\Gamma\mathrm{Acbarc}[\{-p,\ mu,\ m,\ -q,\ i\$8263,\ p+q,\ i\$8269\}]\times\Gamma\mathrm{Acbarc}[\{p,\ nu,\ n,\ -p-q,\ i\$8274,\ q,\ i\$8280\}]\Big\},$$
$$\Big\{-\frac{1}{2}\,\mathrm{Gccbar}[\{-p-q,\ i\$8331,\ p+q,\ i\$8326\}]\times\mathrm{Gccbar}[\{-q,\ i\$8316,\ q,\ i\$8337\}]\times\mathrm{Gccbar}[\{-q,\ i\$8320,\ q,\ i\$8313\}]\times\mathrm{Rdotcbarc}[\{q,\ i\$8313,\ -q,\ i\$8316\}]\times$$
$$\Gamma\mathrm{Acbarc}[\{-p,\ mu,\ m,\ p+q,\ i\$8326,\ -q,\ i\$8320\}]\times\Gamma\mathrm{Acbarc}[\{p,\ nu,\ n,\ q,\ i\$8337,\ -p-q,\ i\$8331\}]\Big\},\ \Big\{-\frac{1}{2}\,\mathrm{GAA}[\{-q,\ mu\$8384,\ i\$8384,\ q,\ mu\$8374,\ i\$8374\}]\times$$
$$\mathrm{GAA}[\{q,\ mu\$8378,\ i\$8378,\ -q,\ mu\$8371,\ i\$8371\}]\times\mathrm{RdotAA}[\{-q,\ mu\$8371,\ i\$8371,\ q,\ mu\$8374,\ i\$8374\}]\times\Gamma\mathrm{AAAA}[\{q,\ mu\$8378,\ i\$8378,\ -q,\ mu\$8384,\ i\$8384,\ -p,\ mu,\ m,\ p,\ nu,\ n\}]\Big\},$$
$$\Big\{-\frac{1}{2}\,\mathrm{Gccbar}[\{-q,\ i\$8414,\ q,\ i\$8419\}]\times\mathrm{Gccbar}[\{-q,\ i\$8426,\ q,\ i\$8411\}]\times\mathrm{Rdotcbarc}[\{q,\ i\$8411,\ -q,\ i\$8414\}]\times\Gamma\mathrm{AAcbarc}[\{-p,\ mu,\ m,\ p,\ nu,\ n,\ q,\ i\$8419,\ -q,\ i\$8426\}]\Big\},$$
$$\Big\{-\frac{1}{2}\,\mathrm{Gccbar}[\{q,\ i\$8454,\ -q,\ i\$8465\}]\times\mathrm{Gccbar}[\{q,\ i\$8458,\ -q,\ i\$8451\}]\times\mathrm{Rdotcbarc}[\{-q,\ i\$8451,\ q,\ i\$8454\}]\times\Gamma\mathrm{AAcbarc}[\{-p,\ mu,\ m,\ p,\ nu,\ n,\ -q,\ i\$8465,\ q,\ i\$8458\}]\Big\},$$
$$\Big\{\frac{1}{2}\,\mathrm{GAA}[\{-p-q,\ mu\$8504,\ i\$8504,\ p+q,\ mu\$8510,\ i\$8510\}]\times\mathrm{GAA}[\{-q,\ mu\$8515,\ i\$8515,\ q,\ mu\$8494,\ i\$8494\}]\times\mathrm{GAA}[\{q,\ mu\$8498,\ i\$8498,\ -q,\ mu\$8491,\ i\$8491\}]\times$$
$$\mathrm{RdotAA}[\{-q,\ mu\$8491,\ i\$8491,\ q,\ mu\$8494,\ i\$8494\}]\times\Gamma\mathrm{AAA}[\{q,\ mu\$8498,\ i\$8498,\ -p-q,\ mu\$8504,\ i\$8504,\ p,\ nu,\ n\}]\times\Gamma\mathrm{AAA}[\{p+q,\ mu\$8510,\ i\$8510,\ -q,\ mu\$8515,\ i\$8515,\ -p,\ mu,\ m\}]\Big\},$$
$$\Big\{-\frac{1}{2}\,\mathrm{Gccbar}[\{-p-q,\ i\$8563,\ p+q,\ i\$8568\}]\times\mathrm{Gccbar}[\{-q,\ i\$8552,\ q,\ i\$8557\}]\times\mathrm{Gccbar}[\{-q,\ i\$8574,\ q,\ i\$8549\}]\times\mathrm{Rdotcbarc}[\{q,\ i\$8549,\ -q,\ i\$8552\}]\times$$
$$\Gamma\mathrm{Acbarc}[\{-p,\ mu,\ m,\ p+q,\ i\$8568,\ -q,\ i\$8574\}]\times\Gamma\mathrm{Acbarc}[\{p,\ nu,\ n,\ q,\ i\$8557,\ -p-q,\ i\$8563\}]\Big\},$$
$$\Big\{-\frac{1}{2}\,\mathrm{Gccbar}[\{q,\ i\$8610,\ -q,\ i\$8631\}]\times\mathrm{Gccbar}[\{q,\ i\$8614,\ -q,\ i\$8607\}]\times\mathrm{Gccbar}[\{p+q,\ i\$8625,\ -p-q,\ i\$8620\}]\times\mathrm{Rdotcbarc}[\{-q,\ i\$8607,\ q,\ i\$8610\}]\times$$
$$\Gamma\mathrm{Acbarc}[\{-p,\ mu,\ m,\ -q,\ i\$8631,\ p+q,\ i\$8625\}]\times\Gamma\mathrm{Acbarc}[\{p,\ nu,\ n,\ -p-q,\ i\$8620,\ q,\ i\$8614\}]\Big\}\Big\}$$

A.3.2. YM: mSTI of Gluon Two-Point Function

The gluon two-point mSTI is given as:

```
DeriveFunctionalEquation[SetupYMLHSmSTI, DerivativeListAAmSTI, "OutputLevel" → "FullDiagrams"]
```

$$\{\{-\Gamma\mathrm{AQcbar}[\{-p,\ mu,\ m,\ p,\ i\$17320\}]\times\Gamma\mathrm{cbarc}[\{-p,\ i\$17320,\ p,\ n\}]\},\ \{\Gamma\mathrm{AA}[\{p,\ mu\$17338,\ i\$17338,\ -p,\ mu,\ m\}]\times\Gamma\mathrm{cQA}[\{p,\ n,\ -p,\ mu\$17338,\ i\$17338\}]\}\}$$

```
DeriveFunctionalEquation[SetupYMmSTI, DerivativeListAAmSTI, "OutputLevel" → "FullDiagrams"]
```

$$\{\{\mathrm{GAA}[\{q,\ mu\$20414,\ i\$20414,\ -q,\ mu\$20410,\ i\$20410\}]\times\mathrm{Gccbar}[\{p+q,\ i\$20425,\ -p-q,\ i\$20420\}]\times$$
$$\mathrm{RAA}[\{-q,\ mu\$20407,\ i\$20407,\ -q,\ mu\$20410,\ i\$20410\}]\times\Gamma\mathrm{Acbarc}[\{q,\ mu\$20414,\ i\$20414,\ -p-q,\ i\$20420,\ p,\ n\}]\times\Gamma\mathrm{AcQA}[\{-p,\ mu,\ m,\ p+q,\ i\$20425,\ -q,\ mu\$20407,\ i\$20407\}]\},$$
$$\{-\mathrm{GAA}[\{p-q,\ mu\$20469,\ i\$20469,\ -p+q,\ mu\$20475,\ i\$20475\}]\times\mathrm{GAA}[\{q,\ mu\$20463,\ i\$20463,\ -q,\ mu\$20459,\ i\$20459\}]\times\mathrm{RAA}[\{-q,\ mu\$20456,\ i\$20456,\ -q,\ mu\$20459,\ i\$20459\}]\times$$
$$\Gamma\mathrm{AAA}[\{q,\ mu\$20463,\ i\$20463,\ p-q,\ mu\$20469,\ i\$20469,\ -p,\ mu,\ m\}]\times\Gamma\mathrm{AcQA}[\{-p+q,\ mu\$20475,\ i\$20475,\ p,\ n,\ -q,\ mu\$20456,\ i\$20456\}]\},$$
$$\{-\mathrm{Gccbar}[\{q,\ i\$20512,\ -q,\ i\$20505\}]\times\mathrm{Gccbar}[\{-p+q,\ i\$20523,\ p-q,\ i\$20518\}]\times\mathrm{Rcbarc}[\{-q,\ i\$20505,\ -q,\ i\$20508\}]\times\Gamma\mathrm{Acbarc}[\{-p,\ mu,\ m,\ p-q,\ i\$20518,\ q,\ i\$20512\}]\times\Gamma\mathrm{Qccc}[\{-q,\ i\$20508,\ -p+q,\ i\$20523,\ p,\ n\}]\}\}$$

A.3.3. YM: DSE of Ghost-Gluon Vertex

The full ghost-gluon vertex DSE is:

```
DeriveFunctionalEquation[SetupYMDSE, DerivativeListAcbarcDSE1, "OutputLevel" → "FullDiagrams"]
```

$$\{\{-\mathrm{SAcbarc}[\{p1,\ mu,\ m,\ p2,\ n,\ -p1-p2,\ o\}]\},$$
$$\{\mathrm{GAA}[\{p1-q,\ mu\$20910,\ i\$20910,\ -p1+q,\ mu\$20919,\ i\$20919\}]\times\mathrm{GAA}[\{q,\ mu\$20929,\ i\$20929,\ -q,\ mu\$20924,\ i\$20924\}]\times\mathrm{Gccbar}[\{-p2-q,\ i\$20936,\ p2+q,\ i\$20913\}]\times\mathrm{SAcbarc}[\{p1-q,\ mu\$20910,\ i\$20910,\ p2+q,\ i\$20913,\ -p1-p2,\ o\}]\times$$
$$\Gamma\mathrm{AAA}[\{-p1+q,\ mu\$20919,\ i\$20919,\ -q,\ mu\$20924,\ i\$20924,\ p1,\ mu,\ m\}]\times\Gamma\mathrm{Acbarc}[\{q,\ mu\$20929,\ i\$20929,\ p2,\ n,\ -p2-q,\ i\$20936\}]\},\ \{-\mathrm{GAA}[\{p1+p2-q,\ mu\$20969,\ i\$20969,\ -p1-p2+q,\ mu\$20978,\ i\$20978\}]\times$$
$$\mathrm{Gccbar}[\{-q,\ i\$20985,\ q,\ i\$20972\}]\times\mathrm{SAcbarc}[\{p1+p2-q,\ mu\$20969,\ i\$20969,\ q,\ i\$20972,\ -p1-p2,\ o\}]\times\Gamma\mathrm{AAcbarc}[\{-p1-p2+q,\ mu\$20978,\ i\$20978,\ p1,\ mu,\ m,\ p2,\ n,\ -q,\ i\$20985\}]\},$$
$$\{-\mathrm{GAA}[\{p1+p2-q,\ mu\$21010,\ i\$21010,\ -p1-p2+q,\ mu\$21019,\ i\$21019\}]\times\mathrm{Gccbar}[\{p1-q,\ i\$21025,\ -p1+q,\ i\$21030\}]\times\mathrm{Gccbar}[\{-q,\ i\$21036,\ q,\ i\$21013\}]\times$$
$$\mathrm{SAcbarc}[\{p1+p2-q,\ mu\$21010,\ i\$21010,\ q,\ i\$21013,\ -p1-p2,\ o\}]\times\Gamma\mathrm{Acbarc}[\{p1,\ mu,\ m,\ -p1+q,\ i\$21030,\ -q,\ i\$21036\}]\times\Gamma\mathrm{Acbarc}[\{-p1-p2-q,\ mu\$21019,\ i\$21019,\ p2,\ n,\ p1-q,\ i\$21025\}]\}\}$$

A.3.4. Yukawa $N_f = 1$: Flow of Two-Point Functions

The flow of the scalar and fermionic two-point function are:

```
FRGDiagramsPhiPhiNf1 = DeriveFunctionalEquation[SetupNf1, DerivativeListScalarTwopoint, "OutputLevel" → "FullDiagrams"]
```

$$\left\{\left\{-\frac{1}{2}\,\text{GPsiPsibar}[\{q, d\$3007, -q, d\$3012\}]\times\text{GPsiPsibar}[\{q, d\$3029, -q, d\$3004\}]\times\right.\right.$$
$$\text{GPsiPsibar}[\{p+q, d\$3018, -p-q, d\$3023\}]\times\text{RdotPsibarPsi}[\{-q, d\$3004, q, d\$3007\}]\times\Gamma\text{PhiPsibarPsi}[\{-p, -q, d\$3012, p+q, d\$3018\}]\times\Gamma\text{PhiPsibarPsi}[\{p, -p-q, d\$3023, q, d\$3029\}]\Big\},$$
$$\Big\{-\frac{1}{2}\,\text{GPsiPsibar}[\{-p-q, d\$3084, p+q, d\$3079\}]\times\text{GPsiPsibar}[\{-q, d\$3069, q, d\$3090\}]\times\text{GPsiPsibar}[\{-q, d\$3073, q, d\$3066\}]\times\text{RdotPsibarPsi}[\{q, d\$3066, -q, d\$3069\}]\times$$
$$\Gamma\text{PhiPsibarPsi}[\{-p, p+q, d\$3079, -q, d\$3073\}]\times\Gamma\text{PhiPsibarPsi}[\{p, q, d\$3090, -p-q, d\$3084\}]\Big\},\Big\{-\frac{1}{2}\,\text{GPhiPhi}[\{-q, q\}]\times\text{GPhiPhi}[\{q, -q\}]\times\text{RdotPhiPhi}[\{-q, q\}]\times\Gamma\text{PhiPhiPhiPhi}[\{q, -q, -p, p\}]\Big\},$$
$$\Big\{-\frac{1}{2}\,\text{GPsiPsibar}[\{-p-q, d\$3174, p+q, d\$3179\}]\times\text{GPsiPsibar}[\{-q, d\$3163, q, d\$3168\}]\times\text{GPsiPsibar}[\{-q, d\$3185, q, d\$3160\}]\times\text{RdotPsibarPsi}[\{q, d\$3160, -q, d\$3163\}]\times$$
$$\Gamma\text{PhiPsibarPsi}[\{-p, p+q, d\$3179, -q, d\$3185\}]\times\Gamma\text{PhiPsibarPsi}[\{p, q, d\$3168, -p-q, d\$3174\}]\Big\},\Big\{-\frac{1}{2}\,\text{GPsiPsibar}[\{q, d\$3221, -q, d\$3242\}]\times\text{GPsiPsibar}[\{q, d\$3225, -q, d\$3218\}]\times$$
$$\text{GPsiPsibar}[\{p+q, d\$3236, -p-q, d\$3231\}]\times\text{RdotPsibarPsi}[\{-q, d\$3218, q, d\$3221\}]\times\Gamma\text{PhiPsibarPsi}[\{-p, -q, d\$3242, p+q, d\$3236\}]\times\Gamma\text{PhiPsibarPsi}[\{p, -p-q, d\$3231, q, d\$3225\}]\Big\}\Big\}$$

```
FRGDiagramsPsibarPsiNf1 = DeriveFunctionalEquation[SetupNf1, DerivativeListFermionTwopoint, "OutputLevel" → "FullDiagrams"]
```

$$\Big\{\Big\{-\frac{1}{2}\,\text{GPhiPhi}[\{-q, q\}]\times\text{GPhiPhi}[\{q, -q\}]\times\text{GPsiPsibar}[\{p+q, d\$3972, -p-q, d\$3977\}]\times\text{RdotPhiPhi}[\{q, -q\}]\times\Gamma\text{PhiPsibarPsi}[\{-q, -p, d, p+q, d\$3972\}]\times\Gamma\text{PhiPsibarPsi}[\{q, -p-q, d\$3977, p, e\}]\Big\},$$
$$\Big\{-\frac{1}{2}\,\text{GPhiPhi}[\{-p-q, p+q\}]\times\text{GPsiPsibar}[\{-q, d\$4018, q, d\$4037\}]\times\text{GPsiPsibar}[\{-q, d\$4022, q, d\$4015\}]\times\text{RdotPsibarPsi}[\{q, d\$4015, -q, d\$4018\}]\times\Gamma\text{PhiPsibarPsi}[\{-p-q, q, d\$4037, p, e\}]\times\Gamma\text{PhiPsibarPsi}[\{p+q, -p, d, -q, d\$4022\}]\Big\},$$
$$\Big\{-\frac{1}{2}\,\text{GPsiPsibar}[\{-q, d\$4074, q, d\$4079\}]\times\text{GPsiPsibar}[\{-q, d\$4086, q, d\$4071\}]\times\text{RdotPsibarPsi}[\{q, d\$4071, -q, d\$4074\}]\times\Gamma\text{PsibarPsibarPsiPsi}[\{q, d\$4079, -p, d, p, e, -q, d\$4086\}]\Big\},$$
$$\Big\{-\frac{1}{2}\,\text{GPsiPsibar}[\{q, d\$4114, -q, d\$4124\}]\times\text{GPsiPsibar}[\{q, d\$4118, -q, d\$4111\}]\times\text{RdotPsibarPsi}[\{-q, d\$4111, q, d\$4114\}]\times\Gamma\text{PsibarPsibarPsiPsi}[\{-p, d, -q, d\$4124, q, d\$4118, p, e\}]\Big\},$$
$$\Big\{-\frac{1}{2}\,\text{GPhiPhi}[\{-q, q\}]\times\text{GPhiPhi}[\{q, -q\}]\times\text{GPsiPsibar}[\{p+q, d\$4166, -p-q, d\$4161\}]\times\text{RdotPhiPhi}[\{-q, q\}]\times\Gamma\text{PhiPsibarPsi}[\{-q, -p, d, p+q, d\$4166\}]\times\Gamma\text{PhiPsibarPsi}[\{q, -p-q, d\$4161, p, e\}]\Big\},$$
$$\Big\{-\frac{1}{2}\,\text{GPhiPhi}[\{-p-q, p+q\}]\times\text{GPsiPsibar}[\{-q, d\$4208, q, d\$4213\}]\times\text{GPsiPsibar}[\{-q, d\$4228, q, d\$4205\}]\times\text{RdotPsibarPsi}[\{q, d\$4205, -q, d\$4208\}]\times\Gamma\text{PhiPsibarPsi}[\{-p-q, q, d\$4213, p, e\}]\times\Gamma\text{PhiPsibarPsi}[\{p+q, -p, d, -q, d\$4228\}]\Big\}\Big\}$$

A.3.5. Yukawa $N_f = 2$: Flow of Two-Point Functions

The flow of the scalar and fermionic two-point function are:

```
FRGDiagramsPhiPhiNf2 = DeriveFunctionalEquation[SetupNf2, DerivativeListScalarTwopoint, "OutputLevel" → "FullDiagrams"]
```

$$\Big\{\Big\{-\frac{1}{2}\,\text{GPsi1Psibar1}[\{q, d\$6596, -q, d\$6601\}]\times\text{GPsi1Psibar1}[\{q, d\$6618, -q, d\$6593\}]\times$$
$$\text{GPsi1Psibar1}[\{p+q, d\$6607, -p-q, d\$6612\}]\times\text{RdotPsibar1Psi1}[\{-q, d\$6593, q, d\$6596\}]\times\Gamma\text{PhiPsibar1Psi1}[\{-p, -q, d\$6601, p+q, d\$6607\}]\times\Gamma\text{PhiPsibar1Psi1}[\{p, -p-q, d\$6612, q, d\$6618\}]\Big\},$$
$$\Big\{-\frac{1}{2}\,\text{GPsi2Psibar2}[\{q, d\$6654, -q, d\$6659\}]\times\text{GPsi2Psibar2}[\{q, d\$6676, -q, d\$6651\}]\times\text{GPsi2Psibar2}[\{p+q, d\$6665, -p-q, d\$6670\}]\times\text{RdotPsibar2Psi2}[\{-q, d\$6651, q, d\$6654\}]\times$$
$$\Gamma\text{PhiPsibar2Psi2}[\{-p, -q, d\$6659, p+q, d\$6665\}]\times\Gamma\text{PhiPsibar2Psi2}[\{p, -p-q, d\$6670, q, d\$6676\}]\Big\},\Big\{-\frac{1}{2}\,\text{GPsi1Psibar1}[\{-p-q, d\$6727, p+q, d\$6722\}]\times\text{GPsi1Psibar1}[\{-q, d\$6712, q, d\$6733\}]\times$$
$$\text{GPsi1Psibar1}[\{-q, d\$6716, q, d\$6709\}]\times\text{RdotPsibar1Psi1}[\{q, d\$6709, -q, d\$6712\}]\times\Gamma\text{PhiPsibar1Psi1}[\{-p, p+q, d\$6722, -q, d\$6716\}]\times\Gamma\text{PhiPsibar1Psi1}[\{p, q, d\$6733, -p-q, d\$6727\}]\Big\},$$
$$\Big\{\frac{1}{2}\,\text{GPsi2Psibar2}[\{-p-q, d\$6785, p+q, d\$6780\}]\times\text{GPsi2Psibar2}[\{-q, d\$6770, q, d\$6791\}]\times\text{GPsi2Psibar2}[\{-q, d\$6774, q, d\$6767\}]\times\text{RdotPsibar2Psi2}[\{q, d\$6767, -q, d\$6770\}]\times$$
$$\Gamma\text{PhiPsibar2Psi2}[\{-p, p+q, d\$6780, -q, d\$6774\}]\times\Gamma\text{PhiPsibar2Psi2}[\{p, q, d\$6791, -p-q, d\$6785\}]\Big\},\Big\{-\frac{1}{2}\,\text{GPhiPhi}[\{-q, q\}]\times\text{GPhiPhi}[\{q, -q\}]\times\text{RdotPhiPhi}[\{-q, q\}]\times\Gamma\text{PhiPhiPhiPhi}[\{q, -q, -p, p\}]\Big\},$$
$$\Big\{-\frac{1}{2}\,\text{GPsi1Psibar1}[\{-p-q, d\$6875, p+q, d\$6880\}]\times\text{GPsi1Psibar1}[\{-q, d\$6864, q, d\$6869\}]\times\text{GPsi1Psibar1}[\{-q, d\$6886, q, d\$6861\}]\times\text{RdotPsibar1Psi1}[\{q, d\$6861, -q, d\$6864\}]\times$$
$$\Gamma\text{PhiPsibar1Psi1}[\{-p, p+q, d\$6880, -q, d\$6886\}]\times\Gamma\text{PhiPsibar1Psi1}[\{p, q, d\$6869, -p-q, d\$6875\}]\Big\},\Big\{-\frac{1}{2}\,\text{GPsi2Psibar2}[\{-p-q, d\$6933, p+q, d\$6938\}]\times\text{GPsi2Psibar2}[\{-q, d\$6922, q, d\$6927\}]\times$$
$$\text{GPsi2Psibar2}[\{-q, d\$6944, q, d\$6919\}]\times\text{RdotPsibar2Psi2}[\{q, d\$6919, -q, d\$6922\}]\times\Gamma\text{PhiPsibar2Psi2}[\{-p, p+q, d\$6938, -q, d\$6944\}]\times\Gamma\text{PhiPsibar2Psi2}[\{p, q, d\$6927, -p-q, d\$6933\}]\Big\},$$
$$\Big\{-\frac{1}{2}\,\text{GPsi1Psibar1}[\{q, d\$6980, -q, d\$7001\}]\times\text{GPsi1Psibar1}[\{q, d\$6984, -q, d\$6977\}]\times\text{GPsi1Psibar1}[\{p+q, d\$6995, -p-q, d\$6990\}]\times\text{RdotPsibar1Psi1}[\{-q, d\$6977, q, d\$6980\}]\times$$
$$\Gamma\text{PhiPsibar1Psi1}[\{-p, -q, d\$7001, p+q, d\$6995\}]\times\Gamma\text{PhiPsibar1Psi1}[\{p, -p-q, d\$6990, q, d\$6984\}]\Big\},\Big\{-\frac{1}{2}\,\text{GPsi2Psibar2}[\{q, d\$7038, -q, d\$7059\}]\times\text{GPsi2Psibar2}[\{q, d\$7042, -q, d\$7035\}]\times$$
$$\text{GPsi2Psibar2}[\{p+q, d\$7053, -p-q, d\$7048\}]\times\text{RdotPsibar2Psi2}[\{-q, d\$7035, q, d\$7038\}]\times\Gamma\text{PhiPsibar2Psi2}[\{-p, -q, d\$7059, p+q, d\$7053\}]\times\Gamma\text{PhiPsibar2Psi2}[\{p, -p-q, d\$7048, q, d\$7042\}]\Big\}\Big\}$$

```
FRGDiagramsPsibar1Psi1Nf2 = DeriveFunctionalEquation[SetupNf2, DerivativeListFermion1Twopoint, "OutputLevel" → "FullDiagrams"]
```

$$\Big\{\Big\{-\frac{1}{2}\,\text{GPhiPhi}[\{-q, q\}]\times\text{GPhiPhi}[\{q, -q\}]\times\text{GPsi1Psibar1}[\{p+q, d\$9430, -p-q, d\$9435\}]\times\text{RdotPhiPhi}[\{q, -q\}]\times\Gamma\text{PhiPsibar1Psi1}[\{-q, -p, d, p+q, d\$9430\}]\times\Gamma\text{PhiPsibar1Psi1}[\{q, -p-q, d\$9435, p, e\}]\Big\},$$
$$\Big\{-\frac{1}{2}\,\text{GPhiPhi}[\{-p-q, p+q\}]\times\text{GPsi1Psibar1}[\{-q, d\$9476, q, d\$9495\}]\times\text{GPsi1Psibar1}[\{-q, d\$9480, q, d\$9473\}]\times\text{RdotPsibar1Psi1}[\{q, d\$9473, -q, d\$9476\}]\times\Gamma\text{PhiPsibar1Psi1}[\{-p-q, q, d\$9495, p, e\}]\times\Gamma\text{PhiPsibar1Psi1}[\{p+q, -p, d, -q, d\$9480\}]\Big\},$$
$$\Big\{\frac{1}{2}\,\text{GPsi1Psibar1}[\{-q, d\$9532, q, d\$9537\}]\times\text{GPsi1Psibar1}[\{-q, d\$9544, q, d\$9529\}]\times\text{RdotPsibar1Psi1}[\{q, d\$9529, -q, d\$9532\}]\times\Gamma\text{Psibar1Psibar1Psi1Psi1}[\{q, d\$9537, -p, d, p, e, -q, d\$9544\}]\Big\},$$
$$\Big\{\frac{1}{2}\,\text{GPsi2Psibar2}[\{-q, d\$9572, q, d\$9577\}]\times\text{GPsi2Psibar2}[\{-q, d\$9584, q, d\$9569\}]\times\text{RdotPsibar2Psi2}[\{q, d\$9569, -q, d\$9572\}]\times\Gamma\text{Psibar1Psibar2Psi1Psi2}[\{-p, d, q, d\$9577, p, e, -q, d\$9584\}]\Big\},$$
$$\Big\{-\frac{1}{2}\,\text{GPsi1Psibar1}[\{q, d\$9612, -q, d\$9622\}]\times\text{GPsi1Psibar1}[\{q, d\$9616, -q, d\$9609\}]\times\text{RdotPsibar1Psi1}[\{-q, d\$9609, q, d\$9612\}]\times\Gamma\text{Psibar1Psibar1Psi1Psi1}[\{-p, d, -q, d\$9622, q, d\$9616, p, e\}]\Big\},$$
$$\Big\{\frac{1}{2}\,\text{GPsi2Psibar2}[\{q, d\$9652, -q, d\$9662\}]\times\text{GPsi2Psibar2}[\{q, d\$9656, -q, d\$9649\}]\times\text{RdotPsibar2Psi2}[\{-q, d\$9649, q, d\$9652\}]\times\Gamma\text{Psibar1Psibar2Psi1Psi2}[\{-p, d, -q, d\$9662, p, e, q, d\$9656\}]\Big\},$$
$$\Big\{\frac{1}{2}\,\text{GPhiPhi}[\{-q, q\}]\times\text{GPhiPhi}[\{q, -q\}]\times\text{GPsi1Psibar1}[\{p+q, d\$9704, -p-q, d\$9699\}]\times\text{RdotPhiPhi}[\{-q, q\}]\times\Gamma\text{PhiPsibar1Psi1}[\{-q, -p, d, p+q, d\$9704\}]\times\Gamma\text{PhiPsibar1Psi1}[\{q, -p-q, d\$9699, p, e\}]\Big\},$$
$$\Big\{-\frac{1}{2}\,\text{GPhiPhi}[\{-p-q, p+q\}]\times\text{GPsi1Psibar1}[\{-q, d\$9746, q, d\$9751\}]\times\text{GPsi1Psibar1}[\{-q, d\$9766, q, d\$9743\}]\times\text{RdotPsibar1Psi1}[\{q, d\$9743, -q, d\$9746\}]\times\Gamma\text{PhiPsibar1Psi1}[\{-p-q, q, d\$9751, p, e\}]\times\Gamma\text{PhiPsibar1Psi1}[\{p+q, -p, d, -q, d\$9766\}]\Big\}\Big\}$$

B. Additional material: On Gauge Invariance in Gauge-Fixed Yang-Mills Theory

B.1. Numerical Implementation

The fRG and mSTI equations were derived using *QMeS* [1, 2], a Mathematica package for the derivation of symbolic functional equations. After projecting onto the respective tensor structures, the equations were traced with *FormTracer* [171, 172]. The resulting momentum-dependent integro-differential and integral equations were solved in Mathematica 12.0.

B.2. Additional Details on the fRG Computation

B.2.1. Projecting onto Tensor Structures

On the level of two-point functions, we have two quantities that contribute to the transverse sector, the gluon and the ghost two-point function. Their tensor structures are,

$$\tau^{ab}_{AA,\mu\nu}(p) = \delta^{ab}\left(\Pi^{\perp}_{\mu\nu}(p)p^2 + \Pi^{\parallel}_{\mu\nu}(p)p^2\right) ,$$
$$\tau^{ab}_{c\bar{c}}(p) = -\delta^{ab}p^2 . \tag{B.1}$$

For the derivation of their respective fRG equations we trace the diagrammatic equations with the projection operators,

$$\mathcal{P}^{ab}_{c\bar{c}}(p) = \tau^{ab}_{c\bar{c}}(p) ,$$
$$\mathcal{P}^{\perp,ab}_{AA,\mu\nu}(p) = \Pi^{\perp}_{\mu\bar{\mu}}(p)\Pi^{\perp}_{\nu\bar{\nu}}(p)\tau^{ab}_{AA,\bar{\mu}\bar{\nu}}(p) ,$$
$$\mathcal{P}^{\parallel,ab}_{AA,\mu\nu}(p) = \Pi^{\parallel}_{\mu\bar{\mu}}(p)\Pi^{\parallel}_{\nu\bar{\nu}}(p)\tau^{ab}_{AA,\bar{\mu}\bar{\nu}}(p) . \tag{B.2}$$

for the ghost and transverse gluon propagator dressing, and for the longitudinal gluon two-point respectively. The tensor structures of the ghost-gluon vertex can be written as,

$$\tau^{abc}_{A\bar{c}c,\mu}(p,q) = if^{abc}\left(\Pi^{\perp}_{\mu\nu}(p) + \Pi^{\parallel}_{\mu\nu}(p)\right)q_\nu . \tag{B.3}$$

The fRG equations for the transverse and longitidunal ghost-gluon dressing are obtained by contracting the equation, Figure B.6,

$$\mathcal{P}^{abc}_{A\bar{c}c,\mu}(p,q) = \Pi^{\perp}_{\mu\bar{\mu}}(p)\tau^{abc}_{A\bar{c}c,\bar{\mu}}(p,q) ,$$
$$\mathcal{P}^{\parallel,abc}_{A\bar{c}c,\mu}(p,q) = \Pi^{\parallel}_{\mu\bar{\mu}}(p)\tau^{abc}_{A\bar{c}c,\bar{\mu}}(p,q) . \tag{B.4}$$

From the longitudinal and transverse/classical ghost-gluon dressing one can compute the non-classical vertex dressing (5.20). The result is shown in Figure B.2. One can see that it is approximately zero for perturbative momenta.

As a tensor basis for the three- and four-gluon vertex, we apply transverse and longitudinal projections of the classical tensor structures,

$$\tau^{abc}_{A^3,\mathrm{cl},\mu\nu\rho}(p,q) = -if^{abc}\left(\delta_{\mu\nu}(p-q)_\rho + \delta_{\nu\rho}(2q+p) + \delta_{\rho\mu}(-2p-q)\right) , \tag{B.5}$$

and

$$\begin{aligned}\tau^{abcd}_{A^4,\mathrm{cl},\mu\nu\rho\sigma}(p,q,r) = {} & f^{abe}f^{cde}\left(\delta_{\mu\rho}\delta_{\nu\sigma} - \delta_{\mu\sigma}\delta_{\nu\rho}\right) \\ & + f^{ace}f^{bde}\left(\delta_{\mu\nu}\delta_{\rho\sigma} - \delta_{\mu\sigma}\delta_{\nu\rho}\right) \\ & + f^{ade}f^{bce}\left(\delta_{\mu\nu}\delta_{\rho\sigma} - \delta_{\mu\rho}\delta_{\nu\sigma}\right) .\end{aligned} \tag{B.6}$$

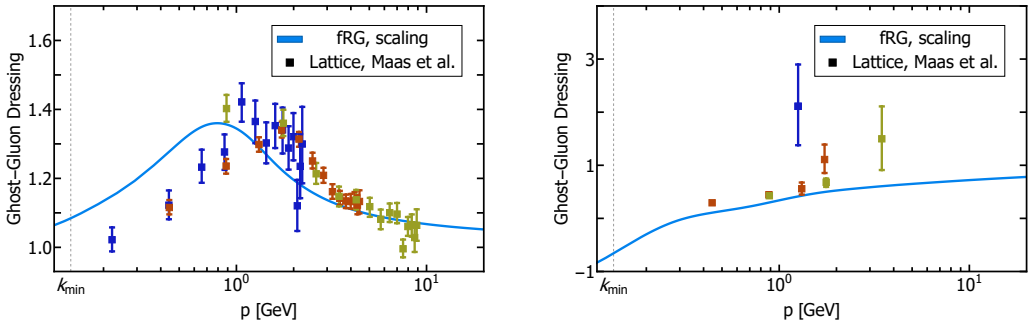

Figure B.1.: Transverse ghost-gluon and three-gluon dressings (blue lines) in comparison to $SU(2)$ lattice results [273–275] with $N = 32^4$, $\beta = \{2.13, 2.39, 2.60\}$ and $a^{-1} = \{0.8\,\text{GeV}, 1.6\,\text{GeV}, 3.2\,\text{GeV}\}$ for the dark blue/rusty red/ocher points.

We obtain the dressings, $\lambda_{A^3,1}$, $\lambda_{A^3,2}$, $\lambda_{A^4,1}$, $\lambda_{A^4,2}$, by contracting the full vertices with the longitudinal and transverse projection operators (5.15) and the classical tensor structures themselves,

$$\begin{aligned}\mathcal{P}^{abc}_{A^3,1,\mu\nu\rho}(p,q) =& \Pi^{\perp}_{\mu\bar{\mu}}(p)\Pi^{\perp}_{\nu\bar{\nu}}(q)\Pi^{\parallel}_{\rho\bar{\rho}}(-p-q)\tau^{abc}_{A^3,\text{cl},\bar{\mu}\bar{\nu}\bar{\rho}}(p,q)\,,\\ \mathcal{P}^{abc}_{A^3,2,\mu\nu\rho}(p,q) =& \Pi^{\perp}_{\mu\bar{\mu}}(p)\Pi^{\parallel}_{\nu\bar{\nu}}(q)\Pi^{\parallel}_{\rho\bar{\rho}}(-p-q)\tau^{abc}_{A^3,\text{cl},\bar{\mu}\bar{\nu}\bar{\rho}}(p,q)\,,\end{aligned} \tag{B.7}$$

and,

$$\begin{aligned}\mathcal{P}^{abcd}_{A^4,1,\mu\nu\rho\sigma}(p,q,r) &= \Pi^{\perp}_{\mu\bar{\mu}}(p)\Pi^{\perp}_{\nu\bar{\nu}}(q)\Pi^{\perp}_{\rho\bar{\rho}}(r)\Pi^{\parallel}_{\sigma\bar{\sigma}}(-p-q-r)\tau^{abcd}_{A^4,\text{cl},\bar{\mu}\bar{\nu}\bar{\rho}\bar{\sigma}}(p,q,r)\,,\\ \mathcal{P}^{abcd}_{A^4,2,\mu\nu\rho\sigma}(p,q,r) &= \Pi^{\perp}_{\mu\bar{\mu}}(p)\Pi^{\perp}_{\nu\bar{\nu}}(q)\Pi^{\parallel}_{\rho\bar{\rho}}(r)\Pi^{\parallel}_{\sigma\bar{\sigma}}(-p-q-r)\tau^{abcd}_{A^4,\text{cl},\bar{\mu}\bar{\nu}\bar{\rho}\bar{\sigma}}(p,q,r)\,.\end{aligned} \tag{B.8}$$

Analogously we define the tensor structures of the BRST-projected two-point vertices,

$$\begin{aligned}\tau^{ab}_{AQ_{\bar{c}},\mu}(p) &= -i\frac{p_\mu}{\xi}\delta^{ab}\,,\\ \tau^{ab}_{cQ_A,\mu}(p) &= -ip_\mu\delta^{ab}\,,\end{aligned} \tag{B.9}$$

and for the BRST three-point functions,

$$\begin{aligned}\tau^{abc}_{ccQ_c}(p,q) =& -f^{abc}\,,\\ \tau^{abc}_{AcQ_A,\mu\nu}(p,q) =& -f^{abc}\left(\Pi^{\perp}_{\mu\nu}(p)+\Pi^{\parallel}_{\mu\nu}(p)\right)\,.\end{aligned} \tag{B.10}$$

The relation between these tensor structures and the pure Yang-Mills ones is further elaborated in Section B.2.5.

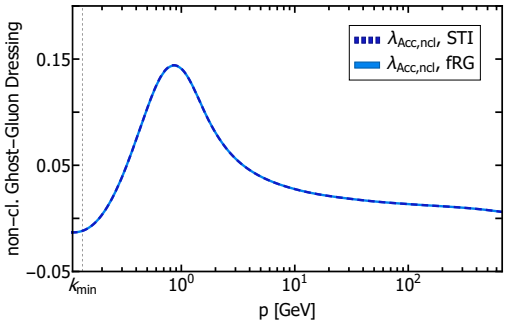

Figure B.2.: Non-classical ghost-gluon dressing from the fRG (solid blue) and STI (dashed dark blue).

B.2.2. Regulators and Gluon Mass

The transverse gluon dressing $Z_A(p)$ contains the gluon mass gap and thus diverges below 1 GeV for $k \to 0$. For the numerical computations we parameterize the gluon two-point function as,

$$\Gamma^{ab}_{AA,\mu\nu}(p) = \Pi^{\perp}_{\mu\nu}(p)\, Z_T(p)\, \left(p^2 + m_T^2\right)\, \delta^{ab} + \Pi^{\parallel}_{\mu\nu}(p)\Gamma^{\parallel}_{AA}(p)\, \delta^{ab}\,,$$

where the longitudinal part $\Gamma^{\parallel}_{AA}$ contains the gauge fixing term p^2/ξ. We obtain the transverse and longitudinal gluon mass from,

$$\begin{aligned} m^2_{\perp,k} &= Z_T(0)\, m_T^2\,, \\ m^2_{\parallel,k} &= \Gamma^{\parallel}_{AA,k}(0)\,. \end{aligned} \tag{B.11}$$

The pole mass as defined in Figure 5.5 is set to $(m^2_{\perp,\text{scaling}} - 0.0004)$ GeV. The longitudinal gluon mass from the mSTI however is extracted from,

$$m^2_{\parallel,k,\text{mSTI}} = \Gamma^{\parallel}_{AA,k,\text{mSTI}}(p = 4k_{min})\,, \tag{B.12}$$

to avoid the influence of IR cutoff effects.

For the ghost and gluon regulator we use respectively,

$$\begin{aligned} (R_A)^{ab}_{\mu\nu}(p) &= \delta^{ab} r(p^2/k^2) \left(\Pi^{\perp}_{\mu\nu}(p)\bar{Z}_T(p)\, p^2 + \Pi^{\parallel}_{\mu\nu}(p)\Gamma^{\parallel}_{AA}(p)\right)\,, \\ (R_c)^{ab}(p) &= \delta^{ab} p^2 Z_c(p) r(p^2/k^2)\,, \end{aligned} \tag{B.13}$$

where k is the RG scale and we parametrise the transverse gluon two-point as,

$$\begin{aligned} \Gamma^{\perp,ab}_{AA,\mu\nu}(p) &= \Pi^{\perp}_{\mu\nu}(p) Z_T(p)(p^2 + m_T^2)\delta^{ab} \\ &= \Pi^{\perp}_{\mu\nu}(p)\left(\bar{Z}_T(p)(p^2 + \bar{m}_T^2 + k^2) - k^2\right)\delta^{ab}\,. \end{aligned} \tag{B.14}$$

The dressing $\bar{Z}_T$ guarantees a well-defined regulator in the infrared. The shape function is defined as an exponential,

$$r(p^2/k^2) = \frac{e^{-p^2/k^2}}{1 - e^{-p^2/k^2}}\,. \tag{B.15}$$

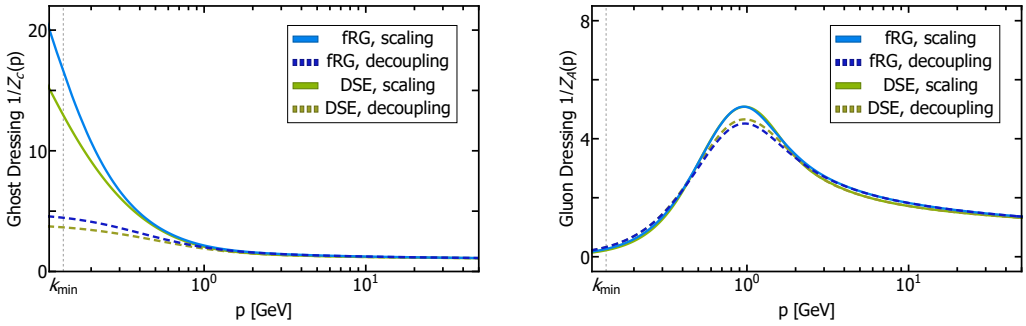

Figure B.3.: Ghost and gluon propagator dressings from the fRG (blue) in comparison to DSE results (green), from [39], for the scaling (solid line) and decoupling (dashed line) solution. The DSE dressings were rescaled such that they agree with the corresponding fRG dressings at $p = \Lambda \approx 672.6\,\mathrm{GeV}$.

B.2.3. Extraction of Scale

We set the momentum scale by positioning the maximum of the gluon dressing $1/Z_A(p)$ at the lattice scale $p \approx 0.955\,\mathrm{GeV}$ from [149].

When comparing our propagators and dressings to the aforementioned lattice results one also has to adjust the global normalization, $Z^{-1}_{\mathrm{Lat}}(p) \to y Z^{-1}_{\mathrm{Lat}}(p)$. This is done via minimizing

$$N_{Z_A}(y) = \sum_i \frac{\Delta x_i}{\Delta E_i^2} \left[\left(Z_A^{-1}(p_i) - y Z^{-1}_{\mathrm{Lat}}(p_i) \right)^2 + \left(\partial_p Z_A^{-1}(p_i) - y \partial_p Z^{-1}_{\mathrm{Lat}}(p_i) \right)^2 \right] \tag{B.16}$$

in the region $0.8\,\mathrm{GeV} \leq p_i \leq 4\,\mathrm{GeV}$, where the lattice input Δx_i denotes the distances to the next point, ΔE_i^2 the statistical error of that point and $Z^{-1}_{\mathrm{Lat}}(p)$ is the gluon dressing obtained from the lattice computation [149]. The normalization procedure for the ghost dressing is done analogously in the fitting range $1.5\,\mathrm{GeV} \leq p_i \leq 6\,\mathrm{GeV}$.

B.2.4. Scaling Exponents

The scaling exponents, c.f. (5.35), obtained from our transverse scaling results in the regime $0.135\,\mathrm{GeV} \leq p \leq 0.471\,\mathrm{GeV}$ are

$$\begin{aligned} \kappa_{gl} &= 0.535 \\ \kappa_{gh} &= 0.541 \end{aligned} \tag{B.17}$$

B.2.5. BRST Projected Vertices

The effective action exhibits shift symmetry in the anti-ghost. This symmetry leads to the identities,

$$\begin{aligned} \partial \cdot \frac{\delta \Gamma}{\delta Q_A} &= \frac{\delta \Gamma}{\delta \bar{c}}\,, \\ \frac{\delta \Gamma}{\delta Q_{\bar{c}}} &= \frac{1}{\xi} \partial \cdot A\,. \end{aligned} \tag{B.18}$$

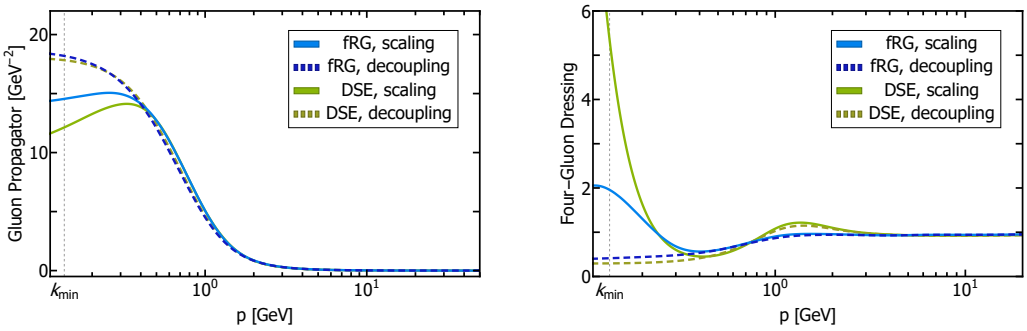

Figure B.4.: Gluon propagator and four-gluon dressing from the fRG (blue) in comparison to DSE results (green), from [39], for the scaling (solid line) and decoupling (dashed line) solution. The DSE dressings were rescaled such that they agree with the corresponding fRG dressings at $p = \Lambda \approx 672.6\,\text{GeV}$.

Fourier transforming both gives,

$$\begin{aligned} -iq_\nu \Gamma_{Q_A,\nu}(q) &= \Gamma_{\bar{c}}(q)\,, \\ \Gamma_{Q_{\bar{c}}}(-p) &= \frac{1}{\xi} ip_\mu A_\mu(p)\,. \end{aligned} \tag{B.19}$$

The first identity relates,

$$\begin{aligned} iq_\nu \Gamma^{adb}_{AcQ_A,\mu\nu}(p,-p-q) &= \Gamma^{abd}_{A\bar{c}c,\mu}(p,q)\,, \\ ip_\mu \Gamma^{ba}_{cQ_A,\mu}(-p) &= \Gamma^{ab}_{\bar{c}c}(p)\,. \end{aligned} \tag{B.20}$$

Generally we can write down the full tensor basis,

$$\Gamma^{adb}_{AcQ_A,\mu\nu}(p,-p-q) = f^{abd}\left(\delta_{\mu\nu}\lambda_1 + p_\mu p_\nu \lambda_2 + q_\mu q_\nu \lambda_3 + p_\mu q_\nu \lambda_4 + q_\mu p_\nu \lambda_5\right)\,. \tag{B.21}$$

The shift symmetry identity (B.20) then relates,

$$\begin{aligned} \lambda_{A\bar{c}c} &= \lambda_1 + q^2\lambda_3 + pq\lambda_5 \\ \lambda_{A\bar{c}c,ncl} &= pq\lambda_2 + q^2\lambda_4 \\ \lambda_{A\bar{c}c,\parallel} &= \lambda_1 + q^2\lambda_3 + pq\lambda_5 - 2pq\lambda_2 - 2q^2\lambda_4\,. \end{aligned} \tag{B.22}$$

The diagrams contributing to the flow of the AcQ_A- and cQ_A-dressings are depicted in Figure B.6. One can see that the identity (B.20) is already diagrammatically fulfilled for the fRG equations. Thus they are exact identities. Therefore applying them in the STIs is valid and the exactness of the identities guarantees gauge parameter independence of the three-gluon STI. However the STIs not only depend on these specific combinations of dressings, therefore a computation of all five from the fRG is nonetheless necessary.

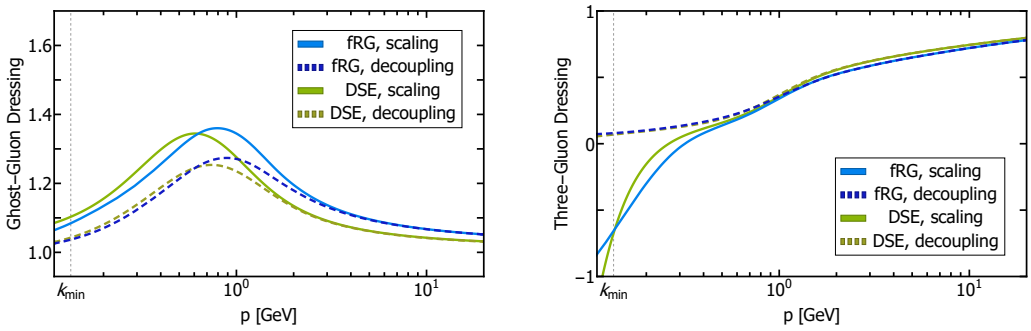

Figure B.5.: Transverse ghost-gluon and three-gluon dressings from the fRG (blue) in comparison to DSE results (green), from [39], for the scaling (solid line) and decoupling (dashed line) solution. The DSE dressings were rescaled such that they agree with the corresponding fRG dressings at $p = \Lambda \approx 672.6\,\mathrm{GeV}$.

We however simplify the approximation by identifying,

$$\lambda_{AcQ_A,1}(p,-p-q) = \lambda_{A\bar{c}c,1}(p,q)\,,$$

$$\lambda_{AcQ_A}(p,-p-q) = \lambda_{A\bar{c}c}(p,q)\,,$$

$$Z_{cQ_A}(p) = Z_c(p)\,, \tag{B.23}$$

where the index 1 indicates a longitudinally projected gluon. This approximation should not lead to qualitative differences.

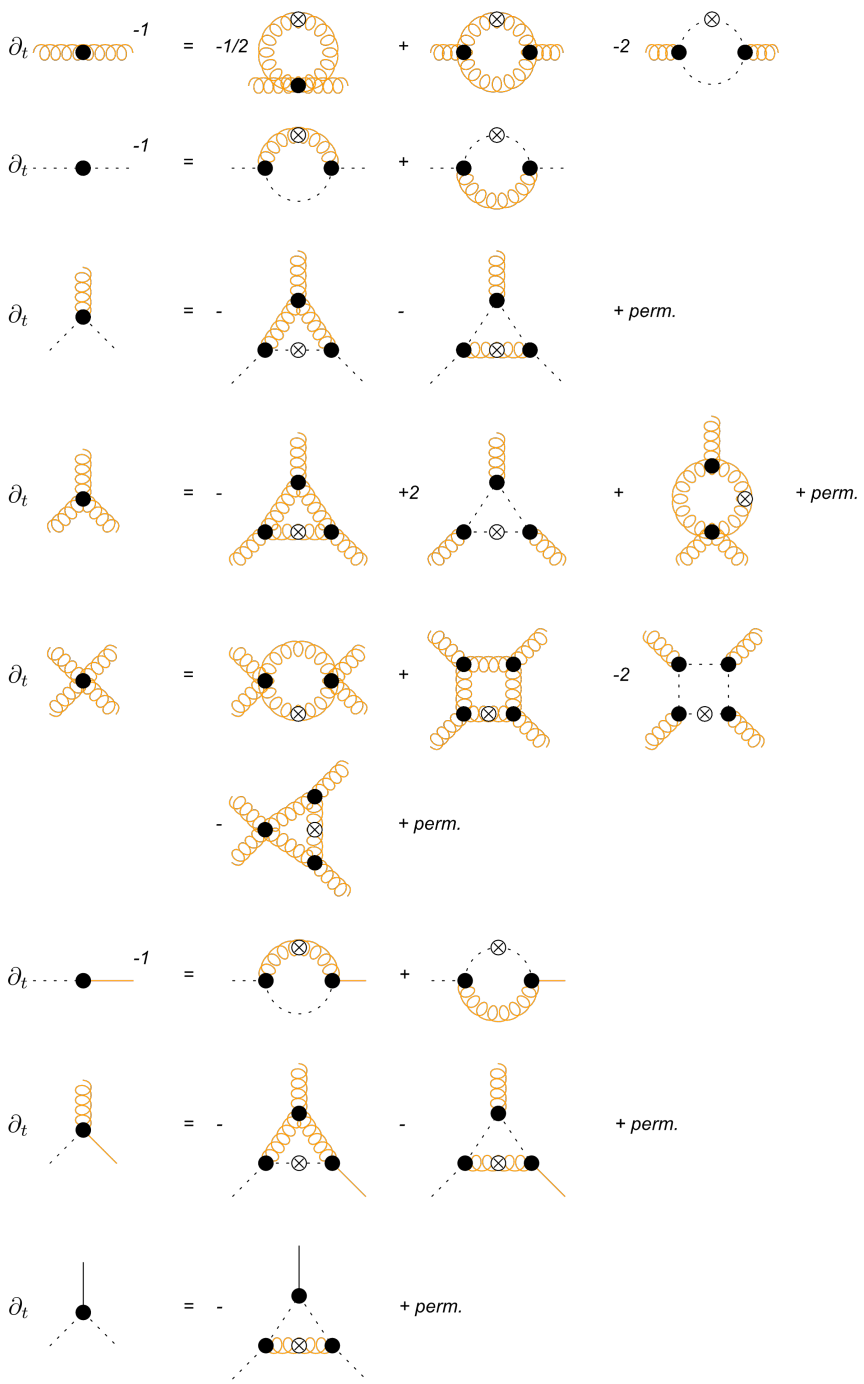

Figure B.6.: Diagrammatic representation of the flow equations of propagators and vertices. The dashed lines represent the fully dressed ghost, curly orange lines the fully dressed gluon, solid black lines to fully dressed Q_c and solid orange lines to the fully dressed Q_A BRST charge. The permutations include permutations of external legs as well as the position of the regulator derivative insertions which is indicated by the crossed circle. The power -1 indicates a full two-point function.

B.3. Additional Details on the mSTI

B.3.1. Longitudinal Gluon Two-Point Function and Gluon Mass

To obtain the mSTI of the longitudinal gluon two-point function one takes the functional derivatives $\delta^2/(\delta A^a_\mu \delta c^b)$ of the mSTI (5.11) projects both sides of the equation with,

$$\mathcal{Q}^{ab}_{AA,\mu} = p_\nu \tau^{ab}_{AA,\nu\mu}(p)\,. \tag{B.24}$$

After normalization, one obtains the STI

$$\Gamma^{\parallel}_{AA,\mathrm{reg}}(p) = 0\,. \tag{B.25}$$

We can compare the one-loop, transverse and longitudinal, mass running from the fRG with the one-loop longitudinal mass from the STI. The different diagrams contributing to the equations can be found in Figure B.6 and B.7. Inserting undressed propagators and vertices with a gauge coupling g and the regulator shape function $r(q^2) \equiv r(q^2/k^2)$, see (B.15), one obtains for the transverse gluon mass from the fRG,

$$\dot{m}^2_\perp = \int dz dq \frac{q^3\sqrt{1-z^2}}{4\pi^3} \frac{g^2 q^2 \dot{r}(q^2)}{q^4(1+r(q^2))^3} \left(3 - 9z^2 + r(q^2)(-7+z^2)\right) \tag{B.26}$$

where $z = \frac{p\cdot q}{|p||q|}$. Performing the loop integration, one arrives at the one-loop running,

$$\dot{m}^2_\perp = k\partial_k m^2_\perp = -\frac{9g^2}{64\pi^2}k^2\,. \tag{B.27}$$

Solving the differential equation yields,

$$m^2_\perp = -\frac{9g^2}{128\pi^2}k^2\,. \tag{B.28}$$

For the longitudinal gluon mass from the fRG one obtains,

$$\dot{m}^2_\parallel = \int dz dq \frac{q^3\sqrt{1-z^2}}{4\pi^3} \frac{g^2 q^2 \dot{r}(q^2)}{q^4(1+r(q^2))^3} \left(2 - 9z^2 + r(q^2)(2+z^2)\right)\,. \tag{B.29}$$

Even though the longitudinal vertices contribute differently, one arrives at the same one-loop running as for the transverse mass and thus the longitudinal mass is,

$$m^2_\parallel = -\frac{9g^2}{128\pi^2}k^2\,. \tag{B.30}$$

For the derivation of the one-loop mass from the mSTI, one has to take the zero momentum limit $p \to 0$ of the equation for $\Gamma^{AA}_{\parallel}(p)$ with the rule of l'Hospital,

$$\lim_{p\to 0}\frac{f(p)}{g(p)} = \lim_{p\to 0}\frac{f'(p)}{g'(p)}\,. \tag{B.31}$$

One then obtains the equation [276],

$$m^2_\parallel = \int dz dq \frac{q^3\sqrt{1-z^2}}{4\pi^3} \frac{g^2 q^2 r(q^2)}{q^4(1+r(q^2))^3} \left((-2+9z^2)(1+r(q^2)) + 8q^2 z^2 \partial_q r(q^2)\right)\,. \tag{B.32}$$

Integrating this, one arrives at the same one-loop mass as from the fRG,

$$m^2_\parallel = -\frac{9g^2}{128\pi^2}k^2\,. \tag{B.33}$$

Although all three equations contain different contributions and diagrams, they yield the same gluonic mass at one-loop level.

B.3.2. Ghost-Gluon Vertex mSTI

We take the functional derivatives $\delta^3/(\delta\bar{c}^a\delta c^b\delta c^c)$ of (5.11). To project onto the dressings we trace the equation with f^{abc}. Thus the projection operator is,

$$\mathcal{Q}^{abc}_{A\bar{c}c}(p,q) = p_\mu \tau^{abc}_{A\bar{c}c,\mu}(p,q)\,. \tag{B.34}$$

After normalization, the STI for the non-classical ghost-gluon dressing at the symmetric point is given as,

$$\lambda_{Qccc}(p) - \lambda_{A\bar{c}c}(p) + 2\lambda_{A\bar{c}c,noncl}(p) = 0\,. \tag{B.35}$$

From this we can derive:

$$\begin{aligned}
\lambda_{A\bar{c}c,ncl}(p) &= \frac{1}{2}\left(\lambda_{A\bar{c}c}(p) - \lambda_{Qccc}(p)\right)\,,\\
\lambda_{A\bar{c}c}(p) &= \lambda_{A\bar{c}c}(p)\,,\\
\lambda_{A\bar{c}c,1}(p) &= \lambda_{A\bar{c}c}(p) - 2\lambda_{A\bar{c}c,ncl}(p) = \lambda_{Qccc}(p)\,.
\end{aligned} \tag{B.36}$$

A comparison of the non-classical ghost-gluon dressing from the mSTI and from the fRG can be found in Figure B.2.

B.3.3. Three-Gluon Vertex mSTI

One can derive the three-gluon mSTI by taking the functional derivatives $\delta^3/\delta A^a_\mu \delta A^b_\nu \delta c^c$. For the projection onto the mSTI for the three-gluon dressings with one and two longitudinal legs, $\lambda_{A^3,1}(p,q)$ and $\lambda_{A^3,2}(p,q)$, one uses,

$$\begin{aligned}
\mathcal{Q}^{abc}_{A^3,1,\mu\nu}(p,q) &= \Pi^{\perp}_{\mu\bar{\mu}}(p)\Pi^{\perp}_{\nu\bar{\nu}}(q)(-p-q)_{\bar{\rho}}\tau^{abc}_{A^3,cl,\bar{\mu}\bar{\nu}\bar{\rho}}(p,q)\,,\\
\mathcal{Q}^{abc}_{A^3,2,\mu\nu}(p,q) &= \Pi^{\perp}_{\mu\bar{\mu}}(p)\Pi^{\parallel}_{\nu\bar{\nu}}(q)(-p-q)_{\bar{\rho}}\tau^{abc}_{A^3,cl,\bar{\mu}\bar{\nu}\bar{\rho}}(p,q)\,.
\end{aligned} \tag{B.37}$$

Since the classical tensor structure has no overlap with the first projection operator, there exists no mSTI for $\lambda_{A^3,1}(p)$ in our truncation, see also (5.37), for the equivalent case in the fRG equations.

B.3.4. Four-Gluon Vertex mSTI

We take the field derivatives $\delta^4/\delta A^a_\mu A^b_\nu A^c_\rho c^d$ of (5.11). The projection operators to obtain mSTI equations for the longitudinal four-gluon dressings $\lambda_{A^4,1}(p,q,r)$ and $\lambda_{A^4,2}(p,q,r)$ are given as,

$$\begin{aligned}
\mathcal{Q}^{abcd}_{A^4,1,\mu\nu\rho}(p,q,r) &= \Pi^{\perp}_{\mu\bar{\mu}}(p)\Pi^{\perp}_{\nu\bar{\nu}}(q)\Pi^{\perp}_{\rho\bar{\rho}}(r)(-p-q-r)_{\bar{\sigma}}\tau^{abcd}_{A^4,cl,\bar{\mu}\bar{\nu}\bar{\rho}\bar{\sigma}}(p,q,r)\,,\\
\mathcal{Q}^{abcd}_{A^4,2,\mu\nu\rho}(p,q,r) &= \Pi^{\perp}_{\mu\bar{\mu}}(p)\Pi^{\perp}_{\nu\bar{\nu}}(q)\Pi^{\parallel}_{\rho\bar{\rho}}(r)(-p-q-r)_{\bar{\sigma}}\tau^{abcd}_{A^4,cl,\bar{\mu}\bar{\nu}\bar{\rho}\bar{\sigma}}(p,q,r)\,.
\end{aligned} \tag{B.38}$$

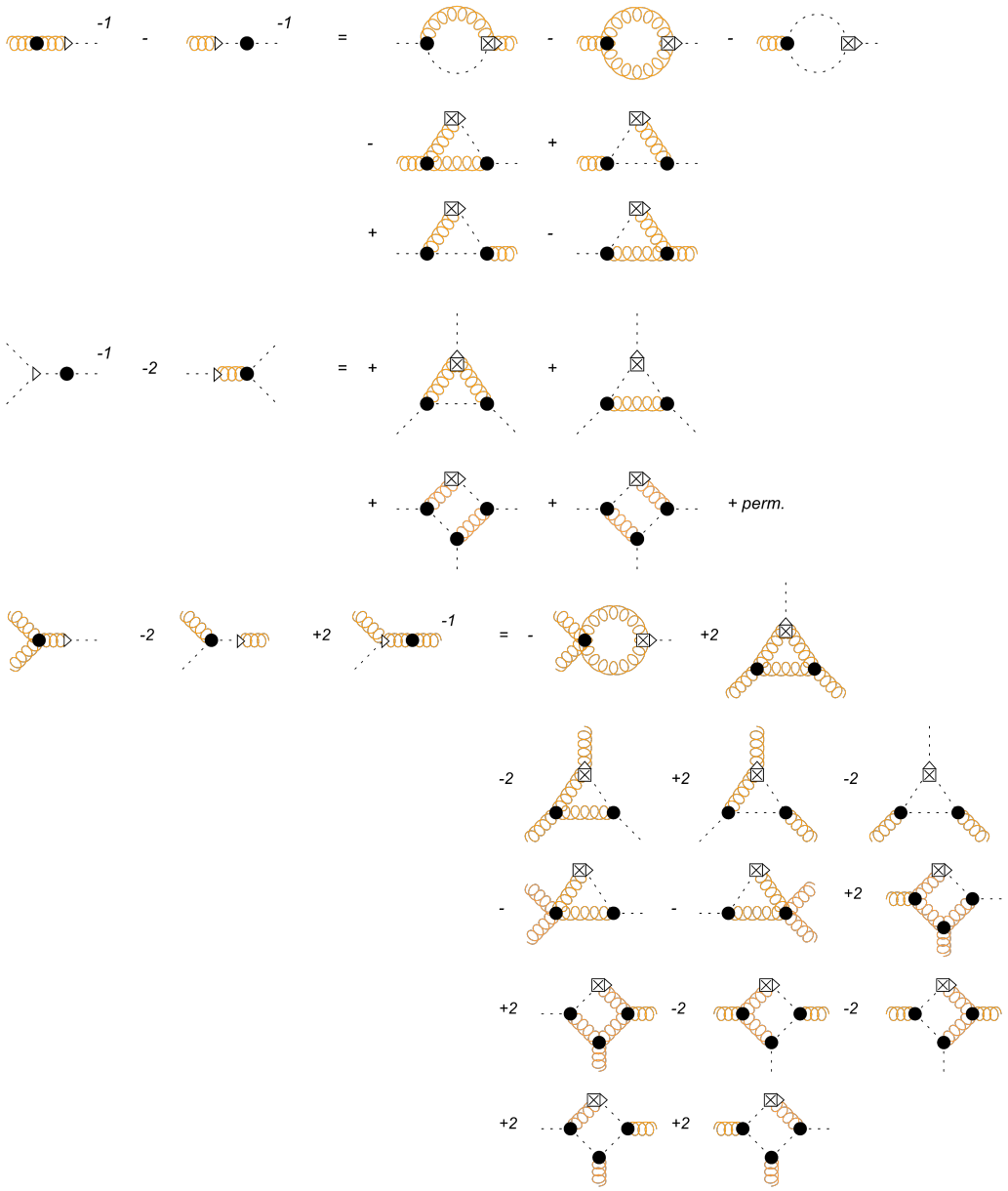

Figure B.7.: Diagrammatic representation of the modified Slavnov-Taylor identities for the longitudinal vertices. The dashed lines represent the fully dressed ghost, curly orange lines the fully dressed gluon. The black circles represent full vertices and the crossed square corresponds to a regulator and the triangle to a BRST vertex. The power -1 indicates a full two-point function. The permutations include permutations of external ghost legs.

C. Additional material: Glueball Masses from the fRG

C.1. Computational Details

C.1.1. Numerical Implementation

The fRG equations were derived using *QMeS* [1, 2], a Mathematica package for the derivation of symbolic functional equations. After projecting onto the respective glueballs tensor structures, the equations were traced with *FormTracer* [171, 172]. The resulting momentum-dependent integro-differential and integral equations were solved in Mathematica 12.0. The Padé approximants and the respective spectral functions were computed using Mathematica 12.0. The Gaussian Process Regression was done and optimized in Python 3, where the integrals were approximated using a Riemann sum.

C.1.2. fRG Equation

The fRG equation for the four-gluon vertex was computed on the scaling solution presented in Chapter 5. We only include the classical transverse tensor structures of vertices. The scalar and pseudoscalar s-channel four-gluon dressings do not feed back into the equation. We approximate the four-gluon dressings in the equations as the classical transverse symmetric point dressing $\lambda_{A^4,cl}(\bar{p})$,

$$\bar{p}^2 = \frac{1}{4}\sum_{i=1}^{4} p_i^2 \,, \tag{C.1}$$

where the momenta p_i are the ones entering the respective four-gluon vertices in the fRG equation. Other details on the approximations and quantities feeding back into the equation can be found in Chapter 5.

C.1.3. RG Consistency

Due to the fact that scalar and pseudo-scalar dressings do not feed back into the fRG equation we are at liberty to choose their respective initial conditions such, that the RG consistency condition (3.21) is fulfilled and we get the classical theory in the UV.

This means in particular that the scalar dressing is equal to the classical transverse four-gluon dressing for large momenta $p \gg \Lambda$, since the scalar projection, (6.21), has overlap with this dressing.

The pseudo-scalar projection operator, (6.25), has per definition no overlap with the scalar and classical transverse dressing. It therefore goes to zero for large momenta.

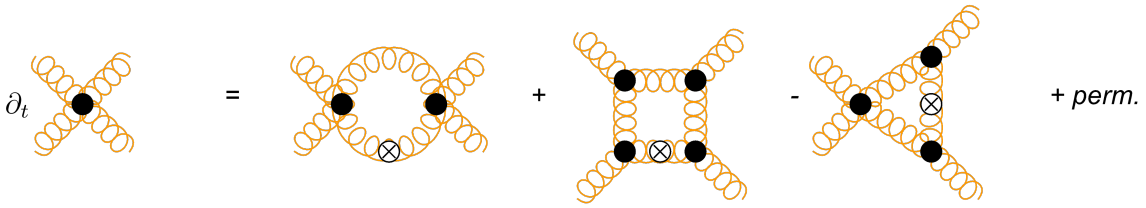

Figure C.1.: fRG equation for the s-channel four-gluon vertex dressing. Wiggly orange lines correspond to fully dressed gluon propagators. The black dots indicate fully dressed vertices. Permutations include permutations of external legs, as well as permutations of the regulator insertion that is marked by a crossed circle.

C.1.4. Momentum Parametrisation

We define the spatial vectors for the two-point functions as,

$$p = \begin{pmatrix} p \\ 0 \\ 0 \\ 0 \end{pmatrix} \qquad p^T = \begin{pmatrix} 0 \\ p \\ 0 \\ 0 \end{pmatrix} \qquad q = q \begin{pmatrix} z \\ \sqrt{1-z^2}y \\ \sqrt{1-z^2}\sqrt{1-y^2}\cos\phi \\ \sqrt{1-z^2}\sqrt{1-y^2}\sin\phi \end{pmatrix}, \tag{C.2}$$

and the spatial scalar products

$$\begin{aligned} p \cdot p &= p^2 \,, \\ p \cdot p^T &= p^2 \,. \end{aligned} \tag{C.3}$$

The loop momentum integration measure is

$$\int d^4q = \int_0^{2\pi} \int_{-1}^{1} \int_{-1}^{1} \int_0^{\infty} \frac{q^3\sqrt{1-z^2}}{(2\pi)^4} dq dz dy d\phi \,. \tag{C.4}$$

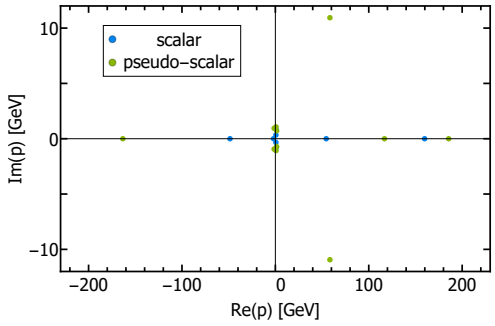

Figure C.2.: Position of poles of the scalar and pseudo-scalar Padé approximants as presented in Figure 6.1 and 6.2 in the complex plane.

C.2. Spectral Functions and Reconstruction

C.2.1. Pole Structure of Padé Approximants

The failure of the Padé spectral functions to reproduce the respective fRG dressings for both projections can be explained by the presence of poles on the Euclidean axis, as well as in the right half-plane, see Figure C.2. The non-analyticities in the right half-plane violate the relation between the spectral function (6.5) and the Källén-Lehmann representation of the dressing (6.3). This explains the failure of even qualitatively reproducing the fRG dressing from the Padé spectral function in Figure 6.1 and 6.2. We therefore also refrain from extracting the glueball masses from the respective Padé spectral function. Further modifications such as smoothing the Euclidean data or constraining them to only certain momentum regimes might remedy this approach. We however defer this strategy to future work.

C.2.2. Optimized Parameters

We perform a grid scan of the log-likelihood (6.20) for different parameter values and additionally include hyperpriors to circumvent obtaining unstable directions in the parameter space. The Gaussian covariance matrix $\mathbf{C_d}$ of the uncertainties of the fRG data was set to $10^{-6}\mathbb{1}$. Throughout the computation we set the mean $\mu = 0$. We slightly modify the Gaussian kernel (6.13) via a non-linear rescaling,

$$\omega \to \frac{1}{e^{(\omega-\omega_0)/l_0}+1}\,. \tag{C.5}$$

This modification enhances the UV and IR asymptotic stability of the spectral function. For a similar procedure, see [217].

The optimized parameters for the scalar and pseudo-scalar spectral function are presented below.

J^{PC}	σ_1^2	σ_2^2	ω_0	l_0
0^{++}	1000	0.0049	1	0.15
0^{-+}	1000	0.0064	1.2	0.2

D. Additional material: Phase Structure of QCD

D.1. Projection Operators

We have three DSEs for the quark propagator dressings, two for the gluon propagator dressings and six for the quark-gluon vertex. We project,

$$\begin{aligned} Z_M(p) \propto & \Pi^M_{\mu\mu'}(p)\Pi^M_{\nu\nu'}(p)\tau_{AA,\mu'\nu'}(p)\Gamma_{AA,\mu\nu}(p) \\ Z_E(p) \propto & \Pi^E_{\mu\mu'}(p)\Pi^E_{\nu\nu'}(p)\tau_{AA,\mu'\nu'}(p)\Gamma_{AA,\mu\nu}(p) \end{aligned}$$

$$\begin{aligned} Z_q(p) \propto & \delta^{ab}\delta^{fg_1f_2} i(\gamma_\nu^{ji} p_\nu - \gamma_0^{ji} p_0)\Gamma^{ab,ij,f_1f_2}_{\bar{q}q}(p) \\ Z_{q,\|}(p) \propto & \delta^{ab}\delta^{f_1f_2}\gamma_0^{ji} p_0 \Gamma^{ab,ij,f_1f_2}_{\bar{q}q}(p) \\ m_q(p) \propto & \delta^{ab}\delta^{fg_1f_2}\delta^{ij}\Gamma^{ab,ij,f_1f_2}_{\bar{q}q}(p)\,, \end{aligned} \tag{D.1}$$

For the dressing we apply a different procedure since the tensor basis is not orthogonal. For this we compute a projection matrix. We know that,

$$\tau^i\tau^j = M^{ij}\,, \tag{D.2}$$

where τ^i with $i = 1, ..., 8$ are the tensor structures of the quark-gluon vertex with indices dropped for simplicity and M^{ij} is a matrix. For a basis that is not orthogonal, such as our basis, this matrix is not diagonal. However we want to find a projection operator σ^i such that,

$$\sigma^i\tau^j = \delta^{ij}\lambda^{(i)}_{A\bar{q}q}\,. \tag{D.3}$$

We obtain,

$$\begin{aligned} (M^{-1})^{ik}\tau^k\tau^j &= (M^{-1})^{ik}M^{kj} \\ \sigma^i\tau^j &= \delta^{ij}\,, \end{aligned} \tag{D.4}$$

with $\sigma^i = (M^{-1})^{ik}\tau^k$.

D.2. Quark-Gluon Vertex

We can write the transverse tensor basis of the quark-gluon vertex as,

$$\Gamma^{a}_{\bar{q}qA,\mu}(p,q) = \mathbb{1}_f T^a_c \Pi^{\perp}_{\mu\nu}(p+q) \sum_{i=1}^{8} \lambda^{(i)}_{A\bar{q}q}(p,q)\tau^{(i)}_{\nu}(p,q)\,, \tag{D.5}$$

with the transverse projection operator,

$$\Pi^{\perp}_{\mu\nu}(p) = \delta_{\mu\nu} - \frac{p_\mu p_\nu}{p^2}\,, \tag{D.6}$$

and where the tensor structures are given as,

$$\begin{aligned}
\tau^{(1)}_{\mu}(p,q) &= -i\gamma_\mu \\
\tau^{(2)}_{\mu}(p,q) &= (p-q)_\mu \mathbb{I}_s \\
\tau^{(3)}_{\mu}(p,q) &= (\not{p} - \not{q})\gamma_\mu \\
\tau^{(4)}_{\mu}(p,q) &= (\not{p} + \not{q})\gamma_\mu \\
\tau^{(5)}_{\mu}(p,q) &= i(\not{p} + \not{q})(p-q)_\mu \\
\tau^{(6)}_{\mu}(p,q) &= i(\not{p} - \not{q})(p-q)_\mu \\
\tau^{(7)}_{\mu}(p,q) &= \frac{i}{2}\left[\not{p},\not{q}\right]\gamma_\mu \\
\tau^{(8)}_{\mu}(p,q) &= \frac{i}{2}\left[\not{p},\not{q}\right](p-q)_\mu\,.
\end{aligned} \tag{D.7}$$

D.3. Thermal Split in the Quark-Gluon Vertex

Generally the projection operators (7.5) acts on all Lorenz indices. We however approximate the thermal split by only acting on the open index μ in the quark-gluon vertex. Thus, the tensor structures of the electric vertex are,

$$\begin{aligned}
\tau_0^{(1)}(p,q) &= -i\gamma_0 \\
\tau_0^{(2)}(p,q) &= (p-q)_0 \mathbb{I}_s \\
\tau_0^{(3)}(p,q) &= (\not{p}-\not{q})\gamma_0 \\
\tau_0^{(4)}(p,q) &= (\not{p}+\not{q})\gamma_0 \\
\tau_0^{(5)}(p,q) &= i(\not{p}+\not{q})(p-q)_0 \\
\tau_0^{(6)}(p,q) &= i(\not{p}-\not{q})(p-q)_0 \\
\tau_0^{(7)}(p,q) &= \frac{i}{2}\left[\not{p},\not{q}\right]\gamma_0 \\
\tau_0^{(8)}(p,q) &= \frac{i}{2}\left[\not{p},\not{q}\right](p-q)_0\,,
\end{aligned} \tag{D.8}$$

and the magnetic vertex tensor structures are given as,

$$\begin{aligned}
\tau_j^{(1)}(p,q) &= -i\gamma_j \\
\tau_j^{(2)}(p,q) &= (p-q)_j \mathbb{I}_s \\
\tau_j^{(3)}(p,q) &= (\not{p}-\not{q})\gamma_j \\
\tau_j^{(4)}(p,q) &= (\not{p}+\not{q})\gamma_j \\
\tau_j^{(5)}(p,q) &= i(\not{p}+\not{q})(p-q)_j \\
\tau_j^{(6)}(p,q) &= i(\not{p}-\not{q})(p-q)_j \\
\tau_j^{(7)}(p,q) &= \frac{i}{2}\left[\not{p},\not{q}\right]\gamma_j \\
\tau_j^{(8)}(p,q) &= \frac{i}{2}\left[\not{p},\not{q}\right](p-q)_j\,,
\end{aligned} \tag{D.9}$$

where $\mu = (0,j)$ and $j = 1,2,3$. The fully dressed vertices are then given as,

$$\begin{aligned}
\Gamma^{a,E}_{\bar{q}qA,\mu}(p,q) &= \mathbb{1}_f T_c^a \Pi^E_{\mu 0}(p+q) \sum_{i=1}^{8} \lambda^{(i)}_{A\bar{q}q,E}(p,q)\tau_0^{(i)}(p,q) \\
\Gamma^{a,M}_{\bar{q}qA,\mu}(p,q) &= \mathbb{1}_f T_c^a \Pi^M_{\mu j}(p+q) \sum_{i=1}^{8} \lambda^{(i)}_{A\bar{q}q,M}(p,q)\tau_j^{(i)}(p,q)\,.
\end{aligned} \tag{D.10}$$

D.4. Spatial Momentum Parametrisation at Finite Temperature

We define the spatial vectors for the two-point functions as,

$$\vec{p} = \begin{pmatrix} p \\ 0 \\ 0 \end{pmatrix} \qquad \vec{q} = \begin{pmatrix} qz \\ q\sqrt{1-z^2}\cos\phi \\ q\sqrt{1-z^2}\sin\phi \end{pmatrix}, \tag{D.11}$$

and the spatial scalar products

$$p_i \cdot p_j = p^2\,, \tag{D.12}$$

For the spatial scalar products of three-points we use

$$p_i \cdot p_j = -\frac{p^2}{2} \quad \text{for} \quad i \neq j\,, \tag{D.13}$$

and

$$\vec{p_1} = \begin{pmatrix} p \\ 0 \\ 0 \end{pmatrix}, \qquad \vec{p_2} = \begin{pmatrix} -1/2p \\ p\sqrt{3}/2 \\ 0 \end{pmatrix}. \tag{D.14}$$

The loop momentum integration measure is

$$\int d^4q = \int_0^{2\pi} \int_{-1}^{1} \int_0^{\infty} \frac{q^2}{(2\pi)^3} dq dz d\phi\,. \tag{D.15}$$

Acknowledgments

First, I would like to thank Jan M. Pawlowski for his supervision and support. I am grateful for all the productive discussions and his great enthusiasm for physics as well as his counsel and advice in general.
Furthermore, I would like to thank Jörg Jäckel for being my second referee.
Special thanks go to all of my collaborators and colleagues for contributing to my scientific understanding and making my PhD studies in Heidelberg enjoyable.
Lastly, I would like to express my gratitude to my friends and family that have supported me during my studies in every way possible.

Bibliography

[1] J. M. Pawlowski, C. S. Schneider, and N. Wink, "QMeS-Derivation: Mathematica package for the symbolic derivation of functional equations," (2021), arXiv:2102.01410 [hep-ph].

[2] J. M. Pawlowski, C. S. Schneider, and N. Wink, "QMeS-Derivation GitHub Repository," (2021), `https://github.com/QMeS-toolbox/QMeS-Derivation`.

[3] J. M. Pawlowski, C. S. Schneider, and N. Wink, "On Gauge Invariance in Gauge-Fixed Yang-Mills Theory," (in preparation).

[4] J. M. Pawlowski, C. S. Schneider, J. Turnwald, and J. M. Urban, "Glueball Masses from the fRG," (in preparation).

[5] F. Gao, J. M. Pawlowski, and C. S. Schneider, "Phase Structure of QCD," (in preparation).

[6] G. Aad *et al.* (ATLAS), "Observation of a new particle in the search for the Standard Model Higgs boson with the ATLAS detector at the LHC," Phys. Lett. B 716, 1 (2012), arXiv:1207.7214 [hep-ex].

[7] S. Chatrchyan *et al.* (CMS), "Observation of a New Boson at a Mass of 125 GeV with the CMS Experiment at the LHC," Phys. Lett. B 716, 30 (2012), arXiv:1207.7235 [hep-ex].

[8] P. W. Higgs, "Broken Symmetries and the Masses of Gauge Bosons," Phys. Rev. Lett. 13, 508 (1964).

[9] G. S. Guralnik, C. R. Hagen, and T. W. B. Kibble, "Global Conservation Laws and Massless Particles," Phys. Rev. Lett. 13, 585 (1964).

[10] F. Englert and R. Brout, "Broken Symmetry and the Mass of Gauge Vector Mesons," Phys. Rev. Lett. 13, 321 (1964).

[11] C.-N. Yang and R. L. Mills, "Conservation of Isotopic Spin and Isotopic Gauge Invariance," Phys. Rev. 96, 191 (1954).

[12] D. J. Gross and F. Wilczek, "Ultraviolet Behavior of Nonabelian Gauge Theories," Phys. Rev. Lett. 30, 1343 (1973).

[13] H. D. Politzer, "Reliable Perturbative Results for Strong Interactions?" Phys. Rev. Lett. 30, 1346 (1973).

[14] R. Alkofer and L. von Smekal, "The Infrared behavior of QCD Green's functions: Confinement dynamical symmetry breaking, and hadrons as relativistic bound states," Phys. Rept. 353, 281 (2001), arXiv:hep-ph/0007355.

[15] Relativistic Heavy Ion Collider (RHIC), https://www.bnl.gov/rhic/.

[16] Large Hadron Collider (LHC), https://home.cern/.

[17] Facility for Antiproton and Ion Research (FAIR), http://www.fair-center.eu/.

[18] Nuclotron-based Ion Collider fAcility (NICA), http://nica.jinr.ru/.

[19] G. Flugge, "EXPERIMENTAL EVIDENCE FOR QUARKS AND GLUONS," Springer Tracts Mod. Phys. 100, 1 (1982).

[20] P. A. Zyla *et al.* (Particle Data Group), "Review of Particle Physics," PTEP 2020, 083C01 (2020).

[21] S. Durr *et al.*, "Ab-Initio Determination of Light Hadron Masses," Science 322, 1224 (2008), arXiv:0906.3599 [hep-lat].

[22] Y. Aoki, G. Endrodi, Z. Fodor, S. D. Katz, and K. K. Szabo, "The Order of the quantum chromodynamics transition predicted by the standard model of particle physics," Nature 443, 675 (2006), arXiv:hep-lat/0611014.

[23] S. Borsanyi, Z. Fodor, C. Hoelbling, S. D. Katz, S. Krieg, C. Ratti, and K. K. Szabo (Wuppertal-Budapest), "Is there still any T_c mystery in lattice QCD? Results with physical masses in the continuum limit III," JHEP 09, 073 (2010), arXiv:1005.3508 [hep-lat].

[24] S. Borsanyi *et al.*, "Calculation of the axion mass based on high-temperature lattice quantum chromodynamics," Nature 539, 69 (2016), arXiv:1606.07494 [hep-lat].

[25] A. Bazavov *et al.*, "The QCD Equation of State to $\mathcal{O}(\mu_B^6)$ from Lattice QCD," Phys. Rev. D 95, 054504 (2017), arXiv:1701.04325 [hep-lat].

[26] M. Troyer and U.-J. Wiese, "Computational complexity and fundamental limitations to fermionic quantum Monte Carlo simulations," Phys. Rev. Lett. 94, 170201 (2005), arXiv:cond-mat/0408370.

[27] P. de Forcrand, "Simulating QCD at finite density," PoS LAT2009, 010 (2009), arXiv:1005.0539 [hep-lat].

[28] L. Fister and J. M. Pawlowski, "Confinement from Correlation Functions," Phys. Rev. D 88, 045010 (2013), arXiv:1301.4163 [hep-ph].

[29] J. Braun, H. Gies, and J. M. Pawlowski, "Quark Confinement from Color Confinement," Phys. Lett. B 684, 262 (2010), arXiv:0708.2413 [hep-th].

[30] J. Braun, A. Eichhorn, H. Gies, and J. M. Pawlowski, "On the Nature of the Phase Transition in SU(N), Sp(2) and E(7) Yang-Mills theory," Eur. Phys. J. C 70, 689 (2010), arXiv:1007.2619 [hep-ph].

[31] A. M. Jaffe and E. Witten, "Quantum Yang-Mills theory," (2000).

[32] J. M. Pawlowski, "Geometrical effective action and Wilsonian flows," (2003), arXiv:hep-th/0310018.

[33] C. S. Fischer and H. Gies, "Renormalization flow of Yang-Mills propagators," JHEP 10, 048 (2004), arXiv:hep-ph/0408089.

[34] C. S. Fischer and J. M. Pawlowski, "Uniqueness of infrared asymptotics in Landau gauge Yang-Mills theory," Phys. Rev. D 75, 025012 (2007), arXiv:hep-th/0609009.

[35] C. S. Fischer, A. Maas, and J. M. Pawlowski, "On the infrared behavior of Landau gauge Yang-Mills theory," Annals Phys. 324, 2408 (2009), arXiv:0810.1987 [hep-ph].

[36] C. S. Fischer and J. M. Pawlowski, "Uniqueness of infrared asymptotics in Landau gauge Yang-Mills theory II," Phys. Rev. D 80, 025023 (2009), arXiv:0903.2193 [hep-th].

[37] A. K. Cyrol, L. Fister, M. Mitter, J. M. Pawlowski, and N. Strodthoff, "Landau gauge Yang-Mills correlation functions," Phys. Rev. D 94, 054005 (2016), arXiv:1605.01856 [hep-ph].

[38] L. Corell, A. K. Cyrol, M. Mitter, J. M. Pawlowski, and N. Strodthoff, "Correlation functions of three-dimensional Yang-Mills theory from the FRG," SciPost Phys. 5, 066 (2018), arXiv:1803.10092 [hep-ph].

[39] M. Q. Huber, "Correlation functions of Landau gauge Yang-Mills theory," Phys. Rev. D 101, 114009 (2020), arXiv:2003.13703 [hep-ph].

[40] G. Eichmann, J. M. Pawlowski, and J. a. M. Silva, "On mass generation in Landau-gauge Yang-Mills theory," (2021), arXiv:2107.05352 [hep-ph].

[41] U. Ellwanger, "Flow equations for N point functions and bound states," , 206 (1993), arXiv:hep-ph/9308260.

[42] U. Ellwanger and C. Wetterich, "Evolution equations for the quark - meson transition," Nucl. Phys. B 423, 137 (1994), arXiv:hep-ph/9402221.

[43] H. Gies and C. Wetterich, "Renormalization flow of bound states," Phys. Rev. D 65, 065001 (2002), arXiv:hep-th/0107221.

[44] H. Gies and C. Wetterich, "Universality of spontaneous chiral symmetry breaking in gauge theories," Phys. Rev. D 69, 025001 (2004), arXiv:hep-th/0209183.

[45] E. E. Salpeter, "Wave Functions in Momentum Space," Phys. Rev. 84, 1226 (1951).

[46] E. E. Salpeter and H. A. Bethe, "A Relativistic equation for bound state problems," Phys. Rev. 84, 1232 (1951).

[47] M. G. Alford, A. Schmitt, K. Rajagopal, and T. Schäfer, "Color superconductivity in dense quark matter," Rev. Mod. Phys. 80, 1455 (2008), arXiv:0709.4635 [hep-ph].

[48] J. Braun, L. M. Haas, F. Marhauser, and J. M. Pawlowski, "Phase Structure of Two-Flavor QCD at Finite Chemical Potential," Phys. Rev. Lett. 106, 022002 (2011), arXiv:0908.0008 [hep-ph].

[49] M. A. Stephanov, K. Rajagopal, and E. V. Shuryak, "Signatures of the tricritical point in QCD," Phys. Rev. Lett. 81, 4816 (1998), arXiv:hep-ph/9806219.

[50] B.-J. Schaefer, J. M. Pawlowski, and J. Wambach, "The Phase Structure of the Polyakov–Quark-Meson Model," Phys. Rev. D 76, 074023 (2007), arXiv:0704.3234 [hep-ph].

[51] T. K. Herbst, J. M. Pawlowski, and B.-J. Schaefer, "Phase structure and thermodynamics of QCD," Phys. Rev. D 88, 014007 (2013), arXiv:1302.1426 [hep-ph].

[52] J. M. Pawlowski and F. Rennecke, "Higher order quark-mesonic scattering processes and the phase structure of QCD," Phys. Rev. D 90, 076002 (2014), arXiv:1403.1179 [hep-ph].

[53] F. Rennecke and B.-J. Schaefer, "Fluctuation-induced modifications of the phase structure in (2+1)-flavor QCD," Phys. Rev. D 96, 016009 (2017), arXiv:1610.08748 [hep-ph].

[54] C. S. Fischer, J. Luecker, and J. A. Mueller, "Chiral and deconfinement phase transitions of two-flavour QCD at finite temperature and chemical potential," Phys. Lett. B 702, 438 (2011), arXiv:1104.1564 [hep-ph].

[55] C. S. Fischer and J. Luecker, "Propagators and phase structure of Nf=2 and Nf=2+1 QCD," Phys. Lett. B 718, 1036 (2013), arXiv:1206.5191 [hep-ph].

[56] C. S. Fischer, J. Luecker, and C. A. Welzbacher, "Phase structure of three and four flavor QCD," Phys. Rev. D 90, 034022 (2014), arXiv:1405.4762 [hep-ph].

[57] R. Contant and M. Q. Huber, "The quark propagators of QCD and QCD-like theories," Acta Phys. Polon. Supp. 10, 1009 (2017), arXiv:1709.03326 [hep-ph].

[58] W.-j. Fu, J. M. Pawlowski, and F. Rennecke, "Strangeness Neutrality and QCD Thermodynamics," SciPost Phys. Core 2, 002 (2020), arXiv:1808.00410 [hep-ph].

[59] C. S. Fischer, "QCD at finite temperature and chemical potential from Dyson–Schwinger equations," Prog. Part. Nucl. Phys. 105, 1 (2019), arXiv:1810.12938 [hep-ph].

[60] W.-j. Fu, J. M. Pawlowski, and F. Rennecke, "QCD phase structure at finite temperature and density," Phys. Rev. D 101, 054032 (2020), arXiv:1909.02991 [hep-ph].

[61] M. Leonhardt, M. Pospiech, B. Schallmo, J. Braun, C. Drischler, K. Hebeler, and A. Schwenk, "Symmetric nuclear matter from the strong interaction," Phys. Rev. Lett. 125, 142502 (2020), arXiv:1907.05814 [nucl-th].

[62] J. Braun, M. Leonhardt, and M. Pospiech, "Fierz-complete NJL model study III: Emergence from quark-gluon dynamics," Phys. Rev. D 101, 036004 (2020), arXiv:1909.06298 [hep-ph].

[63] J. Braun, W.-j. Fu, J. M. Pawlowski, F. Rennecke, D. Rosenblüh, and S. Yin, "Chiral susceptibility in (2+1)-flavor QCD," Phys. Rev. D 102, 056010 (2020), arXiv:2003.13112 [hep-ph].

[64] N. Dupuis, L. Canet, A. Eichhorn, W. Metzner, J. M. Pawlowski, M. Tissier, and N. Wschebor, "The nonperturbative functional renormalization group and its applications," Phys. Rept. 910, 1 (2021), arXiv:2006.04853 [cond-mat.stat-mech].

[65] F. Gao and J. M. Pawlowski, "QCD phase structure from functional methods," Phys. Rev. D 102, 034027 (2020), arXiv:2002.07500 [hep-ph].

[66] F. Gao and J. M. Pawlowski, "Chiral phase structure and critical end point in QCD," Phys. Lett. B 820, 136584 (2021), arXiv:2010.13705 [hep-ph].

[67] J. Bernhardt, C. S. Fischer, P. Isserstedt, and B.-J. Schaefer, "The critical endpoint of QCD in a finite volume," (2021), arXiv:2107.05504 [hep-ph].

[68] W. Ochs, "The Status of Glueballs," J. Phys. G 40, 043001 (2013), arXiv:1301.5183 [hep-ph].

[69] A. K. Cyrol, M. Mitter, J. M. Pawlowski, and N. Strodthoff, "Nonperturbative quark, gluon, and meson correlators of unquenched QCD," Phys. Rev. D 97, 054006 (2018), arXiv:1706.06326 [hep-ph].

[70] R. Alkofer and J. Greensite, "Quark Confinement: The Hard Problem of Hadron Physics," J. Phys. G 34, S3 (2007), arXiv:hep-ph/0610365.

[71] C. S. Fischer, "Infrared properties of QCD from Dyson-Schwinger equations," J. Phys. G 32, R253 (2006), arXiv:hep-ph/0605173.

[72] A. Maas, "Describing gauge bosons at zero and finite temperature," Phys.Rept. 524, 203 (2013), arXiv:1106.3942 [hep-ph].

[73] N. Vandersickel and D. Zwanziger, "The Gribov problem and QCD dynamics," Phys. Rept. 520, 175 (2012), arXiv:1202.1491 [hep-th].

[74] G. S. Bali, "QCD forces and heavy quark bound states," Phys. Rept. 343, 1 (2001), arXiv:hep-ph/0001312.

[75] J. Greensite, "The Confinement problem in lattice gauge theory," Prog. Part. Nucl. Phys. 51, 1 (2003), arXiv:hep-lat/0301023.

[76] D. Diakonov, "Topology and confinement," Nucl. Phys. B Proc. Suppl. 195, 5 (2009), arXiv:0906.2456 [hep-ph].

[77] R. Alkofer, D. Diakonov, J. Pawlowski, H. Reinhardt, V. Zakharov, D. Zwanziger, and J. Greensite, "Panel discussion: What \it don't we know about confinement?" AIP Conf. Proc. 1343, 17 (2011), arXiv:1012.3192 [hep-th].

[78] T. P. Cheng and L. F. Li, *GAUGE THEORY OF ELEMENTARY PARTICLE PHYSICS* (1984).

[79] J. M. Pawlowski, "Exact flow equations and the U(1) problem," Phys. Rev. D 58, 045011 (1998), arXiv:hep-th/9605037.

[80] M. Mitter, J. M. Pawlowski, and N. Strodthoff, "Chiral symmetry breaking in continuum QCD," Phys. Rev. D 91, 054035 (2015), arXiv:1411.7978 [hep-ph].

[81] K.-I. Aoki, K.-i. Morikawa, J.-I. Sumi, H. Terao, and M. Tomoyose, "Nonperturbative renormalization group analysis of the chiral critical behaviors in QED," Prog. Theor. Phys. 97, 479 (1997), arXiv:hep-ph/9612459.

[82] K.-I. Aoki, K. Morikawa, J.-I. Sumi, H. Terao, and M. Tomoyose, "Wilson renormalization group equations for the critical dynamics of chiral symmetry," Prog. Theor. Phys. 102, 1151 (1999), arXiv:hep-th/9908042.

[83] K.-I. Aoki, K. Morikawa, J.-I. Sumi, H. Terao, and M. Tomoyose, "Analysis of the Wilsonian effective potentials in dynamical chiral symmetry breaking," Phys. Rev. D 61, 045008 (2000), arXiv:hep-th/9908043.

[84] K.-I. Aoki, K. Takagi, H. Terao, and M. Tomoyose, "Nonladder extended renormalization group analysis of the dynamical chiral symmetry breaking," Prog. Theor. Phys. 103, 815 (2000), arXiv:hep-th/0002038.

[85] E. Meggiolaro and C. Wetterich, "Evolution equations for the effective four quark interactions in QCD," Nucl. Phys. B 606, 337 (2001), arXiv:hep-ph/0012081.

[86] K.-I. Aoki and K. Miyashita, "Evaluation of the spontaneous chiral symmetry breaking scale in general gauge theories with non-perturbative renormalization group," Prog. Theor. Phys. 121, 875 (2009).

[87] K.-I. Aoki and D. Sato, "Solving the QCD non-perturbative flow equation as a partial differential equation and its application to the dynamical chiral symmetry breaking," PTEP 2013, 043B04 (2013), arXiv:1212.0063 [hep-th].

[88] K.-I. Aoki, S.-I. Kumamoto, and D. Sato, "Weak solution of the non-perturbative renormalization group equation to describe dynamical chiral symmetry breaking," PTEP 2014, 043B05 (2014), arXiv:1403.0174 [hep-th].

[89] J. Braun, L. Fister, J. M. Pawlowski, and F. Rennecke, "From Quarks and Gluons to Hadrons: Chiral Symmetry Breaking in Dynamical QCD," Phys. Rev. D 94, 034016 (2016), arXiv:1412.1045 [hep-ph].

[90] F. Rennecke, "Vacuum structure of vector mesons in QCD," Phys. Rev. D 92, 076012 (2015), arXiv:1504.03585 [hep-ph].

[91] F. Gao, J. Papavassiliou, and J. M. Pawlowski, "Fully coupled functional equations for the quark sector of QCD," Phys. Rev. D 103, 094013 (2021), arXiv:2102.13053 [hep-ph].

[92] M. E. Peskin and D. V. Schroeder, *An Introduction to quantum field theory* (Addison-Wesley, Reading, USA, 1995).

[93] C. Itzykson and J. B. Zuber, *Quantum Field Theory*, International Series In Pure and Applied Physics (McGraw-Hill, New York, 1980).

[94] J. M. Pawlowski, J. A. Bonnet, S. Rechenberger, M. Reichert, and N. Wink, "-the functional renormalization group- & applications to gauge theories and gravity," (in preparation).

[95] J. M. Pawlowski and T. Plehn, "QCD," (in preparation).

[96] V. N. Gribov, "Quantization of Nonabelian Gauge Theories," Nucl. Phys. B 139, 1 (1978).

[97] I. M. Singer, "Some Remarks on the Gribov Ambiguity," Commun. Math. Phys. 60, 7 (1978).

[98] L. D. Faddeev and V. N. Popov, "Feynman Diagrams for the Yang-Mills Field," Phys. Lett. B 25, 29 (1967).

[99] J. S. Bell and R. Jackiw, "A PCAC puzzle: $\pi^0 \to \gamma\gamma$ in the σ model," Nuovo Cim. A 60, 47 (1969).

[100] S. L. Adler, "Axial vector vertex in spinor electrodynamics," Phys. Rev. 177, 2426 (1969).

[101] S. L. Adler and W. A. Bardeen, "Absence of higher order corrections in the anomalous axial vector divergence equation," Phys. Rev. 182, 1517 (1969).

[102] K. Fujikawa, "Path Integral Measure for Gauge Invariant Fermion Theories," Phys. Rev. Lett. 42, 1195 (1979).

[103] G. 't Hooft, "Symmetry Breaking Through Bell-Jackiw Anomalies," Phys. Rev. Lett. 37, 8 (1976).

[104] Y. Nambu and G. Jona-Lasinio, "Dynamical Model of Elementary Particles Based on an Analogy with Superconductivity. 1." Phys. Rev. 122, 345 (1961).

[105] Y. Nambu, "Quasiparticles and Gauge Invariance in the Theory of Superconductivity," Phys. Rev. 117, 648 (1960).

[106] J. Goldstone, "Field Theories with Superconductor Solutions," Nuovo Cim. 19, 154 (1961).

[107] J. Goldstone, A. Salam, and S. Weinberg, "Broken Symmetries," Phys. Rev. 127, 965 (1962).

[108] M. Gell-Mann, R. J. Oakes, and B. Renner, "Behavior of current divergences under SU(3) x SU(3)," Phys. Rev. 175, 2195 (1968).

[109] G. 't Hooft, "Naturalness, chiral symmetry, and spontaneous chiral symmetry breaking," NATO Sci. Ser. B 59, 135 (1980).

[110] C. Becchi, A. Rouet, and R. Stora, "Renormalization of Gauge Theories," Annals Phys. 98, 287 (1976).

[111] I. V. Tyutin, "Gauge Invariance in Field Theory and Statistical Physics in Operator Formalism," (1975), arXiv:0812.0580 [hep-th].

[112] J. Berges, N. Tetradis, and C. Wetterich, "Non-perturbative renormalization flow in quantum field theory and statistical physics," Phys. Rept. 363, 223 (2002), arXiv:hep-ph/0005122.

[113] J. Polonyi, "Lectures on the functional renormalization group method," Central Eur.J.Phys. 1, 1 (2003), arXiv:hep-th/0110026 [hep-th].

[114] B. Delamotte, D. Mouhanna, and M. Tissier, "Nonperturbative renormalization group approach to frustrated magnets," Phys.Rev. B69, 134413 (2004), arXiv:cond-mat/0309101 [cond-mat].

[115] J. M. Pawlowski, "Aspects of the functional renormalisation group," Annals Phys. 322, 2831 (2007), arXiv:hep-th/0512261.

[116] B.-J. Schaefer and J. Wambach, "Renormalization group approach towards the QCD phase diagram," Phys.Part.Nucl. 39, 1025 (2008), arXiv:hep-ph/0611191 [hep-ph].

[117] H. Gies, "Introduction to the functional RG and applications to gauge theories," Lect.Notes Phys. 852, 287 (2012), arXiv:hep-ph/0611146 [hep-ph].

[118] B. Delamotte, "An Introduction to the nonperturbative renormalization group," Lect. Notes Phys. 852, 49 (2012), arXiv:cond-mat/0702365 [cond-mat.stat-mech].

[119] Y. Igarashi, K. Itoh, and H. Sonoda, "Realization of Symmetry in the ERG Approach to Quantum Field Theory," Prog. Theor. Phys. Suppl. 181, 1 (2010), arXiv:0909.0327 [hep-th].

[120] O. J. Rosten, "Fundamentals of the Exact Renormalization Group," Phys. Rept. 511, 177 (2012), arXiv:1003.1366 [hep-th].

[121] P. Kopietz, L. Bartosch, and F. Schütz, *Introduction to the functional renormalization group*, Vol. 798 (2010).

[122] J. Braun, "Fermion Interactions and Universal Behavior in Strongly Interacting Theories," J.Phys. G39, 033001 (2012), arXiv:1108.4449 [hep-ph].

[123] D. F. Litim, "Renormalisation group and the Planck scale," Phil. Trans. Roy. Soc. Lond. A 369, 2759 (2011), arXiv:1102.4624 [hep-th].

[124] W. Metzner, M. Salmhofer, C. Honerkamp, V. Meden, and K. Schönhammer, "Functional renormalization group approach to correlated fermion systems," Reviews of Modern Physics 84, 299–352 (2012).

[125] M. Salmhofer, "Renormalization in condensed matter: Fermionic systems – from mathematics to materials," Nucl. Phys. B 941, 868 (2019), arXiv:1807.01766 [cond-mat.str-el].

[126] A. Eichhorn, "An asymptotically safe guide to quantum gravity and matter," Front. Astron. Space Sci. 5, 47 (2019), arXiv:1810.07615 [hep-th].

[127] M. Reuter and F. Saueressig, *Quantum Gravity and the Functional Renormalization Group: The Road towards Asymptotic Safety* (Cambridge University Press, 2019).

[128] A. Bonanno, A. Eichhorn, H. Gies, J. M. Pawlowski, R. Percacci, M. Reuter, F. Saueressig, and G. P. Vacca, "Critical reflections on asymptotically safe gravity," Front. in Phys. 8, 269 (2020), arXiv:2004.06810 [gr-qc].

[129] J. M. Pawlowski and M. Reichert, "Quantum gravity: a fluctuating point of view," (2020), arXiv:2007.10353 [hep-th].

[130] C. D. Roberts and S. M. Schmidt, "Dyson-Schwinger equations: Density, temperature and continuum strong QCD," Prog. Part. Nucl. Phys. 45, S1 (2000), arXiv:nucl-th/0005064.

[131] D. Binosi and J. Papavassiliou, "Pinch Technique: Theory and Applications," Phys. Rept. 479, 1 (2009), arXiv:0909.2536 [hep-ph].

[132] P. Boucaud, J. P. Leroy, A. L. Yaouanc, J. Micheli, O. Pene, and J. Rodriguez-Quintero, "The Infrared Behaviour of the Pure Yang-Mills Green Functions," Few Body Syst. 53, 387 (2012), arXiv:1109.1936 [hep-ph].

[133] A. C. Aguilar, D. Binosi, and J. Papavassiliou, "The Gluon Mass Generation Mechanism: A Concise Primer," Front. Phys. (Beijing) 11, 111203 (2016), arXiv:1511.08361 [hep-ph].

[134] G. Eichmann, H. Sanchis-Alepuz, R. Williams, R. Alkofer, and C. S. Fischer, "Baryons as relativistic three-quark bound states," Prog. Part. Nucl. Phys. 91, 1 (2016), arXiv:1606.09602 [hep-ph].

[135] H. Sanchis-Alepuz and R. Williams, "Recent developments in bound-state calculations using the Dyson–Schwinger and Bethe–Salpeter equations," Comput. Phys. Commun. 232, 1 (2018), arXiv:1710.04903 [hep-ph].

[136] M. Q. Huber, "Nonperturbative properties of Yang–Mills theories," Phys. Rept. 879, 1 (2020), arXiv:1808.05227 [hep-ph].

[137] F. Dyson, "The S matrix in quantum electrodynamics," Phys. Rev. 75, 1736 (1949).

[138] J. S. Schwinger, "On the Green's functions of quantized fields. 1." Proc. Nat. Acad. Sci. 37, 452 (1951).

[139] K. Symanzik, "Small distance behavior in field theory and power counting," Commun. Math. Phys. 18, 227 (1970).

[140] C. Wetterich, "Exact evolution equation for the effective potential," Phys.Lett. B301, 90 (1993).

[141] M. Bonini, M. D'Attanasio, and G. Marchesini, "Perturbative renormalization and infrared finiteness in the Wilson renormalization group: The Massless scalar case," Nucl. Phys. B 409, 441 (1993), arXiv:hep-th/9301114.

[142] T. R. Morris, "The Exact renormalization group and approximate solutions," Int. J. Mod. Phys. A9, 2411 (1994), arXiv:hep-ph/9308265.

[143] J. Zinn-Justin, "Renormalization of Gauge Theories," Lect. Notes Phys. 37, 1 (1975).

[144] J. Zinn-Justin, "Renormalization of gauge theories and master equation," Mod. Phys. Lett. A 14, 1227 (1999), arXiv:hep-th/9906115.

[145] J. Braun, M. Leonhardt, and J. M. Pawlowski, "Renormalization group consistency and low-energy effective theories," SciPost Phys. 6, 056 (2019), arXiv:1806.04432 [hep-ph].

[146] D. F. Litim, "Derivative expansion and renormalization group flows," JHEP 11, 059 (2001), arXiv:hep-th/0111159.

[147] D. F. Litim, "Optimized renormalization group flows," Phys. Rev. D 64, 105007 (2001), arXiv:hep-th/0103195.

[148] D. F. Litim, "Optimization of the exact renormalization group," Phys. Lett. B 486, 92 (2000), arXiv:hep-th/0005245.

[149] A. Sternbeck, E. M. Ilgenfritz, M. Muller-Preussker, A. Schiller, and I. L. Bogolubsky, "Lattice study of the infrared behavior of QCD Green's functions in Landau gauge," PoS LAT2006, 076 (2006), arXiv:hep-lat/0610053.

[150] V. Branchina, K. A. Meissner, and G. Veneziano, "The Price of an exact, gauge invariant RG flow equation," Phys. Lett. B 574, 319 (2003), arXiv:hep-th/0309234.

[151] S. Arnone, T. R. Morris, and O. J. Rosten, "A Generalised manifestly gauge invariant exact renormalisation group for SU(N) Yang-Mills," Eur. Phys. J. C 50, 467 (2007), arXiv:hep-th/0507154.

[152] O. J. Rosten, "A Manifestly gauge invariant and universal calculus for SU(N) Yang-Mills," Int. J. Mod. Phys. A 21, 4627 (2006), arXiv:hep-th/0602229.

[153] C. Wetterich, "Gauge invariant flow equation," Nucl. Phys. B 931, 262 (2018), arXiv:1607.02989 [hep-th].

[154] C. Wetterich, "Gauge-invariant fields and flow equations for Yang–Mills theories," Nucl. Phys. B 934, 265 (2018), arXiv:1710.02494 [hep-th].

[155] S. Asnafi, H. Gies, and L. Zambelli, "BRST invariant RG flows," Phys. Rev. D 99, 085009 (2019), arXiv:1811.03615 [hep-th].

[156] L. Corell, A. K. Cyrol, M. Heller, and J. M. Pawlowski, "Flowing with the temporal renormalization group," Phys. Rev. D 104, 025005 (2021), arXiv:1910.09369 [hep-th].

[157] C. Wetterich and M. Yamada, "Variable Planck mass from the gauge invariant flow equation," Phys. Rev. D 100, 066017 (2019), arXiv:1906.01721 [hep-th].

[158] T. Gasenzer and J. M. Pawlowski, "Towards far-from-equilibrium quantum field dynamics: A functional renormalisation-group approach," Phys. Lett. B 670, 135 (2008), arXiv:0710.4627 [cond-mat.other].

[159] J. Berges and G. Hoffmeister, "Nonthermal fixed points and the functional renormalization group," Nucl. Phys. B 813, 383 (2009), arXiv:0809.5208 [hep-th].

[160] J. Berges and D. Mesterhazy, "Introduction to the nonequilibrium functional renormalization group," Nucl. Phys. B Proc. Suppl. 228, 37 (2012), arXiv:1204.1489 [hep-ph].

[161] T. Gasenzer, S. Kessler, and J. M. Pawlowski, "Far-from-equilibrium quantum many-body dynamics," Eur. Phys. J. C 70, 423 (2010), arXiv:1003.4163 [cond-mat.quant-gas].

[162] J. M. Pawlowski and N. Strodthoff, "Real time correlation functions and the functional renormalization group," Phys. Rev. D 92, 094009 (2015), arXiv:1508.01160 [hep-ph].

[163] R. Alkofer, M. Q. Huber, and K. Schwenzer, "Algorithmic derivation of Dyson-Schwinger Equations," Comput. Phys. Commun. 180, 965 (2009), arXiv:0808.2939 [hep-th].

[164] M. Q. Huber and J. Braun, "Algorithmic derivation of functional renormalization group equations and Dyson-Schwinger equations," Comput.Phys.Commun. 183, 1290 (2012), arXiv:1102.5307 [hep-th].

[165] M. Q. Huber, A. K. Cyrol, and J. M. Pawlowski, "Dofun 3.0: Functional equations in mathematica," Computer Physics Communications 248, 107058 (2020).

[166] M. Q. Huber and A. K. Cyrol, "DoFun GitHub Repository," (2019), https://github.com/markusqh/DoFun.

[167] J. A. M. Vermaseren, "New features of FORM," (2000), arXiv:math-ph/0010025.

[168] J. Vermaseren, "FORM GitHub Repository," (2016), https://github.com/vermaseren/form.

[169] F. Feng and R. Mertig, "FormLink/FeynCalcFormLink : Embedding FORM in Mathematica and FeynCalc," (2012), arXiv:1212.3522.

[170] F. Feng and R. Mertig, "FormLink/FeynCalcFormLink GitHub Repository," (2012), https://github.com/FormLink/formlink.

[171] A. K. Cyrol, M. Mitter, and N. Strodthoff, "FormTracer - A Mathematica Tracing Package Using FORM," Comput. Phys. Commun. 219, 346 (2017), arXiv:1610.09331 [hep-ph].

[172] A. K. Cyrol, M. Mitter, J. M. Pawlowski, and N. Strodthoff, "FormTracer GitHub Repository," (2016), https://github.com/FormTracer/FormTracer.

[173] D. F. Litim and T. Steudtner, "ARGES – Advanced Renormalisation Group Equation Simplifier," (2020), arXiv:2012.12955 [hep-ph].

[174] D. F. Litim and T. Steudtner, "ARGES GitHub Repository," (2020), https://github.com/TomSteu/ARGES.

[175] M. Tissier and N. Wschebor, "Infrared propagators of Yang-Mills theory from perturbation theory," Phys. Rev. D 82, 101701 (2010), arXiv:1004.1607 [hep-ph].

[176] M. Tissier and N. Wschebor, "An Infrared Safe perturbative approach to Yang-Mills correlators," Phys. Rev. D 84, 045018 (2011), arXiv:1105.2475 [hep-th].

[177] J. Serreau and M. Tissier, "Lifting the Gribov ambiguity in Yang-Mills theories," Phys. Lett. B 712, 97 (2012), arXiv:1202.3432 [hep-th].

[178] U. Reinosa, J. Serreau, M. Tissier, and N. Wschebor, "How nonperturbative is the infrared regime of Landau gauge Yang-Mills correlators?" Phys. Rev. D 96, 014005 (2017), arXiv:1703.04041 [hep-th].

[179] J. Zinn-Justin, "Renormalization of Gauge Theories," Lect. Notes Phys. 37, 1 (1975).

[180] J. Zinn-Justin, "Renormalization of gauge theories and master equation," Mod. Phys. Lett. A 14, 1227 (1999), arXiv:hep-th/9906115.

[181] M. Q. Huber, A. K. Cyrol, and L. von Smekal, "On Dyson-Schwinger studies of Yang-Mills theory and the four-gluon vertex," Acta Phys. Polon. Supp. 8, 497 (2015), arXiv:1506.03908 [hep-ph].

[182] H. Gies, "Running coupling in Yang-Mills theory: A flow equation study," Phys. Rev. D 66, 025006 (2002), arXiv:hep-th/0202207.

[183] T. Kugo and I. Ojima, "Local Covariant Operator Formalism of Nonabelian Gauge Theories and Quark Confinement Problem," Prog. Theor. Phys. Suppl. 66, 1 (1979).

[184] N. Nakanishi and I. Ojima, *Covariant operator formalism of gauge theories and quantum gravity*, Vol. 27 (1990).

[185] C. S. Fischer, "Infrared behavior of QCD from the Dyson-Schwinger formalism," PoS LC2008, 048 (2008), arXiv:0810.2526 [hep-ph].

[186] A. Maas, "Constraining the gauge-fixed Lagrangian in minimal Landau gauge," SciPost Phys. 8, 071 (2020), arXiv:1907.10435 [hep-lat].

[187] C. J. Morningstar and M. J. Peardon, "The Glueball spectrum from an anisotropic lattice study," Phys. Rev. D 60, 034509 (1999), arXiv:hep-lat/9901004.

[188] G. S. Bali, K. Schilling, A. Hulsebos, A. C. Irving, C. Michael, and P. W. Stephenson (UKQCD), "A Comprehensive lattice study of SU(3) glueballs," Phys. Lett. B 309, 378 (1993), arXiv:hep-lat/9304012.

[189] Y. Chen *et al.*, "Glueball spectrum and matrix elements on anisotropic lattices," Phys. Rev. D 73, 014516 (2006), arXiv:hep-lat/0510074.

[190] E. Gregory, A. Irving, B. Lucini, C. McNeile, A. Rago, C. Richards, and E. Rinaldi, "Towards the glueball spectrum from unquenched lattice QCD," JHEP 10, 170 (2012), arXiv:1208.1858 [hep-lat].

[191] A. Athenodorou and M. Teper, "The glueball spectrum of SU(3) gauge theory in 3 + 1 dimensions," JHEP 11, 172 (2020), arXiv:2007.06422 [hep-lat].

[192] J. Meyers and E. S. Swanson, "Spin Zero Glueballs in the Bethe-Salpeter Formalism," Phys. Rev. D 87, 036009 (2013), arXiv:1211.4648 [hep-ph].

[193] H. Sanchis-Alepuz, C. S. Fischer, C. Kellermann, and L. von Smekal, "Glueballs from the Bethe-Salpeter equation," Phys. Rev. D 92, 034001 (2015), arXiv:1503.06051 [hep-ph].

[194] E. V. Souza, M. Narciso Ferreira, A. C. Aguilar, J. Papavassiliou, C. D. Roberts, and S.-S. Xu, "Pseudoscalar glueball mass: a window on three-gluon interactions," Eur. Phys. J. A 56, 25 (2020), arXiv:1909.05875 [nucl-th].

[195] L. P. Kaptari and B. Kämpfer, "Mass Spectrum of Pseudo-Scalar Glueballs from a Bethe–Salpeter Approach with the Rainbow–Ladder Truncation," Few Body Syst. 61, 28 (2020), arXiv:2004.06523 [hep-ph].

[196] M. Q. Huber, C. S. Fischer, and H. Sanchis-Alepuz, "Spectrum of scalar and pseudoscalar glueballs from functional methods," Eur. Phys. J. C 80, 1077 (2020), arXiv:2004.00415 [hep-ph].

[197] V. Mathieu, N. Kochelev, and V. Vento, "The Physics of Glueballs," Int. J. Mod. Phys. E 18, 1 (2009), arXiv:0810.4453 [hep-ph].

[198] F. Brau and C. Semay, "Semirelativistic potential model for glueball states," Phys. Rev. D 70, 014017 (2004), arXiv:hep-ph/0412173.

[199] V. Mathieu, C. Semay, and B. Silvestre-Brac, "Semirelativistic potential model for three-gluon glueballs," Phys. Rev. D 77, 094009 (2008), arXiv:0803.0815 [hep-ph].

[200] F. Buisseret, V. Mathieu, and C. Semay, "Glueball phenomenology and the relativistic flux tube model," Phys. Rev. D 80, 074021 (2009), arXiv:0906.3098 [hep-ph].

[201] A. B. Kaidalov and Y. A. Simonov, "Glueball masses and Pomeron trajectory in nonperturbative QCD approach," Phys. Lett. B 477, 163 (2000), arXiv:hep-ph/9912434.

[202] E. Klempt and A. Zaitsev, "Glueballs, Hybrids, Multiquarks. Experimental facts versus QCD inspired concepts," Phys. Rept. 454, 1 (2007), arXiv:0708.4016 [hep-ph].

[203] A. Szczepaniak, E. S. Swanson, C.-R. Ji, and S. R. Cotanch, "Glueball spectroscopy in a relativistic many body approach to hadron structure," Phys. Rev. Lett. 76, 2011 (1996), arXiv:hep-ph/9511422.

[204] A. P. Szczepaniak and E. S. Swanson, "The Low lying glueball spectrum," Phys. Lett. B 577, 61 (2003), arXiv:hep-ph/0308268.

[205] D. Dudal, M. S. Guimaraes, and S. P. Sorella, "Glueball masses from an infrared moment problem and nonperturbative Landau gauge," Phys. Rev. Lett. 106, 062003 (2011), arXiv:1010.3638 [hep-th].

[206] S. Janowski, D. Parganlija, F. Giacosa, and D. H. Rischke, "The Glueball in a Chiral Linear Sigma Model with Vector Mesons," Phys. Rev. D 84, 054007 (2011), arXiv:1103.3238 [hep-ph].

[207] W. I. Eshraim, S. Janowski, F. Giacosa, and D. H. Rischke, "Decay of the pseudoscalar glueball into scalar and pseudoscalar mesons," Phys. Rev. D 87, 054036 (2013), arXiv:1208.6474 [hep-ph].

[208] D. Dudal, M. S. Guimaraes, and S. P. Sorella, "Pade approximation and glueball mass estimates in $3d$ and $4d$ with $N_c = 2, 3$ colors," Phys. Lett. B 732, 247 (2014), arXiv:1310.2016 [hep-ph].

[209] H. Padé, "Sur la représentation approchée d'une fonction par des fractions rationalles." Annales Scientifiques de l'Êcole Normale Supérieure 9, 1 (1892).

[210] G. Frobenius, "Über Relationen zwischen den Näherungsbrüchen von Potenzreihen," Journal für die reine und angewandte Mathematik 90, 1 (1881).

[211] D. G. Krige, "A statistical approach to some basic mine valuation problems on the witwatersrand," Journal of the Southern African Insitute of Mining and Metallurgy 52 (1951).

[212] M. Kanagawa, P. Hennig, D. Sejdinovic, and B. K. Sriperumbudur, "Gaussian processes and kernel methods: A review on connections and equivalences," (2018), arXiv:1807.02582 [stat.ML].

[213] J. Horak, J. M. Pawlowski, and N. Wink, "Spectral functions in the ϕ^4-theory from the spectral DSE," Phys. Rev. D 102, 125016 (2020), arXiv:2006.09778 [hep-th].

[214] J. Horak, J. Papavassiliou, J. M. Pawlowski, and N. Wink, "Ghost spectral function from the spectral Dyson-Schwinger equation," (2021), arXiv:2103.16175 [hep-th].

[215] Y.-y. Tan, Y.-r. Chen, and W.-j. Fu, "Real-time dynamics of the $O(4)$ scalar theory within the fRG approach," (2021), arXiv:2107.06482 [hep-ph].

[216] A. K. Cyrol, J. M. Pawlowski, A. Rothkopf, and N. Wink, "Reconstructing the gluon," SciPost Phys. 5, 065 (2018), arXiv:1804.00945 [hep-ph].

[217] J. Horak, J. M. Pawlowski, J. Rodríguez-Quintero, J. Turnwald, J. M. Urban, N. Wink, and S. Zafeiropoulos, "Reconstructing QCD Spectral Functions with Gaussian Processes," (2021), arXiv:2107.13464 [hep-ph].

[218] A. Wightman, *Fields as Operator-valued Distributions in Relativistic Quantum Theory*, Arkiv för fysik (Almqvist & Wiksell, 1964).

[219] N. N. Bogolyubov, A. A. Logunov, and I. T. Todorov, *Introduction to Axiomatic Quantum Field Theory* (1975).

[220] J. Glimm and A. M. Jaffe, *QUANTUM PHYSICS. A FUNCTIONAL INTEGRAL POINT OF VIEW* (1987).

[221] G. Kallen, "On the definition of the Renormalization Constants in Quantum Electrodynamics," Helv. Phys. Acta 25, 417 (1952).

[222] H. Lehmann, "On the Properties of propagation functions and renormalization contants of quantized fields," Nuovo Cim. 11, 342 (1954).

[223] J. Hubbard, "Calculation of partition functions," Phys. Rev. Lett. 3, 77 (1959).

[224] R. L. Stratonovich, "On a Method of Calculating Quantum Distribution Functions," Soviet Physics Doklady 2, 416 (1957).

[225] G. Cuniberti, E. De Micheli, and G. A. Viano, "Reconstructing the thermal Green functions at real times from those at imaginary times," Commun. Math. Phys. 216, 59 (2001), arXiv:cond-mat/0109175.

[226] Y. Burnier, M. Laine, and L. Mether, "A Test on analytic continuation of thermal imaginary-time data," Eur. Phys. J. C 71, 1619 (2011), arXiv:1101.5534 [hep-lat].

[227] M. Hobson and A. Lasenby, "The entropic prior for distributions with positive and negative values," Mon. Not. Roy. Astron. Soc. 298, 905 (1998), arXiv:astro-ph/9810240.

[228] A. Rothkopf, "Bayesian inference of nonpositive spectral functions in quantum field theory," Phys. Rev. D 95, 056016 (2017), arXiv:1611.00482 [hep-ph].

[229] Y. Burnier and A. Rothkopf, "Bayesian Approach to Spectral Function Reconstruction for Euclidean Quantum Field Theories," Phys. Rev. Lett. 111, 182003 (2013), arXiv:1307.6106 [hep-lat].

[230] J. Schmidhuber, "Deep learning in neural networks: An overview," CoRR abs/1404.7828 (2014), arXiv:1404.7828.

[231] Y. LeCun, Y. Bengio, and G. Hinton, "Deep Learning," Nature 521, 436 (2025).

[232] H. Yoon, J.-H. Sim, and M. J. Han, "Analytic continuation via domain knowledge free machine learning," Physical Review B 98 (2018), 10.1103/physrevb.98.245101.

[233] L. Kades, J. M. Pawlowski, A. Rothkopf, M. Scherzer, J. M. Urban, S. J. Wetzel, N. Wink, and F. P. G. Ziegler, "Spectral Reconstruction with Deep Neural Networks," Phys. Rev. D 102, 096001 (2020), arXiv:1905.04305 [physics.comp-ph].

[234] R. Fournier, L. Wang, O. V. Yazyev, and Q. Wu, "Artificial neural network approach to the analytic continuation problem," Physical Review Letters 124 (2020), 10.1103/physrevlett.124.056401.

[235] M. Zhou, F. Gao, J. Chao, Y.-X. Liu, and H. Song, "Application of radial basis functions neutral networks in spectral functions," (2021), arXiv:2106.08168 [hep-ph].

[236] M. Haas, L. Fister, and J. M. Pawlowski, "Gluon spectral functions and transport coefficients in Yang–Mills theory," Phys. Rev. D 90, 091501 (2014), arXiv:1308.4960 [hep-ph].

[237] M. Ulybyshev, C. Winterowd, and S. Zafeiropoulos, "Collective charge excitations and the metal-insulator transition in the square lattice Hubbard-Coulomb model," Phys. Rev. B 96, 205115 (2017), arXiv:1707.04212 [cond-mat.str-el].

[238] D. Dudal, O. Oliveira, M. Roelfs, and P. Silva, "Spectral representation of lattice gluon and ghost propagators at zero temperature," Nucl. Phys. B 952, 114912 (2020), arXiv:1901.05348 [hep-lat].

[239] D. Dudal, O. Oliveira, and M. Roelfs, "Källén-Lehmann Spectral Representation of the Scalar SU(2) Glueball," (2021), arXiv:2103.11846 [hep-lat].

[240] L.-F. Arsenault, R. Neuberg, L. A. Hannah, and A. J. Millis, "Projected regression methods for inverting fredholm integrals: Formalism and application to analytical continuation," (2016), arXiv:1612.04895 [cond-mat.str-el].

[241] S. Offler, G. Aarts, C. Allton, J. Glesaaen, B. Jäger, S. Kim, M. P. Lombardo, S. M. Ryan, and J.-I. Skullerud, "News from bottomonium spectral functions in thermal QCD," PoS LATTICE2019, 076 (2019), arXiv:1912.12900 [hep-lat].

[242] M. Jarrell and J. E. Gubernatis, "Bayesian inference and the analytic continuation of imaginary-time quantum Monte Carlo data," Phys. Rept. 269, 133 (1996).

[243] M. Asakawa, T. Hatsuda, and Y. Nakahara, "Maximum entropy analysis of the spectral functions in lattice QCD," Prog. Part. Nucl. Phys. 46, 459 (2001), arXiv:hep-lat/0011040.

[244] J. Fei, C.-N. Yeh, and E. Gull, "Nevanlinna analytical continuation," Physical Review Letters 126 (2021), 10.1103/physrevlett.126.056402.

[245] J. Fei, C.-N. Yeh, D. Zgid, and E. Gull, "Analytical continuation of matrix-valued functions: Carathéodory formalism," (2021), arXiv:2107.00788 [cond-mat.str-el].

[246] R.-A. Tripolt, I. Haritan, J. Wambach, and N. Moiseyev, "Threshold energies and poles for hadron physical problems by a model-independent universal algorithm," Phys. Lett. B 774, 411 (2017), arXiv:1610.03252 [hep-ph].

[247] R.-A. Tripolt, P. Gubler, M. Ulybyshev, and L. Von Smekal, "Numerical analytic continuation of Euclidean data," Comput. Phys. Commun. 237, 129 (2019), arXiv:1801.10348 [hep-ph].

[248] D. Binosi and R.-A. Tripolt, "Spectral functions of confined particles," Phys. Lett. B 801, 135171 (2020), arXiv:1904.08172 [hep-ph].

[249] A. P. Valentine and M. Sambridge, "Gaussian process models—I. A framework for probabilistic continuous inverse theory," Geophysical Journal International 220, 1632 (2019), https://academic.oup.com/gji/article-pdf/220/3/1632/31578341/ggz520.pdf.

[250] A. Rothkopf, "Heavy Quarkonium in Extreme Conditions," Phys. Rept. 858, 1 (2020), arXiv:1912.02253 [hep-ph].

[251] C. Rasmussen and C. Williams, *Gaussian Processes for Machine Learning*, Adaptive Computation and Machine Learning (MIT Press, Cambridge, MA, USA, 2006) p. 248.

[252] M. Krasser, "Gaussian Processes," (2018), https://krasserm.github.io/2018/03/19/gaussian-processes/.

[253] H. Liu, Y.-S. Ong, X. Shen, and J. Cai, "When gaussian process meets big data: A review of scalable gps," (2019), arXiv:1807.01065 [stat.ML].

[254] W. Menke and R. Creel, "Gaussian process regression reviewed in the context of inverse theory," Surveys in Geophysics 42, 473 (2021).

[255] A. J. Helmboldt, J. M. Pawlowski, and N. Strodthoff, "Towards quantitative precision in the chiral crossover: masses and fluctuation scales," Phys. Rev. D 91, 054010 (2015), arXiv:1409.8414 [hep-ph].

[256] J. M. Pawlowski, N. Strodthoff, and N. Wink, "Finite temperature spectral functions in the O(N)-model," Phys. Rev. D 98, 074008 (2018), arXiv:1711.07444 [hep-th].

[257] G. Eichmann, C. S. Fischer, and W. Heupel, "Four-point functions and the permutation group S4," Phys. Rev. D 92, 056006 (2015), arXiv:1505.06336 [hep-ph].

[258] X. Luo and N. Xu, "Search for the QCD Critical Point with Fluctuations of Conserved Quantities in Relativistic Heavy-Ion Collisions at RHIC : An Overview," Nucl. Sci. Tech. 28, 112 (2017), arXiv:1701.02105 [nucl-ex].

[259] L. Adamczyk *et al.* (STAR), "Bulk Properties of the Medium Produced in Relativistic Heavy-Ion Collisions from the Beam Energy Scan Program," Phys. Rev. C 96, 044904 (2017), arXiv:1701.07065 [nucl-ex].

[260] A. Andronic, P. Braun-Munzinger, K. Redlich, and J. Stachel, "Decoding the phase structure of QCD via particle production at high energy," Nature 561, 321 (2018), arXiv:1710.09425 [nucl-th].

[261] M. A. Stephanov, "QCD phase diagram: An Overview," PoS LAT2006, 024 (2006), arXiv:hep-lat/0701002.

[262] J. O. Andersen, W. R. Naylor, and A. Tranberg, "Phase diagram of QCD in a magnetic field: A review," Rev. Mod. Phys. 88, 025001 (2016), arXiv:1411.7176 [hep-ph].

[263] E. Shuryak, "Strongly coupled quark-gluon plasma in heavy ion collisions," Rev. Mod. Phys. 89, 035001 (2017), arXiv:1412.8393 [hep-ph].

[264] J. M. Pawlowski, "Equation of state and phase diagram of strongly interacting matter," Nucl. Phys. A 931, 113 (2014).

[265] Y. Yin, "The QCD critical point hunt: emergent new ideas and new dynamics," (2018), arXiv:1811.06519 [nucl-th].

[266] A. Bazavov *et al.* (HotQCD), "Skewness and kurtosis of net baryon-number distributions at small values of the baryon chemical potential," Phys. Rev. D 96, 074510 (2017), arXiv:1708.04897 [hep-lat].

[267] C. Bonati, M. D'Elia, F. Negro, F. Sanfilippo, and K. Zambello, "Curvature of the pseudocritical line in QCD: Taylor expansion matches analytic continuation," Phys. Rev. D 98, 054510 (2018), arXiv:1805.02960 [hep-lat].

[268] S. Borsanyi, Z. Fodor, J. N. Guenther, S. K. Katz, K. K. Szabo, A. Pasztor, I. Portillo, and C. Ratti, "Higher order fluctuations and correlations of conserved charges from lattice QCD," JHEP 10, 205 (2018), arXiv:1805.04445 [hep-lat].

[269] A. Bazavov *et al.* (HotQCD), "Chiral crossover in QCD at zero and non-zero chemical potentials," Phys. Lett. B 795, 15 (2019), arXiv:1812.08235 [hep-lat].

[270] J. N. Guenther, S. Borsanyi, Z. Fodor, S. K. Katz, K. K. Szabó, A. Pasztor, I. Portillo, and C. Ratti, "Lattice thermodynamics at finite chemical potential from analytical Continuation," J. Phys. Conf. Ser. 1070, 012002 (2018).

[271] H. T. Ding *et al.* (HotQCD), "Chiral Phase Transition Temperature in (2+1)-Flavor QCD," Phys. Rev. Lett. 123, 062002 (2019), arXiv:1903.04801 [hep-lat].

[272] S. Borsanyi, Z. Fodor, J. N. Guenther, R. Kara, S. D. Katz, P. Parotto, A. Pasztor, C. Ratti, and K. K. Szabo, "QCD Crossover at Finite Chemical Potential from Lattice Simulations," Phys. Rev. Lett. 125, 052001 (2020), arXiv:2002.02821 [hep-lat].

[273] A. Cucchieri, A. Maas, and T. Mendes, "Exploratory study of three-point Green's functions in Landau-gauge Yang-Mills theory," Phys. Rev. D 74, 014503 (2006), arXiv:hep-lat/0605011.

[274] A. Cucchieri, A. Maas, and T. Mendes, "Three-point vertices in Landau-gauge Yang-Mills theory," Phys. Rev. D 77, 094510 (2008), arXiv:0803.1798 [hep-lat].

[275] A. Maas, "(in preparation)," .

[276] U. Ellwanger, "Flow equations and BRS invariance for Yang-Mills theories," Phys. Lett. B 335, 364 (1994), arXiv:hep-th/9402077.